CORRELATION OF SPACECRAFT PASSIVE MICROWAVE SYSTEM DATA WITH SOIL MOISTURE INDICES (API)

By
Bruce J. Blanchard
Marshall J. McFarland
Sidney Theis
John G. Richter
Remote Sensing Center
Texas A&M University
College Station, Texas 77843

February 1981

Prepared for
Goddard Space Flight Center
Greenbelt, Maryland 20771
Contract No.: NSG-5193

TEXAS A&M UNIVERSITY
REMOTE SENSING CENTER
COLLEGE STATION, TEXAS

Correlation of Spacecraft Passive Microwave System Data with Soil Moisture Indices (API)

By

Bruce J. Blanchard

Marshall J. McFarland

Sidney Theis

John G. Richter

Prepared for

Goddard Space Flight Center
Greenbelt, Maryland 80721

Contract No.: NSG-5193

TABLE OF CONTENTS

LIST OF FIGURES

LIST OF FIGURES (continued)

LIST OF FIGURES (continued)

LIST OF TABLES

1.0 INTRODUCTION

1.1 Necessity of This Research

Estimates of surface soil moisture in a large area context are primarily useful for large area crop monitoring, crop yield forecasting, estimating flood hazards, and as inputs into dynamic atmospheric models. Such estimates may also provide indications of soil moisture below the surface as well as provide a means for the determination of drought and the aerial extent of drought conditions. Conventional soil moisture measurements are very time consuming and not widely or regularly obtained over most of the United States. The spatial variations of soil moisture make it difficult to extrapolate conventional point measurements to represent an integrated value over a large area.

The benefits of crop yield forecasting are so wide ranging that some forecast methods are practiced in almost all countries (Idso et al., 1975). A yield forecast is of use in estimating supply, location of crop shortage areas, and in allocation of harvest resources such as harvesters and railroad cars. Inaccurate forecasts cause producers and shippers to make inefficient use of facilities. Early prediction of crop yields would also allow adjustment of current inventories. As more dependence is placed on these forecasts, accuracy must be improved. The loss in "social well-being" due to forecast errors has been modeled by Hayami and Peterson (1972). Their model computes the cost of a one percent error in a crop's yield forecast. When the model is used with 1978 United States data from Agricultural Statistics (1979) it is calculated that a one percent error in wheat yield estimation would result in a $30,000,000 decrease in social well-being. This loss would be felt by consumers in the form of higher prices.

The current crop yield forecasting technique used by the United States Department of Agriculture (USDA) includes the use of test plots. According to Idso et al. (1975) the crop condition for this predictive estimate is visually determined. Climatologically predicted rainfall is then used as an additional input to forecast the final yield for the test plots. The results are extrapolated to the total acreage in the vicinity of the test plots. This method presents difficulties when applied on a large scale. Rainfall can be very localized, which may make the test plots unrepresentative of true local conditions. Wide variations in crop condition estimation can occur as the result of the subjective nature of visual observations. A large number of test observations must be used to obtain a statistically significant sample.

The difficulty in using common meteorological variables and point measurements as inputs into soil moisture and crop models has led to research in remote sensing techniques to develop methods of obtaining inexpensive and large scale assessments of soil moisture and crop condition. Interpolation of point measurements and the resulting inaccuracies would no longer be a problem if the spatial variation can be mapped. Sensing devices, particularly when satellite mounted, give an integrated value for soil and crop conditions on a large scale; thus such a tool could be useful in several ways. Drought areas could be determined easily. During the growing season, the current crop conditions could be used to forecast a range of possible final yields. The final yield could also be predicted for inaccessible developing countries and hostile areas.

1.2 Background

The fundamental concepts of thermal microwave radiation that pertain to this study are presented in detail in texts by Paris (1969 and 1971), Newton (1977), Hess (1959), Marion (1965), and Lintz and Simonett (1976).

1.2.1 Soil Moisture Estimation

The 1.55 cm ESMR is a quasi-operational spacecraft system from which digital data can be acquired over the same area on approximately a 3-day repeat cycle. This affords the opportunity to use time series data for multi-temporal mapping. Recent investigations by Cihlar and Ulaby (1975), Meneely (1977), Schmugge et al. (1974, 1976a and 1976b), Schmugge (1976 and 1977) and Newton (1977) have demonstrated that surface emissivity at the 1.55 cm. wavelength is inversely related to soil moisture content in the surface layer. Sensitivity of this emissivity to moisture content is significantly diminished by an increase in surface roughness, and/or an increase in vegetation density. Consequently, the most significant results have been obtained on relatively bare, smooth soils.

Schmugge et al. (1977) presented case studies of ESMR's spatial response to recent rainfall as related to vegetation and surface roughness. Relative vegetation densities were obtained from Landsat false color infrared images and surface roughness features were inferred from U. S. Geological Survey surface land forms. Their results show that variations in surface roughness and vegetative cover, plus the absence of large areas of bare soils, restrict the spatial mapping capabilities of soil moisture at satellite altitudes.

Temporal mapping of soil moisture shows a greater potential than other methods because the adverse effects of point-to-point variations of surface roughness and vegetation cover are minimized (McFarland and Blanchard, 1977). The moisture content and temperature of the emitting layer integrated over the sensor footprint forms the major variations of temporal brightness temperature changes. Since the emitting layer temperature can be approximated, the brightness temperature changes may provide a fairly accurate indication of soil moisture changes from rainfall and subsequent drying. By using temporal mapping techniques with ESMR, McFarland and Blanchard obtained high correlations between microwave emissivity and soil moisture modeled by antecedent precipitation indices (API) during the autumn (minimum vegetative period) over relatively flat terrain.

1.2.2 Plant Stress Estimation

The immediate effect of a water deficit is a loss in plant turgor and closing of the stomates. This results in a rise in leaf temperature and a reduction in photosynthetic activity according to Ehrler and van Bavel (1967). When these effects occur the plant is said to be undergoing stress. Chinoy (1962) studied the effects of a water deficit at several phenological stages of the wheat plant. His results show stress acts to reduce the size and quantity of wheat grains. The reductions were highest when the period of stress came in the latter stages of development. This is due to the increasing water requirement of the plant as it grows. A similar study by Day and Intalap (1970) found reduced grain yield and a lower weight per volume for wheat that had undergone stress. Day and Barmore (1971) showed that a stress period near heading lowered the quality of the resulting flour.

The use of highly instrumented test plots has produced useful results. Ehrler (1973) measured plant canopy temperature (T_V) and ambient air temperature (T_A). He found T_A to be larger than T_V when the plant had adequate moisture supplies. As the soil dried out, the temperature difference became smaller. This study was expanded by Idso and Ehrler (1976). They found T_A to exceed T_V by up to 6°C for unstressed plants. For stressed plants, T_V exceeded T_A by up to 8°C. The measurements were taken around local noon when the temperature differences should be near the maximum.

A study of the diurnal change in leaf-air temperature differential was carried out by Ehrler et al. (1978). They showed that T_V was larger than T_A for stressed plants during the daytime only. At night there was little difference in temperature differential between stressed and unstressed plants. They also showed that the diurnal change in temperature differential was twice as large for stressed plants as for unstressed plants.

The difference between leaf temperature and ambient air temperature for stressed plants is adaptable to remote sensing methods. Bartholic et al. (1972) used an airborne thermal scanner over cotton fields that were undergoing varying amounts of stress. Their results showed a high degree of correlation between leaf-air temperature differential and leaf-water potential. A study by Heilman et al. (1976) developed a method of calculating evapotranspiration using an airborne thermal scanner. The only drawback is that the model requires ground level measurement of net radiation.

The ability to use remote sensing techniques to obtain evapotranspiration values would be of use in models such as the one by Hiler and

Clark (1971). They developed an irrigation scheduling technique that introduced the stress degree index (SDI) defined as

$$SDI = \sum_{i=1}^{n} (SD_i \times CS_i) \qquad (1)$$

The stress day factor (SD) is characterized as:

$$SD = 1 - (ET_A/ETp) \qquad (2)$$

where ET_A is the actual evapotranspiration and ETp is the potential evapotranspiration. The crop susceptibility factor (CS) is dependent upon the water requirement when stress is encountered. It serves as a weighting function for the stress day factor.

A study by Idso et al. (1978) outlined the use of a stress degree day (SDD) summation. It is analogous to the familiar growing degree day and is formulated as

$$Yield = \partial - \alpha \sum_{i=1}^{n} SSD_i \qquad (3)$$

where SDD is the 2 pm value of

$$SDD = T_{veg} - T_{air}$$

This model assumes a mixmum possivle yield (∂) with no stress encountered. The value of SDD is changed to amount of yield reduction when multiplied by α. The model requires in situ measurement of air temperature (T_{air}) a few meters above the crop while the plant canopy temperature (T_{veg}) can be remotely measured with an infrared thermometer.

1.3 Objectives

The two satellite mounted microwave systems to be used were the Electrically Scanning Microwave Radiometer (ESMR) and the Scanning Multichannel Microwave Radiometer (SMMR). This study only considered ESMR because processing difficulties of the SMMR data have delayed receipt of the data until early 1981.

The thrust of this study was to use ESMR brightness temperatures (BT), meteorological data, climatological data and crop information over the southern Great Plains to accomplish three objectives.

The objectives are:

1. Test and improve correlations between passive microwave brightness temperature and indices of soil moisture.
2. Detect free water after storm frontal passage.
3. Examine the feasibility of adapting a stress degree index (SDI) that accepts passive microwave input data in order to indicate drought conditions and/or predict winter wheat yield.

2.0 SITE DESCRIPTION

A large region of the southern Great Plains was used in this study (Figure 1). This region was selected for two reasons: first, it encompasses the area used by McFarland and Blanchard (1977) in the preliminary study of ESMR data (Figure 2), and, secondly, the area is a principle source of hard winter wheat. The study region has a wide range of roughness, soil types, vegetative cover, and average yearly rainfall amounts. General characteristics of the study region are: (1) there are no mountain ranges in this region; (2) the climate varies from arid to moderate; (3) the plains are cut by river headwater erosion; and (4) the eastern half of the preliminary study area has timber along the steams thickening along the eastern boundary to some solid timber areas. A general soils map for the preliminary study area is shown in Figure 3.

2.1 Data Available

Basic data used in this study consisted of meteorological point measurements, passive microwave return of the ESMR, and crop yield information. Meteorological data over the study area was obtained from the NOAA climatological network. The information available includes daily rainfall and maximum and minimum temperatures. These data lend well to gridding to 25 km because station spacing is also approximately 25 km. All data over the region was related to a 25 x 25 km grid. The block of grid points used by McFarland and shown in Figure 2 was used as a preliminary study area to test and improve the relationship between passive microwave response and soil moisture indices.

ESMR brightness temperatures on digital magnetic tape were furnished by the Goddard Spaceflight Center for the period from August 1973

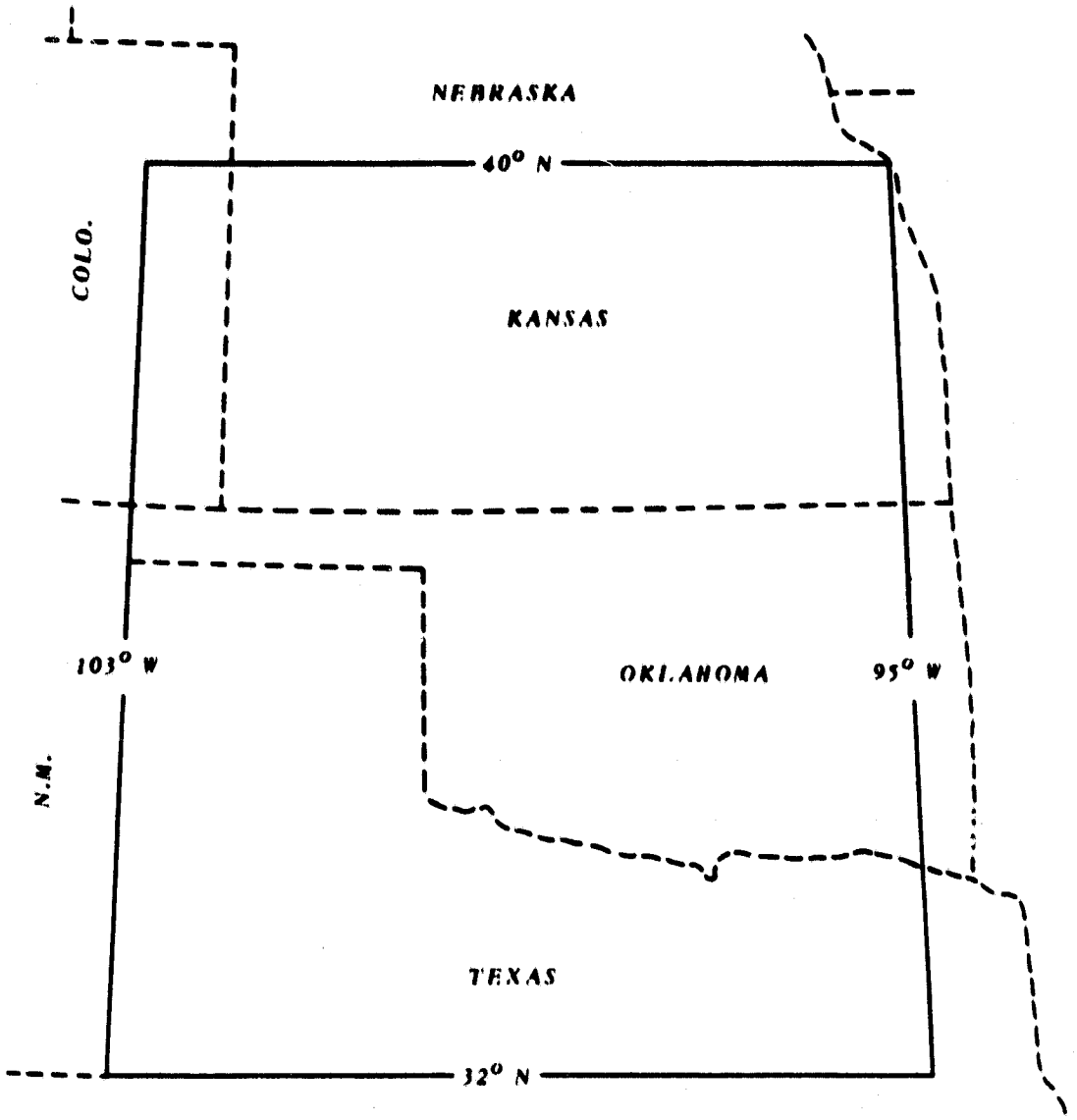

FIGURE 1: Southern great plains area used as a basis for calibration of ESMR.

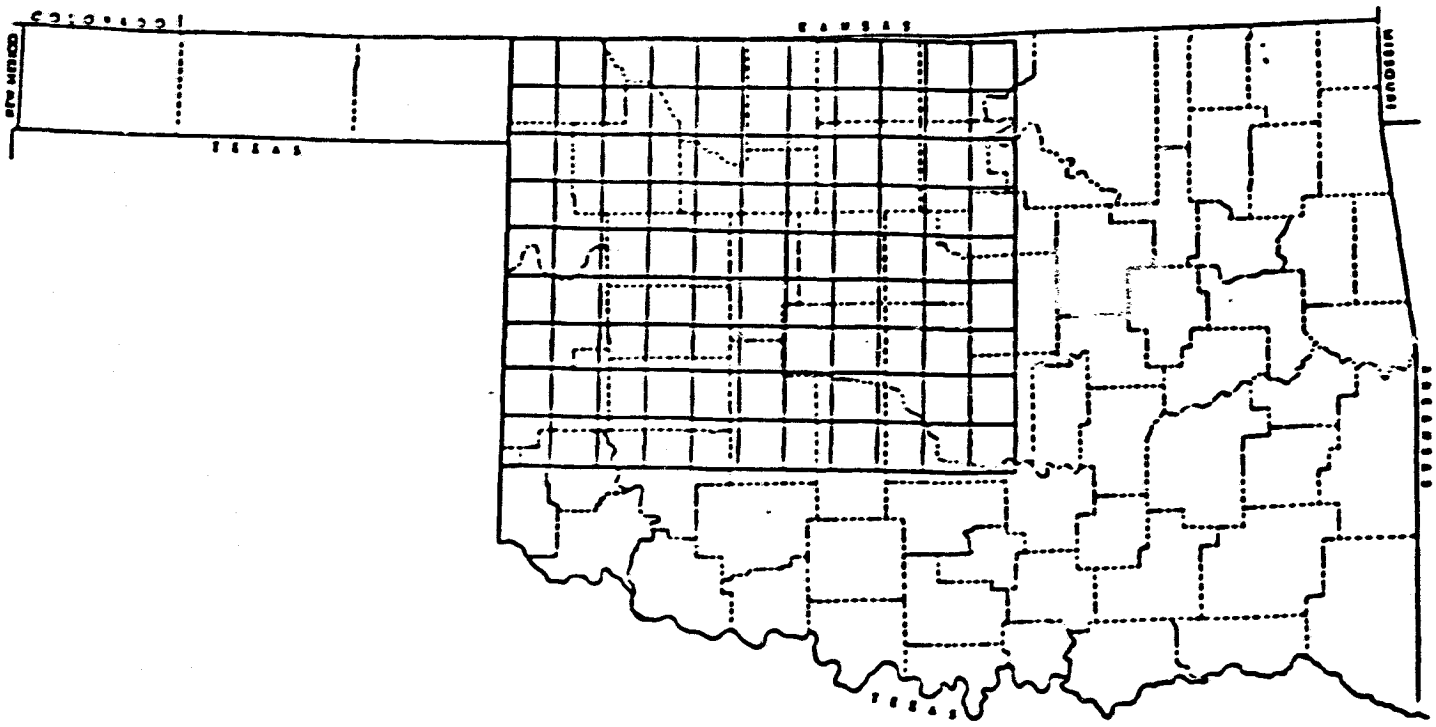

Figure 2. Gridded area used by McFarland in preliminary study and as training site grid.

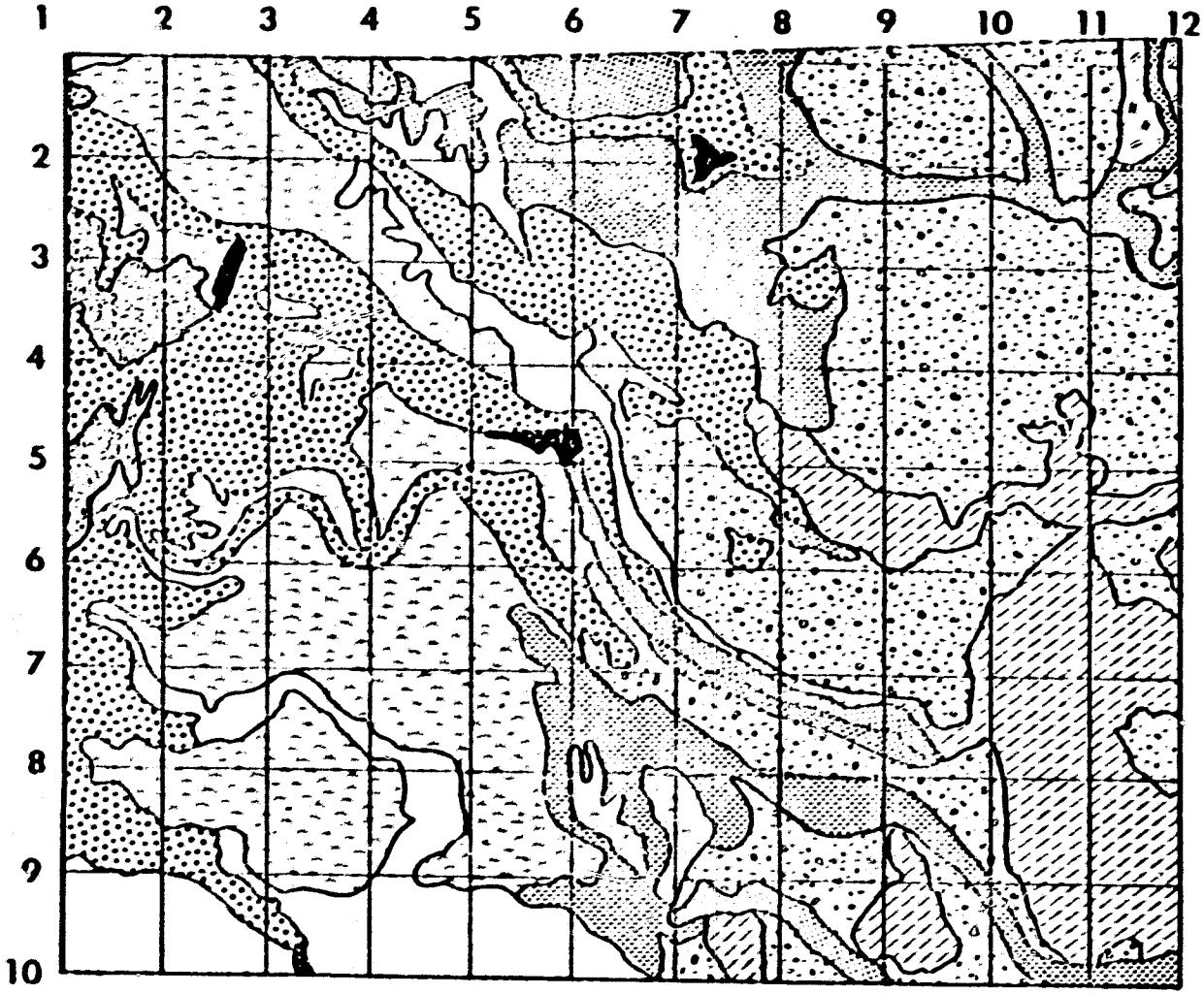

Figure 3. Soils map of the preliminary study area.

OKLAHOMA SOILS MAP LEGEND

Cross Timbers

Light-colored sandy soils with reddish subsoils on various sandy materials developed under oak-hickory forests with prairie openings (savannah).

Eastern (Cherokee) Prairies

Dark-colored soils mostly with clayey subsoils developed on shales, sandstones, and limestones under tall grasses.

Western (Rolling Red) Plains

Dark or reddish soils with clay subsoils developed in clayey Red Beds under mid and short grasses.

Reddish or dark soils with loam subsoils developed in loamy Red Beds.

Brown and light brown loams and sands with clay loam to sandy subsoils on unconsolidated sandy and loam deposits developed under grasses, scrub oaks, shinnery oak, and sage.

High Plains and Breaks

Dark-colored loams and clay loams with moderately clayey subsoils on limy unconsolidated loams, silts and caliche. Developed under mid and short grasses.

Central Reddish Prairies

Dark soils with clayey subsoils developed under tall grass mostly in clayey Red Beds.

Loamy soils with loamy subsoils developed under tall grass in loamy Red Beds or alluvium.

Bottomlands

Nearly level, deep sandy to clayey bottomland soils. Some areas flood frequently; most flood occasionally, and some rarely. Soils are developed under lowland hardwoods which decrease in density from east to west.

Figure 3 (continued). Soils map of the preliminary study area.

through May 1975. Data for the summer months were not available. The interval between days with ESMR data ranged between 1 and 7 days, with an average of approximately 3 days. The brightness temperatures used in the analysis were observed near 1700 GMT.

Crop information was derived from state agricultural statistics on a county basis. These data are very inaccurate and become even more so when relaxed to the grid. Percentages of area devoted to winter wheat and total croplands by county are shown for the preliminary study area in Figure 4. The inaccuracy of some of this information becomes apparent when the spacial variability of winter wheat areas are observed from Landsat false color composites.

The percentages of grid area covered by cropland and continuously cropped dryland winter wheat are shown in the form of graymaps, Figures 5 and 6. Figure 7 is a graymap of the 1974 dryland winter wheat yield (bushels/acre). At the top of each graymap are the percentage limits for each grayshade.

Several crops in addition to wheat are grown in the grid area. Since the coarse resolution of the ESMR precludes sensing only wheat fields, some contamination of the data is inescapable. However, a comparison of Figures 5 and 6 shows that continuously cropped winter wheat is the predominant crop in the central areas of the grid.

2.2 Cropping Practices

Normal cultural practices for winter wheat in Oklahoma and Texas begin the cropping season with plowing in July and seedbed preparation in late August to late September. Depending upon the availability of soil moisture, seeding takes place from mid-September through late October. The halfway point of planting is near October 1. Early plant-

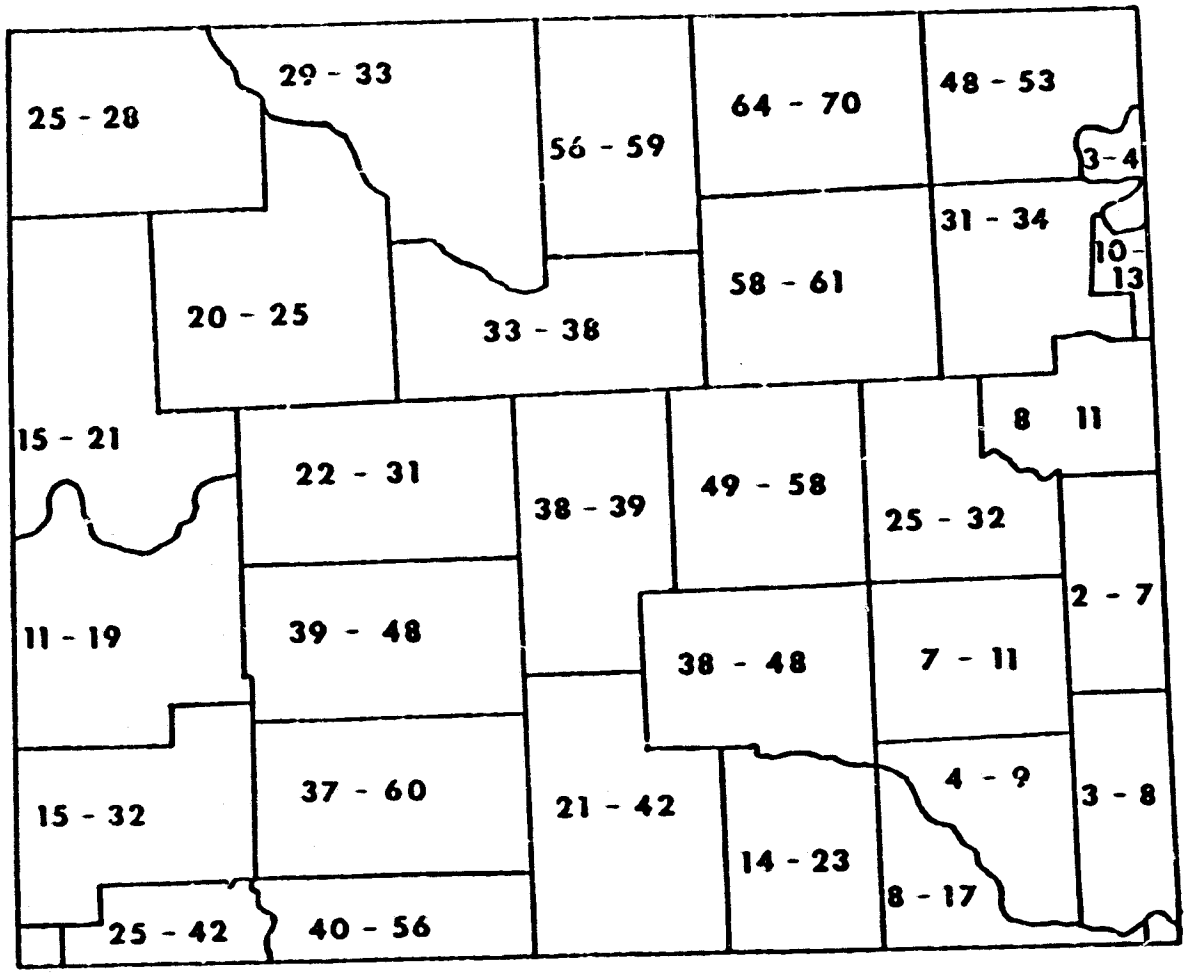

Figure 4. Percentages of preliminary study area devoted to winter wheat and total croplands by county. The first number is percent winter wheat. The second is percent croplands including winter wheat.

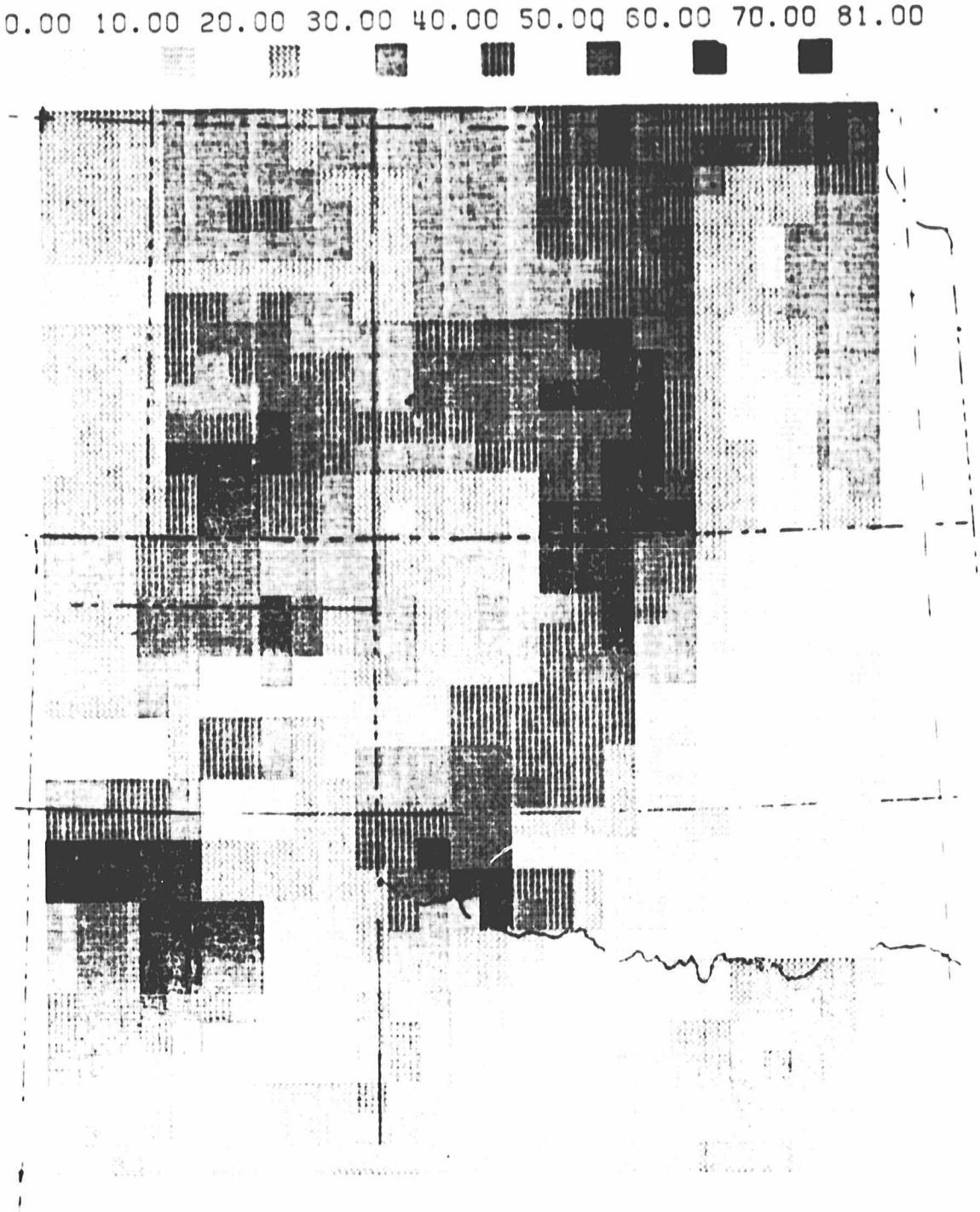

Figure 5. A graymap representing the percentage of each gridpoint covered by cropland.

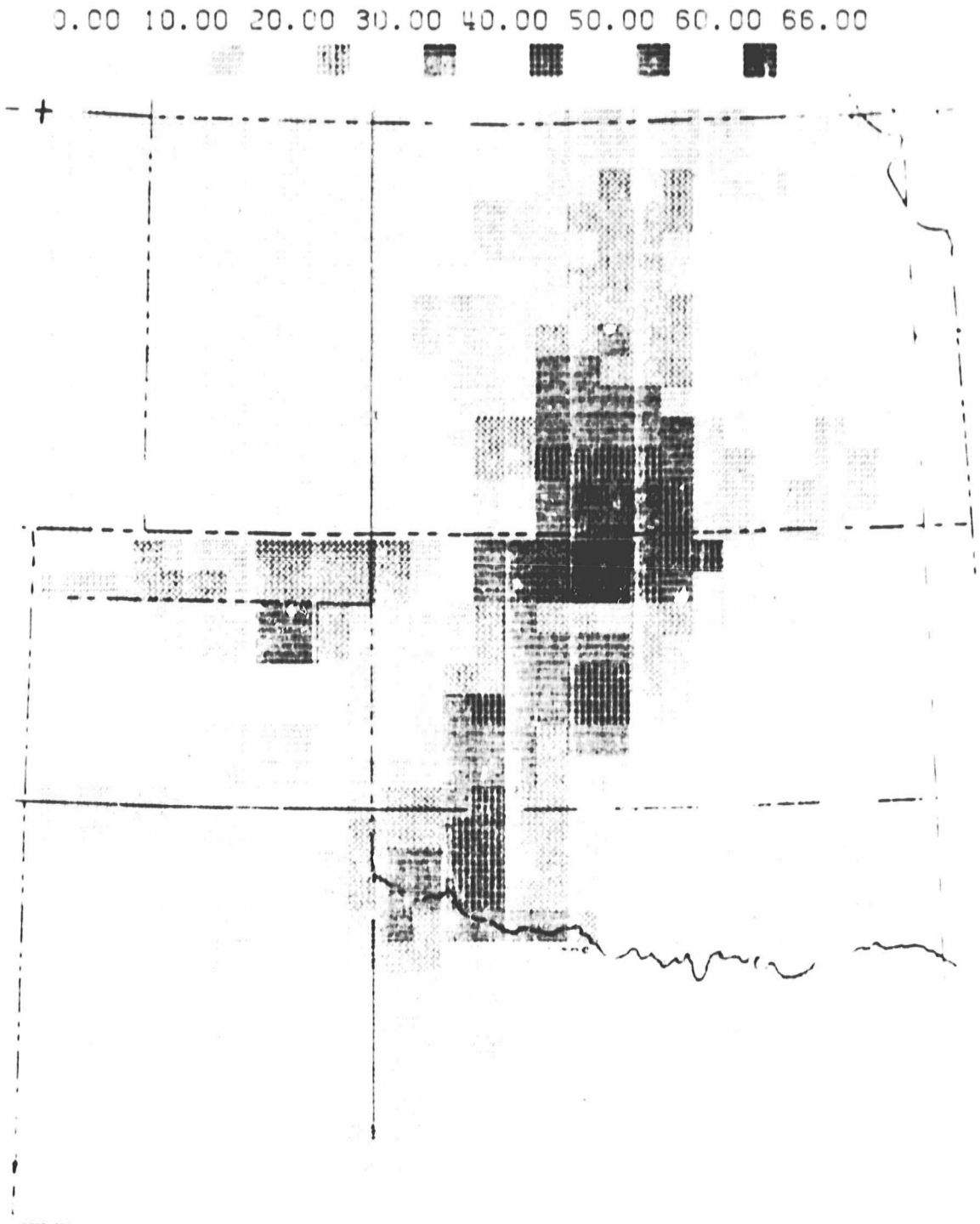

Figure 6. A graymap depicting the percentage of each grid point covered by continuously cropped dryland winter wheat.

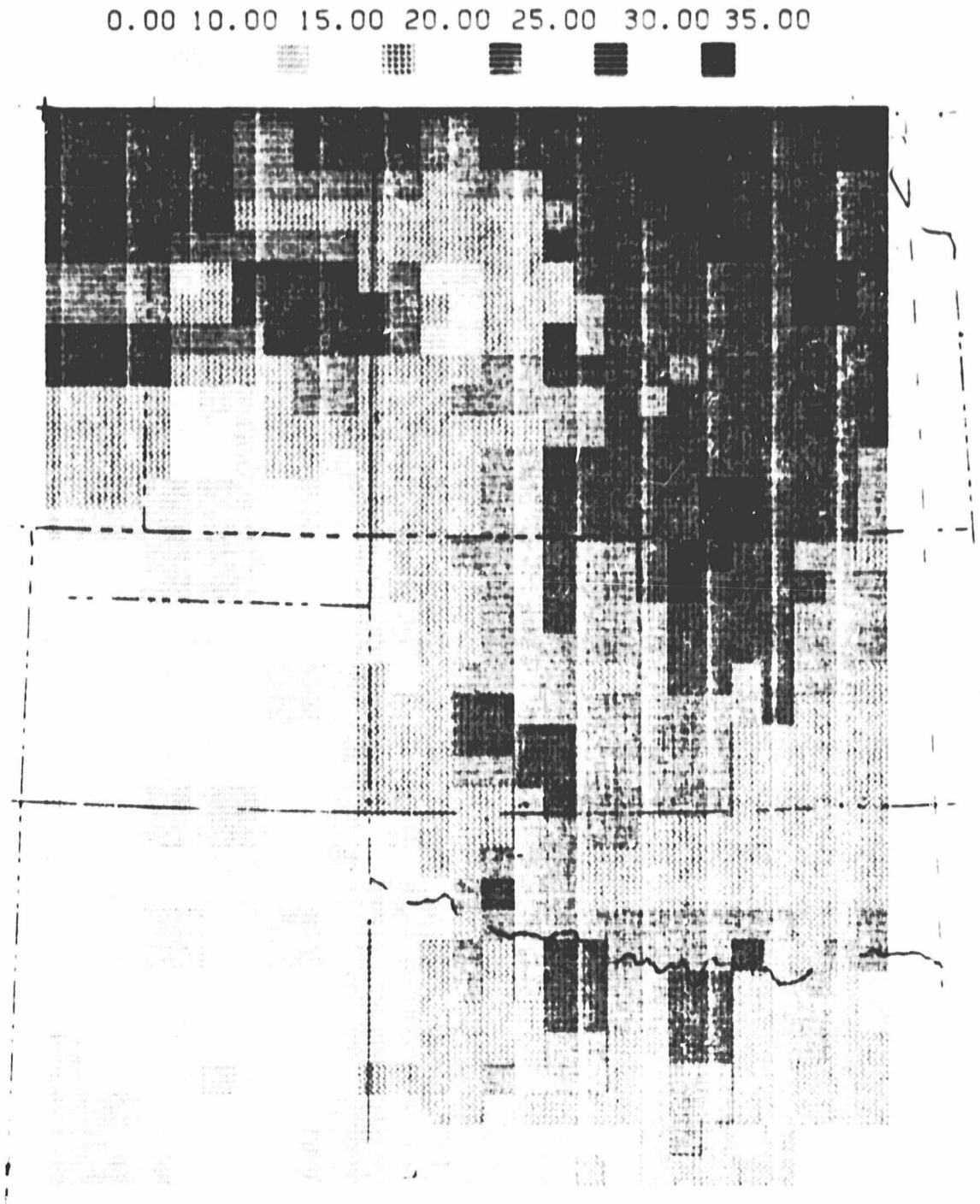

Figure 7. A graymap representing the 1974 continuously cropped dryland winter wheat yield, in bushels per acre, for each grid point.

ings to be used for winter pastures normally will have sufficient growth for grazing by December 1. Consequently, the soils are essentially bare from July into November for the winter wheat land of Oklahoma.

Grazing begins around December 1 when the wheat is 5 to 25 cm tall. Grazing continues until approximately two weeks before jointing, which occurs in March or April. The water used by the wheat crop increases from about 0.23 cm per day in March to 0.89 cm per day in April. The wheat begins to boot in mid-April and continues to mature until harvest in June.

Other crops that are grown in this area have different phenologies. In the early Spring the crops such as cotton and grain sorghums are being planted whereas the winter wheat is already 15 to 25 cm tall. In May all crops and rangelands have significant vegetative cover. The non-wheat crops continue to mature through the Summer. Most are harvested in October.

The phenological stage of the wheat crop varies up to four weeks due to latitudinal differences, with the southern crops leading in development. Figure 8 shows the number of weeks that wheat development in other areas lags that of the Texas crop. State agricultural statistics compiled by Whitehead (1979) were used as a basis to prepare Figure 8.

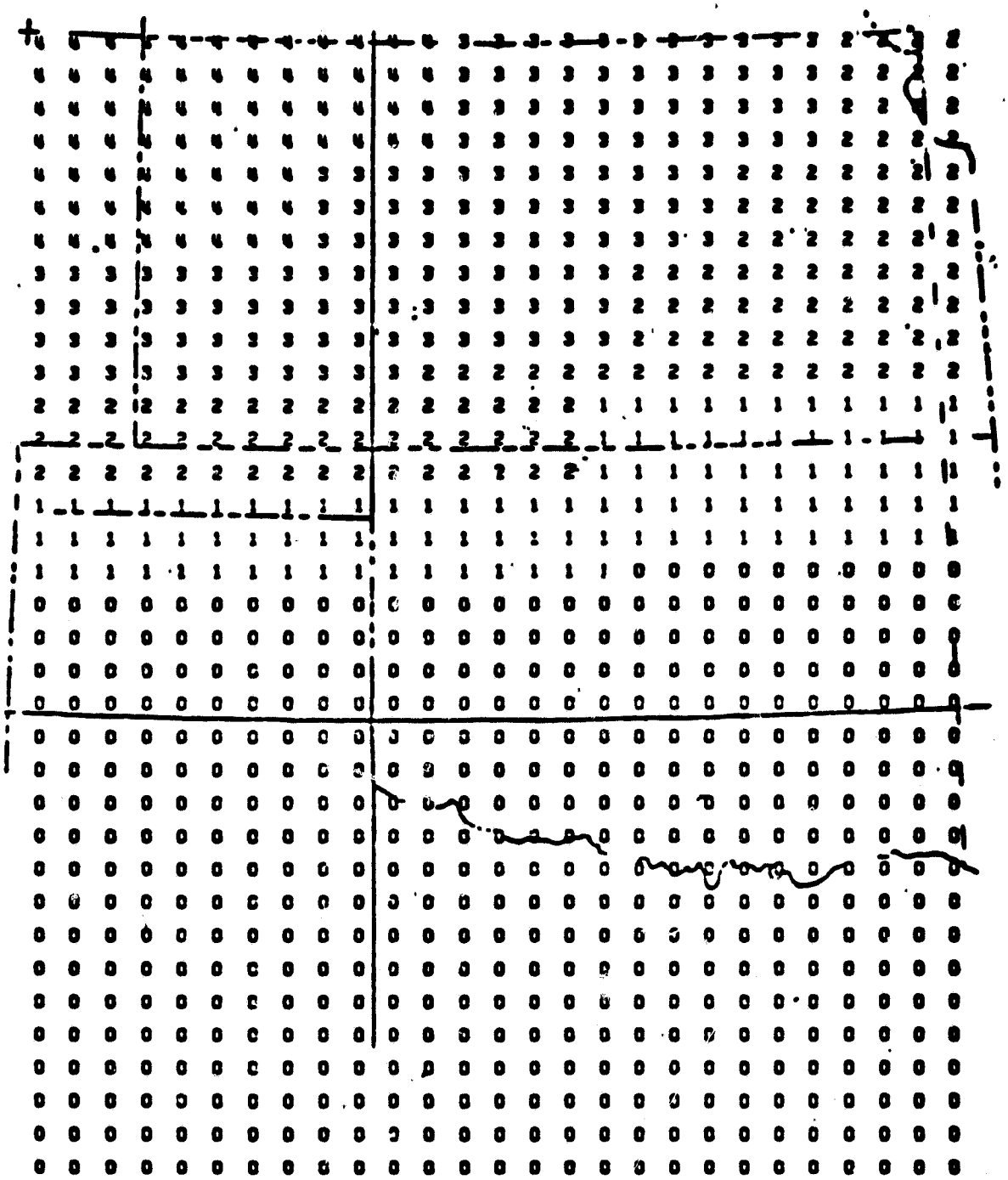

Figure 8. Number of weeks that the phenological development of wheat lags that of the Texas crop.

3.0 NIMBUS 5 ESMR DATA

The Nimbus 5 satellite was launched in December 1972 into a circular orbit at an altitude of 1112 km. The satellite is sun-synchronous with a local noon (ascending) and a midnight (descending) equator crossing. The period of the orbit is about 107 min with successive orbits crossing the equator with longitudinal separation of 27 deg. This orbit affords daylight temporal coverage of the entire earth with approximately a 3-day repeat cycle. One instrument on Nimbus 5, the ESMR, is a horizontally polarized radiometer with a central frequency of 19.35 GHz and an intermediate frequency bandpass from 5 to 125 MHz; thus it is sensitive to radiation from 19.22 to 19.475 GHz. Every 4 sec, the unit scans perpendicular to the spacecraft velocity vector from 50 deg to the left of nadir to 50 deg to the right of nadir in 78 discrete steps. From an altitude of 1112 km, the resolution is 25 km x 25 km near nadir and degrades to 160 km crosstrack x 45 km downtrack at the ends of the scan, as shown in Figure 9 (Wilheit, 1972).

For this study antenna brightness temperatures (BT) were restricted to resolutions less than 50 km. Wilheit (1973) reported a cross polarized grating lobe in the ESMR. This correction has not been incorporated in the data.

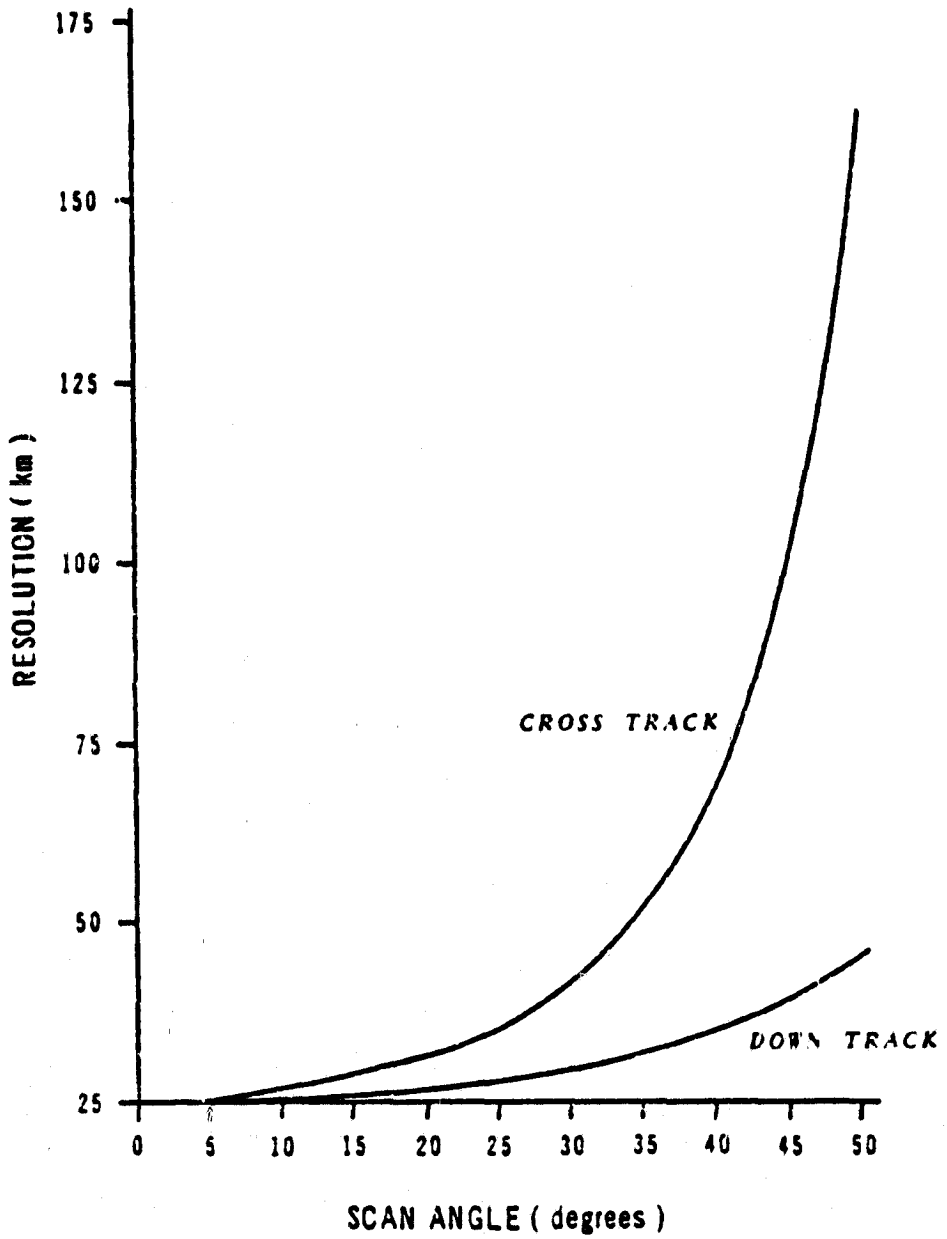

Figure 9. ESMR ground resolution as a function of scan angle from nadir.

4.0 TECHNIQUES OF DATA HANDLING

The brightness temperatures, precipitation, and air temperatures were resampled to emulate a grid having 25 km cells. The grid established is based on a polar stereographic projection.

The grid point values are determined from

$$\phi_{ij} = \frac{\Sigma w_m \phi_m}{\Sigma w_m} \qquad (5)$$

where ϕ_m is the value of the variable at observation point m and ϕ_{ij} is the interpolated value at grid point ij. The distance-dependent weight function, w, is a modified Barnes exponential (Barnes, 1973)

$$w_m = \exp\left(\frac{-d^2}{a}\right) \qquad (6)$$

where d is the distance from the grid point to the observation point and a is the response parameter to control the shape of the weight function.

4.1 The Soil Moisture Model

In the absence of actual soil moisture measurements, a simple soil moisture model was used to account for changes in moisture in the ESMR emitting layer. An antecedent precipitation index (API) was selected because of its simplicity and its ability to infer upper-level soil moisture. The only input required by the API model is the precipitation which, for large areas, is readily available at raingage locations from climatological data. Effective precipitation was considered a direct input to the soil water storage that is estimated by the API. Losses of soil moisture due to evaporation and transpiration were assumed to decrease exponentially with time (Linsley, Kohler, and Paulhus, 1975).

Shown mathematically, the relationship for a single rainfall event is:

$$API_{i+t} = P_i k^t \qquad (7)$$

where P is effective precipitation, i is the day number when rainfall occurred, t is the time after rainfall, and k is a recession factor which accounts for seasonal differences in evapotranspiration losses.

Rather than total the combined influence of all the rainfall events in a period, daily indexes can be calculated by setting t equal to 1 in equation 7 and repeatedly using the following form (Saxton and Lenz, 1967):

$$API_i = P_i + (API_{i-1} \times k) \qquad (8)$$

Before the first API value was used in a correlation with emissivity, the API model was allowed to stabilize by using a minimum of 30 days of rainfall history. The relationship between rainfall amount (R) and effective precipitation, developed by Blanchard et al. (1979), was used to account for runoff. Am empirical recession curve developed at the SEA/AR (Southern Great Plains Watershed Research Center, Chickasha, Oklahoma) by DeCoursey (1974) was used for calculating the daily recession factor, k. The final form of the soil moisture model was

$$API_i = R_i^{.891} + (API_{i-1} \times k_i) \qquad (9)$$

where

R_i = daily rainfall amount (cm).

4.2 Emissivity Model

The temperature of the emitting layer was approximated by the daily maximum temperature (T_{MT}) in the emissivity model,

$$\epsilon = T_{BT}/T_{MT} \qquad (10)$$

where T_{BT} is the ESMR brightness temperature and ϵ is the emissivity.

The emitting layer for the short wavelength ESMR is most likely limited to the top centimeter of the surface being observed. The overpass time of ESMR over the study area is near local noon and maximum air temperature usually occurs several hours later. Because the maximum soil temperature usually leads the maximum air temperature, this is believed to be a sound approximation. The sensitivity of this model to errors in the emitting layer temperature is small. An error of 10°K will only yield a 4 percent error in the predicted emissivity.

Since the study period encompassed winter periods, consideration was made of the influence of frozen ground on the ESMR return. The dielectric properties of ice are completely different from water. Ice is not a dipole molecule and has a low dielectric constant. When a soil is frozen the emissivity is high and independent of soil moisture. Therefore, to avoid the confusion possible from observations of frozen ground, the emissivity values were not used in this study if the maximum air temperature was less than 283°K.

Rain in an atmosphere can also have a very significant effect on upwelling radiation, Paris (1971). Radar summary charts from the NWS were used in determining the presence of rain between the ESMR and the earth surface for each grid point. When rainfall occurred at the time of the ESMR overpass, the emissivity data for affected grid points were omitted.

4.3 Stress Degree Index Model

This study exploited the difference between canopy temperature and air temperature for stress measurement. Two models were used to describe stress. One model requires only remotely sensed data and climatological temperatures. The other model uses air temperatures

modeled from daily maximum and minimum temperatures. These two models were chosen so that this study could not only determine whether or not the stress measurement works, but also whether or not local temperature data were needed to make it work.

The general form of the stress degree index (SDI) model used in this study was patterned after the Hiler and Clark (1971) model. The form of the model used was

$$SDI = \sum_{i=1}^{n} (SDD_i \times CS_i)$$

where SDD_i = number of stress degree days for day i,

and CS_i = crop susceptibility factor for day i,

n = number of days in the growing season.

Both models calculated SDI using

$$SDD_i = T_{VEG} - T_{AIR} \qquad \text{If } T_{VEG} > T_{AIR}$$

or (12)

$$SDD_i = 0 \qquad \text{If } T_{VEG} < T_{AIR}$$

T_{VEG} is the vegetation temperature and T_{AIR} is the air temperature at the time of overpass. T_{VEG} was calculated using

$$T_{VEG} = T_B/0.92 \qquad (13)$$

The 0.92 was assumed to be an average emissivity of a vegetated surface. This number was chosen because it is a representative value of emissivity when the scene is dry and/or vegetated. The first model, hereafter called Model 1, defined T_{AIR} as

$$T_{AIR} = 0.75\ (T_{MAX} - T_{MIN}) + T_{MIN}, \qquad (14)$$

where T_{MAX} is the daily maximum temperature and T_{MIN} is the daily minimum temperature. T_{AIR} is an estimation of the air temperature at the time of the 11 a.m. ESMR sensor overpass.

Both models calculated SDI using

$$SDD_i = T_{VEG} - T_{AIR} \qquad \text{If } T_{VEG} > T_{AIR}$$

or (12)

$$SDD_i = 0 \qquad \text{If } T_{VEG} < T_{AIR}$$

T_{VEG} is the vegetation temperature and T_{AIR} is the air temperature at the time of overpass. T_{VEG} was calculated using

$$T_{VEG} = T_B/0.92 \tag{13}$$

The 0.92 was assumed to be an average emissivity of a vegetated surface. This number was chosen because it is a representative value of emissivity when the scene is dry and/or vegetated.The first model, hereafter called Model 1, defined T_{AIR} as

$$T_{AIR} = 0.75\ (T_{MAX} - T_{MIN}) + T_{MIN}, \tag{14}$$

where T_{MAX} is the daily maximum temperature and T_{MIN} is the daily minimum temperature. T_{AIR} is an estimation of the air temperature at the time of the 11 a.m. ESMR sensor overpass.

The CS curve used with Model 1 is shown in Figure 10. The standardized CS curve was calculated using water use requirements measured for winter wheat at the Bushland, Texas USDA research station. Since phenological development is slower in the northern portion of the grid, the CS curve must shift to the right when used north of the Texas area. The amount of the shift, in weeks, is shown for each grid point in Figure 8.

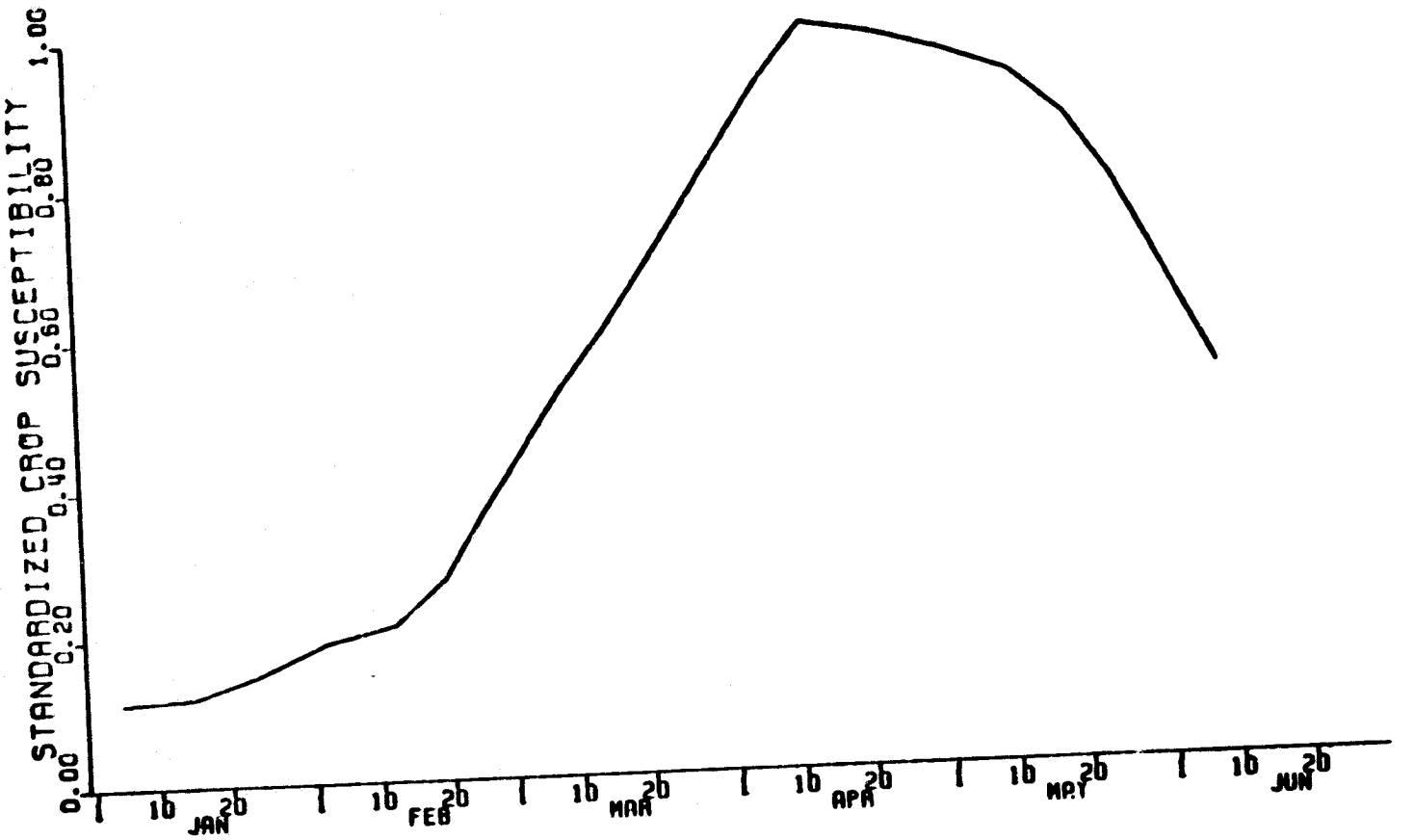

Figure 10. **A plot of the crop susceptibility curve developed for this study.**

The second model, hereafter referred to as Model 2, required only microwave brightness temperature as a real time input. The SDD was formulated as before only T_{AVG} is now the climatological estimate of the temperature at the time of overpass. It was calculated using the average daily maximum and minimum temperatures for Oklahoma City, Oklahoma and Wichita, Kansas. These two cities were chosen because they lie in a predominantly winter wheat area. For each day of the summation the average maximum temperatures for the two cities were averaged. The same was done for each day's minimum temperature. The resulting two curves are shown in Figure 11. From these curves a climatological estimate of maximum and minimum air temperature for the central grid area can be obtained. These estimates were then used with Eq. (14) to calculated T_{AIR}. The remaining computation proceeded as in Model 1.

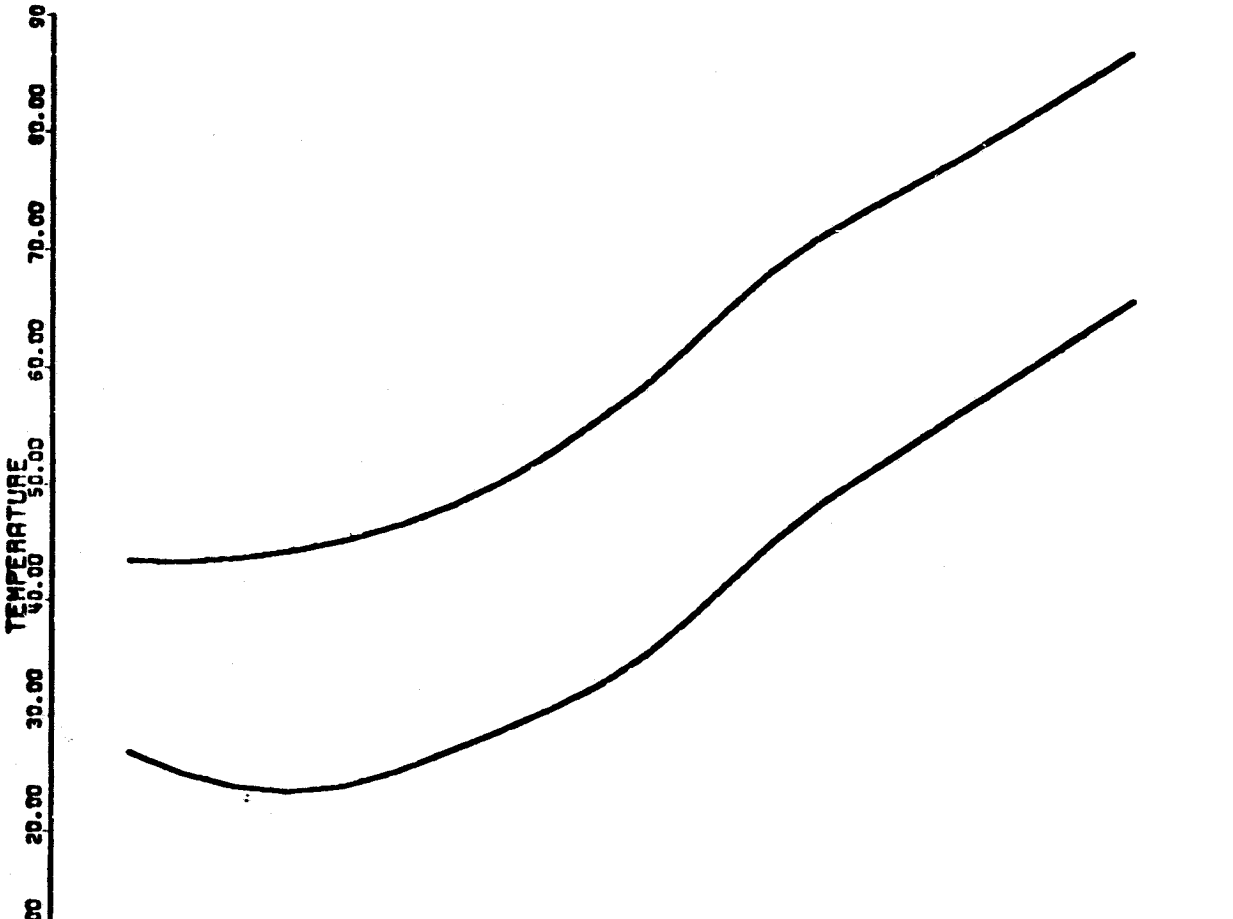

Figure 11. A plot of the mean daily maximum and minimum temperatures used in model 2.

5.0 ANALYSIS AND DISCUSSION

5.1 Correlation Between API and Emissivity

This section was directed toward developing relationships between emissivity and API over the training grid area in Oklahoma (Figure 2). The results were presented in a thesis by Theis (1979) and in a paper presented at the 1979 AGU Spring Meeting (abstracts in Appendix A). The results are summarized and presented here.

The calendar year was divided into four new-standard ESMR seasons because of climatological factors, crop phenologies and cultivation practices. Percentages of areas devoted to winter wheat and total croplands for the grid area are presented in Figure 4. Fall was defined from August 12 to November 1 which corresponded to a minimum vegetation period when fields are relatively flat. This is the period studied by McFarland and Blanchard (1977) and their results were duplicated. The fall correlation coefficients between emissivity and API for each grid point are presented in Figure 12. By comparing the areas of greater than 0.80 to Figure 4 and Landsat color composites (not presented) it is apparent that cultivated agricultural lands give the best correlations.

Winter, as defined by this study (November 2-February 27), is characterized by periods of frozen soil surfaces and upward movement of moisture due to temperature gradients. The correlations during this period are much less significant with values generally around -0.60. Both the emissivity and API models are not well suited for the winter. The API model is very simple and does not account for movement of water due to temperature gradients. The dielectric properties of ice are significantly different from water, making the emissivity independent of soil moisture in the frozen state.

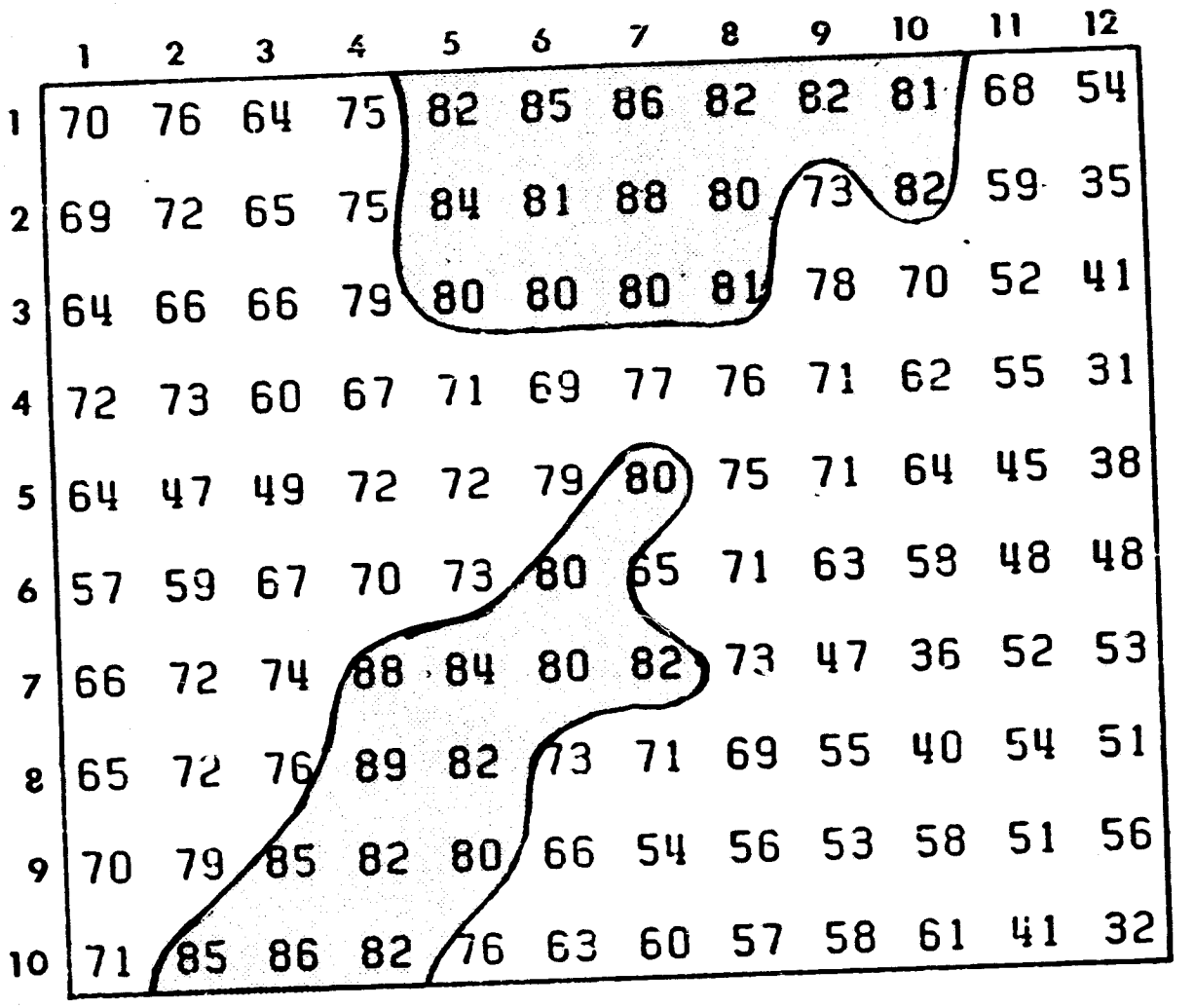

Figure 12. Fall (August 12-November 1) correlation coefficients for each grid point (values are multiplied by -100).

Spring (February 28-April 15) was defined as a rather short season generally bounded by the end of frozen soil surfaces and the beginning of the winter wheat "boot" stage. This is a period of smooth soil surface with increasing vegetative cover over winter wheat acreage. Over other agricultural croplands the soil surface is bare, but is either in a rough bedded condition or freshly planted in rows. The good correlation areas, shown in Figure 13, generally correspond with predominantly winter wheat agricultural areas. This shows up quite well when the grid is overlayed onto a Landsat color composite taken during April when the only growing vegetation is winter wheat.

All croplands are densely vegetated during summer (April 16-June 8) as defined in this study. Correlation coefficients are corresponding poorly with values averaging around -0.50.

The differences between the spring correlations of winter wheat and non-wheat croplands were investigated further by plotting six grid points from each area. The plots for fall, shown in Figures 14 and 15, indicate very little differences in the two areas. The values of the slopes and intercept agree closely with those obtained by McFarland and Blanchard (1977) (slope = -0.0232, intercept = 0.92). It should be pointed out that McFarland used one year's data and this study used two.

Spring scatter plots are presented in Figure 16 and 17. Correlations for the winter wheat area are significantly higher than non-wheat croplands. The slope for the winter wheat areas has slightly decreased from the fall value (-0.0227 to -0.0156). This indicates that the small winter wheat vegetation may affect but does not destroy the good relationship. The summer slope for the same grid points decreases to -0.0081 with a corresponding correlation coefficient of -0.48. Dur-

	1	2	3	4	5	6	7	8	9	10	11	12
1	72	76	69	68	60	78	80	72	74	78	56	44
2	67	70	75	79	81	79	71	76	78	81	45	32
3	71	72	78	80	77	81	76	72	77	72	53	39
4	68	34	57	75	75	79	78	72	72	62	32	46
5	50	61	69	73	72	73	69	69	58	61	65	70
6	39	57	65	63	70	70	72	71	79	61	64	59
7	57	56	64	81	75	68	62	76	65	55	63	64
8	66	63	63	71	64	54	65	68	59	54	71	71
9	57	69	69	62	58	57	65	54	58	66	73	79
10	58	66	50	49	43	58	64	62	69	68	79	75

Figure 13. Spring (February 28-April 15) correlation coefficients for each grid point (values are multiplied by -100).

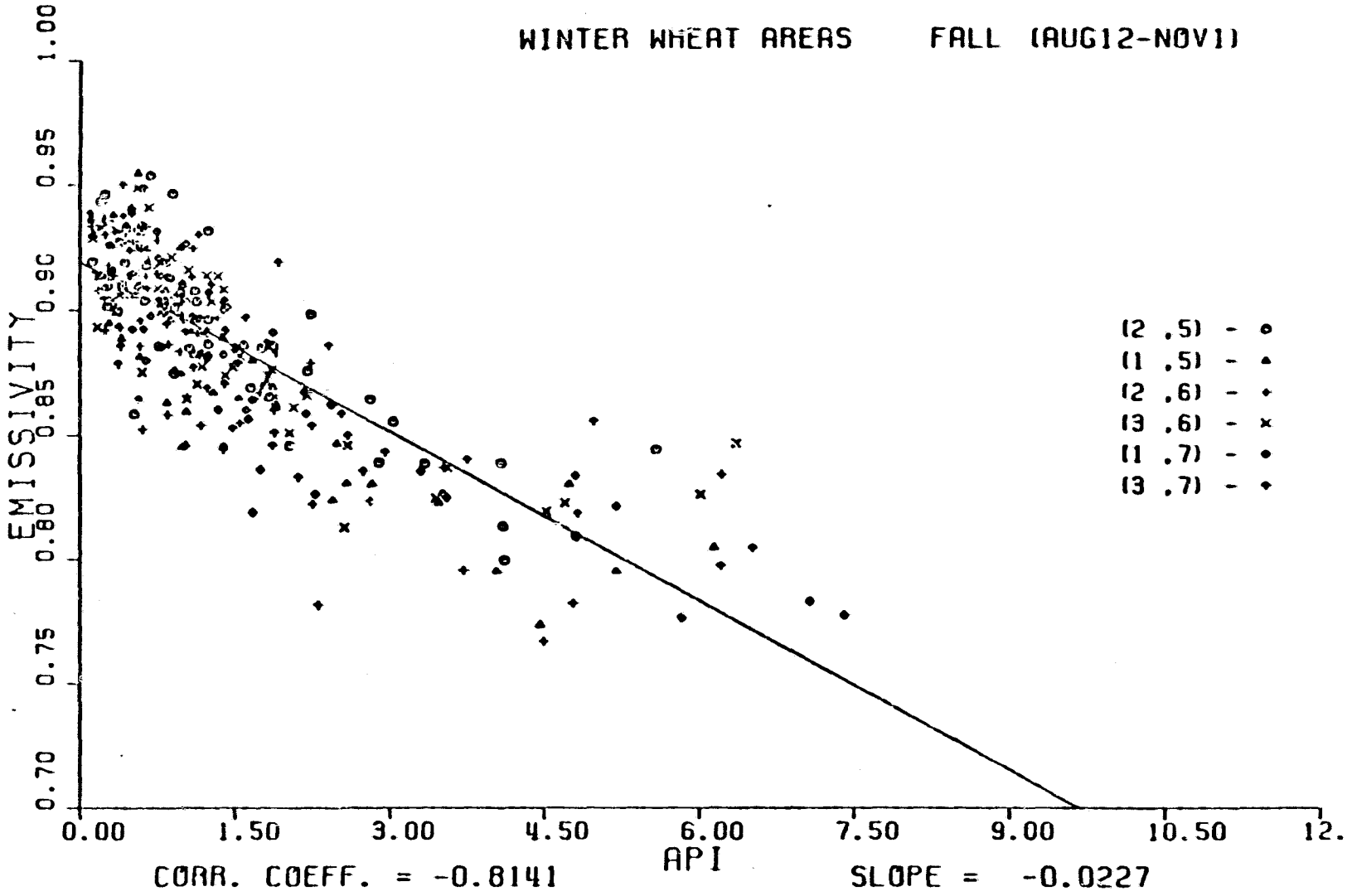

Figure 14. Fall scatter plot for six winter wheat grid points.

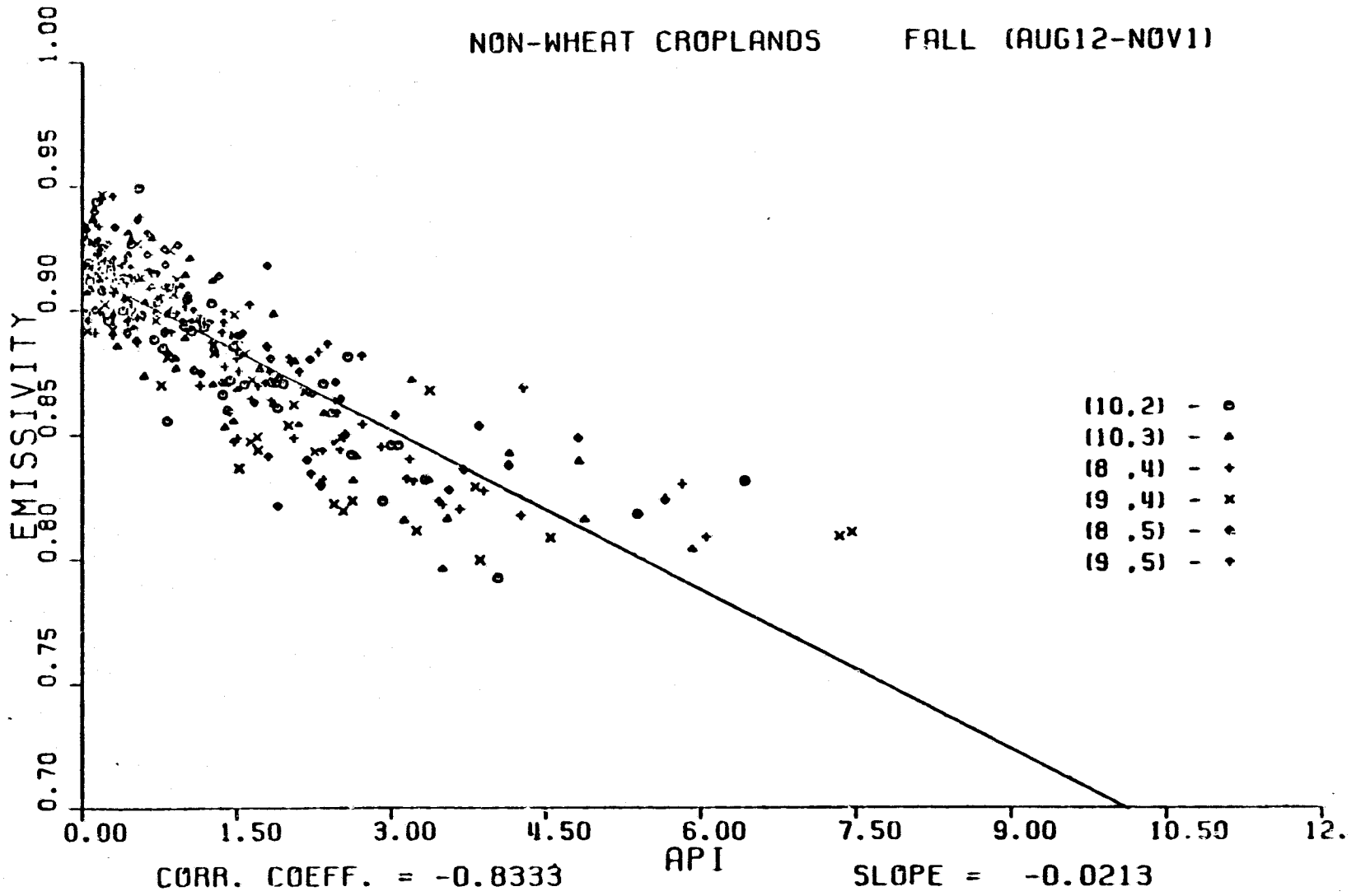

Figure 15. Fall scatter plot for six non-wheat croplands grid points.

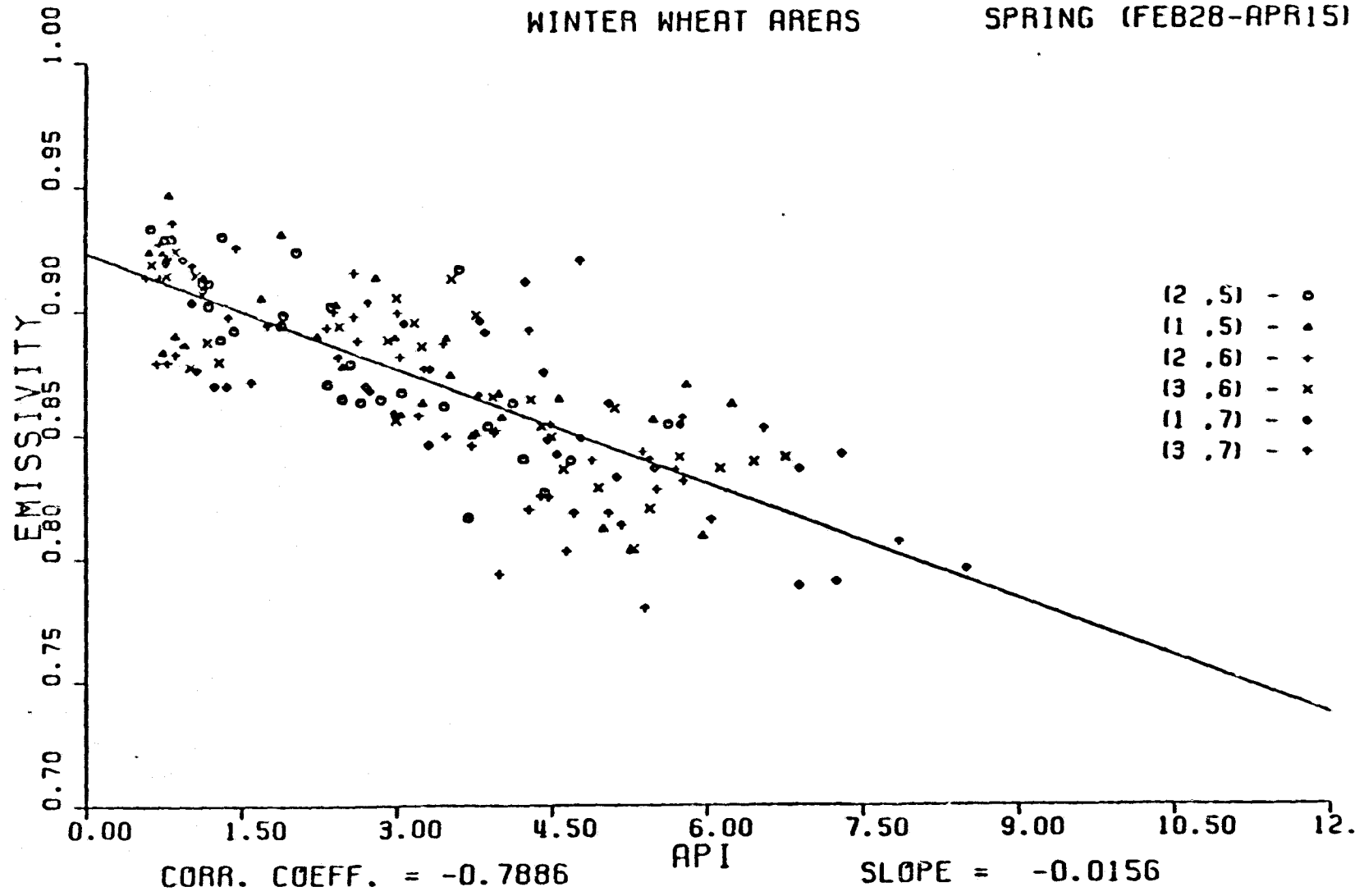

Figure 16. Spring scatter plot for six winter wheat grid points.

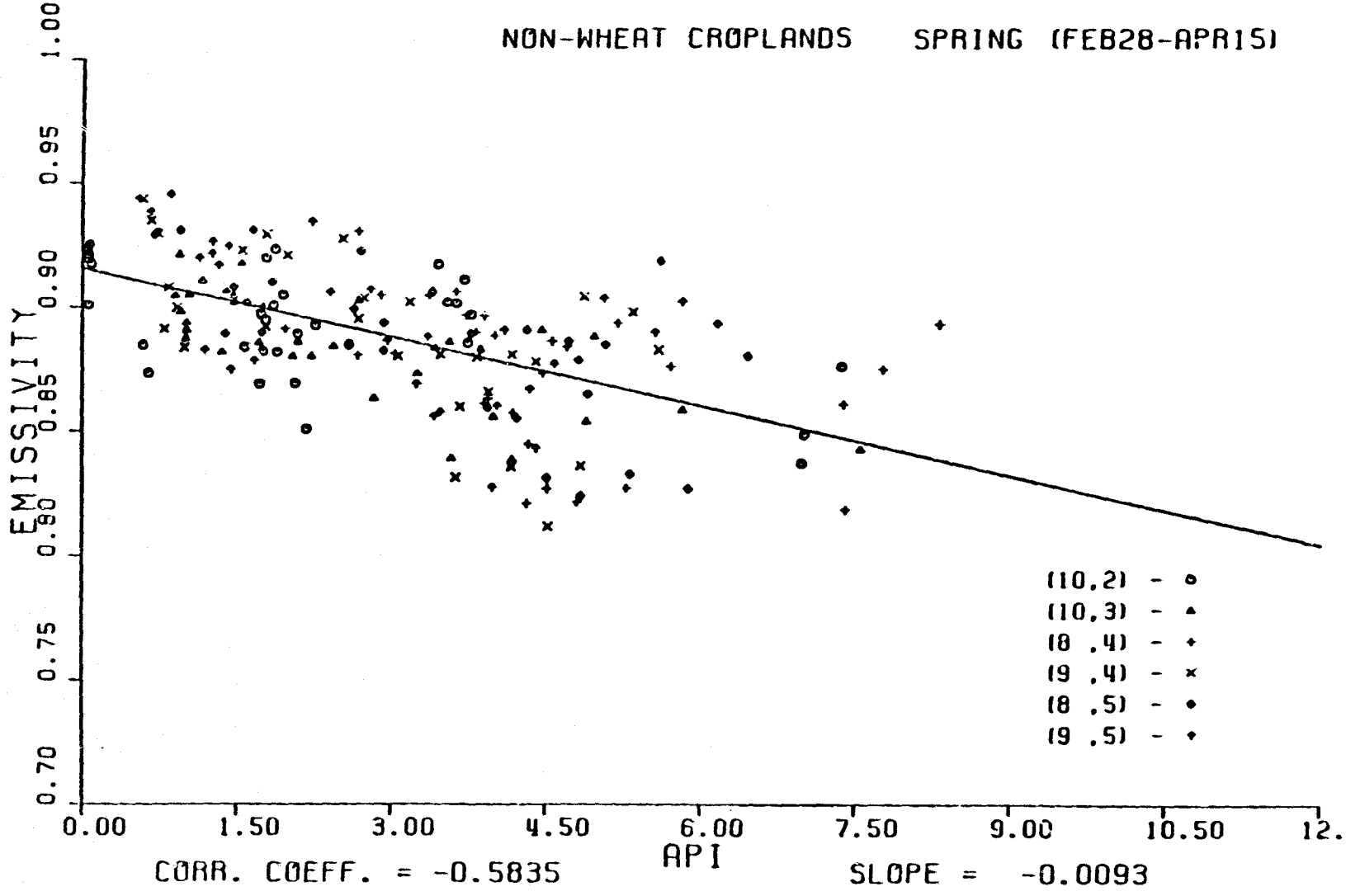

Figure 17. Spring scatter plot for six non-wheat croplands grid points.

ing summer the vegetation has reached a threshold density so that the ESMR's response to API becomes masked by the vegetation.

5.2 Free Water After Storm Frontal Passage

The same techniques were used to map both API and emissivity over a large portion of the Southern Great Plains.

API and emissivity gray maps were made for each day that an ESMR pass occurred over the test region. API values were calculated for each day in each cell and then merged into a spatial map for each day. Density slices were chosen for the API gray scale such that intermediate steps in gray tone represent a range of one centimeter while the maximum and minimum gray tone may represent more or less than one centimeter. Gray tones were selected for emissivity maps by first fitting a regression line to the API and emissivity data for each date and calculating emissivity values to correspond to the API divisions. This admittedly enhances the visual correlation between the two gray scale maps for each date. It is significant, however, that differences in the scales for emissivity are minor throughout the different seasons.

Figures 18 and 19, 20 and 21, 22 and 23, 24 and 25, 26 and 27 are pairs of gray scale maps that have been selected to illustrate moisture conditions after major storms. In each pair of maps for a particular date, a remarkable correlation can be seen between the ESMR emissivity and the API.

A preliminary 16mm film was produced with daily gray maps of API and emissivity on each frame. By visual inspection, several modeling problems appeared. Whenever the dynamic range of API was small (low API throughout the grid) correlation was poor. When the range of API was large there was a good correlation. API grey maps during the winter

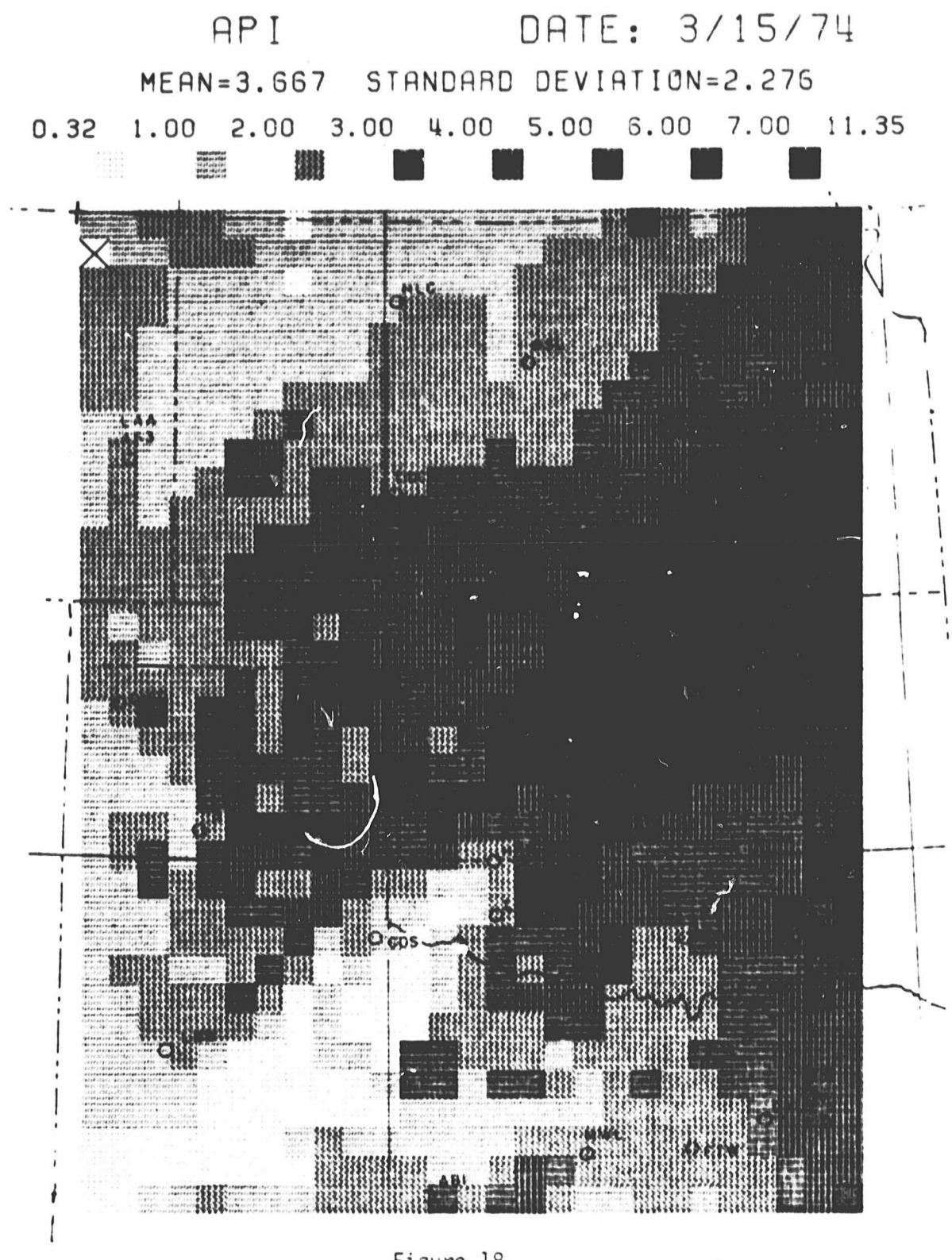

Figure 18

EMISSIVITY DATE: 3/15/74

MEAN=0.885 STANDARD DEVIATION=0.028

0.816 0.862 0.869 0.876 0.883 0.890 0.897 0.904 0.950

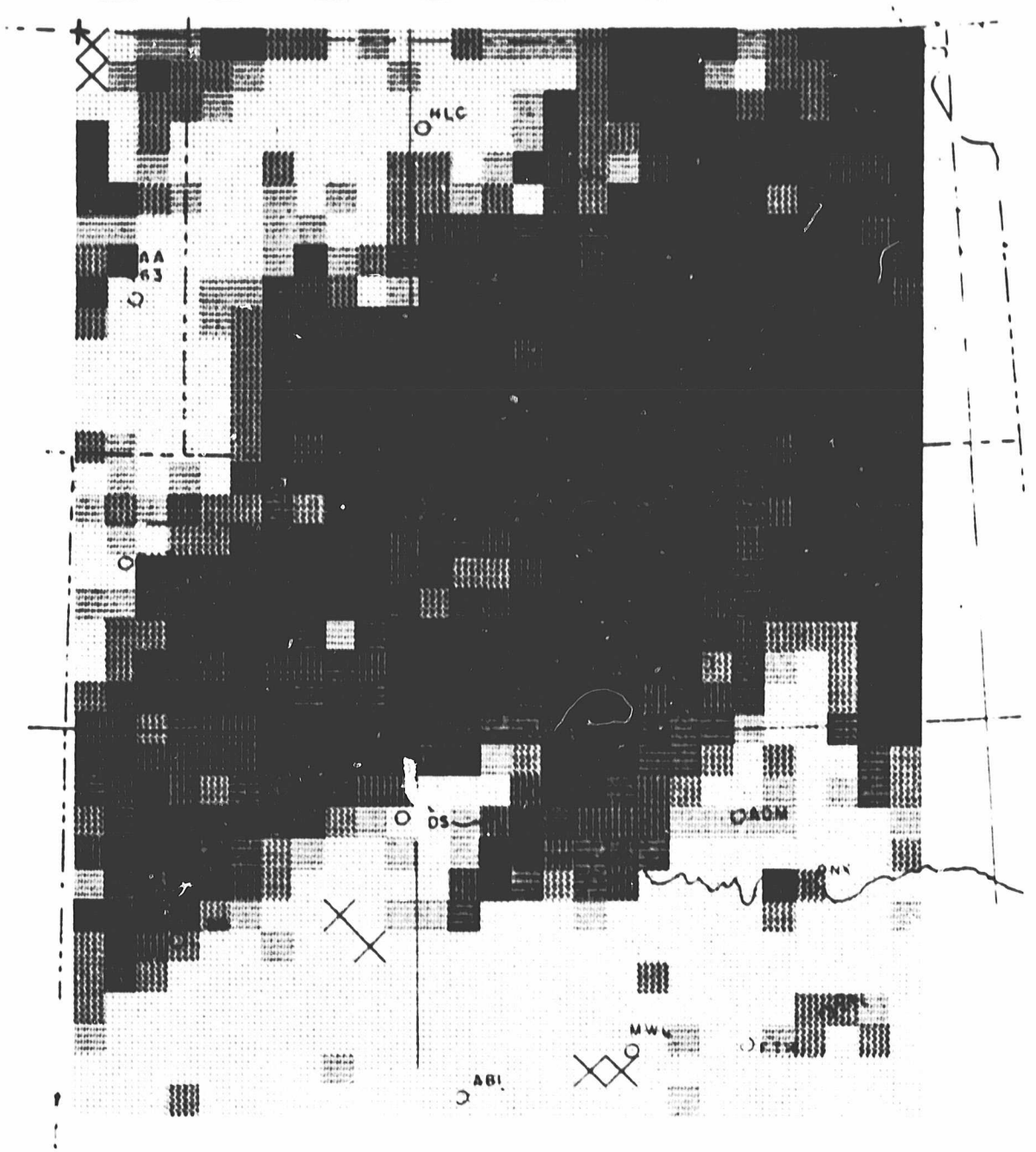

Figure 19

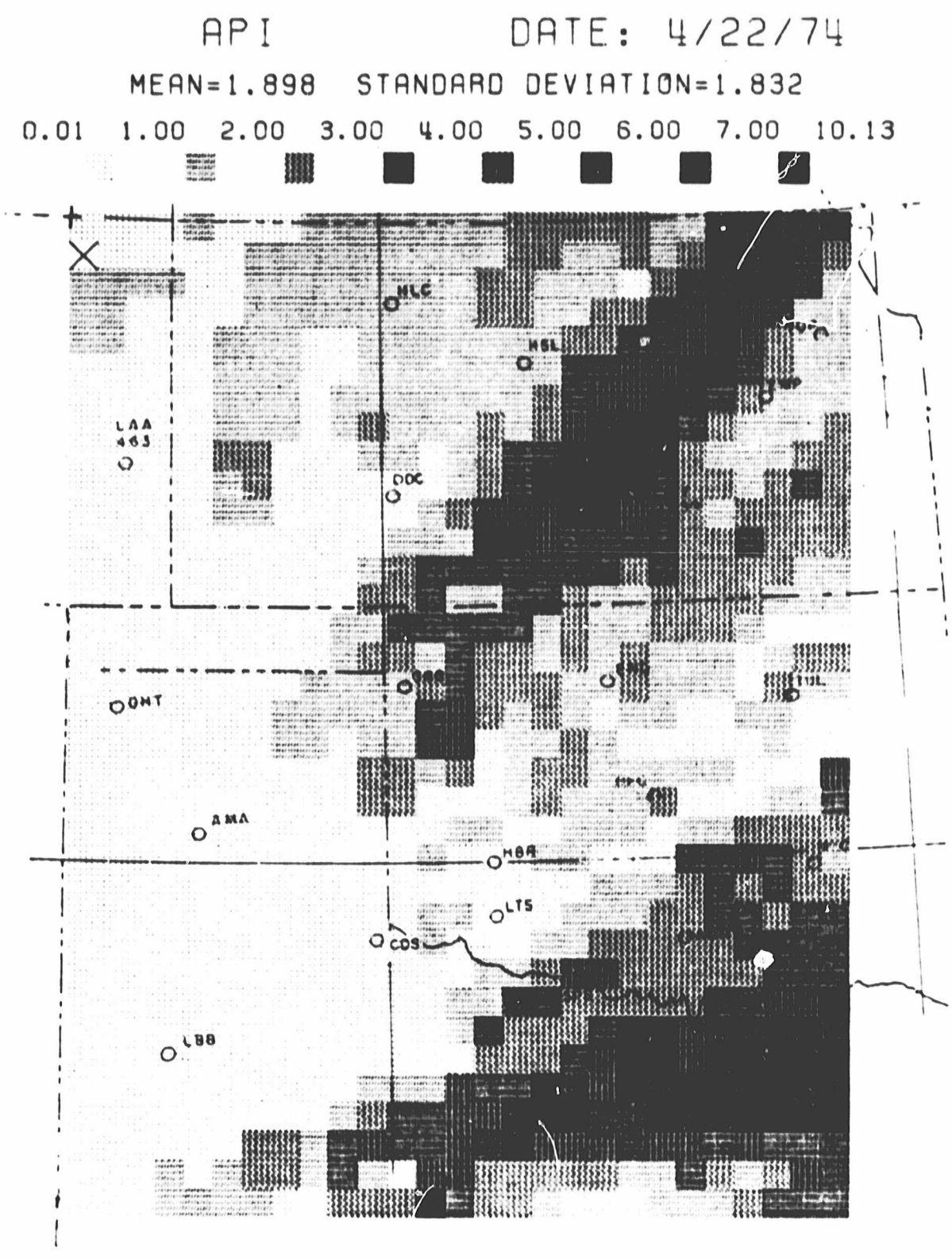
API
DATE: 4/22/74
MEAN=1.898 STANDARD DEVIATION=1.832
0.01 1.00 2.00 3.00 4.00 5.00 6.00 7.00 10.13
HLC
HSL
LAA
DDC
GAG
OKT
AMA
HOB
LTS
CDS
LBB

Figure 20

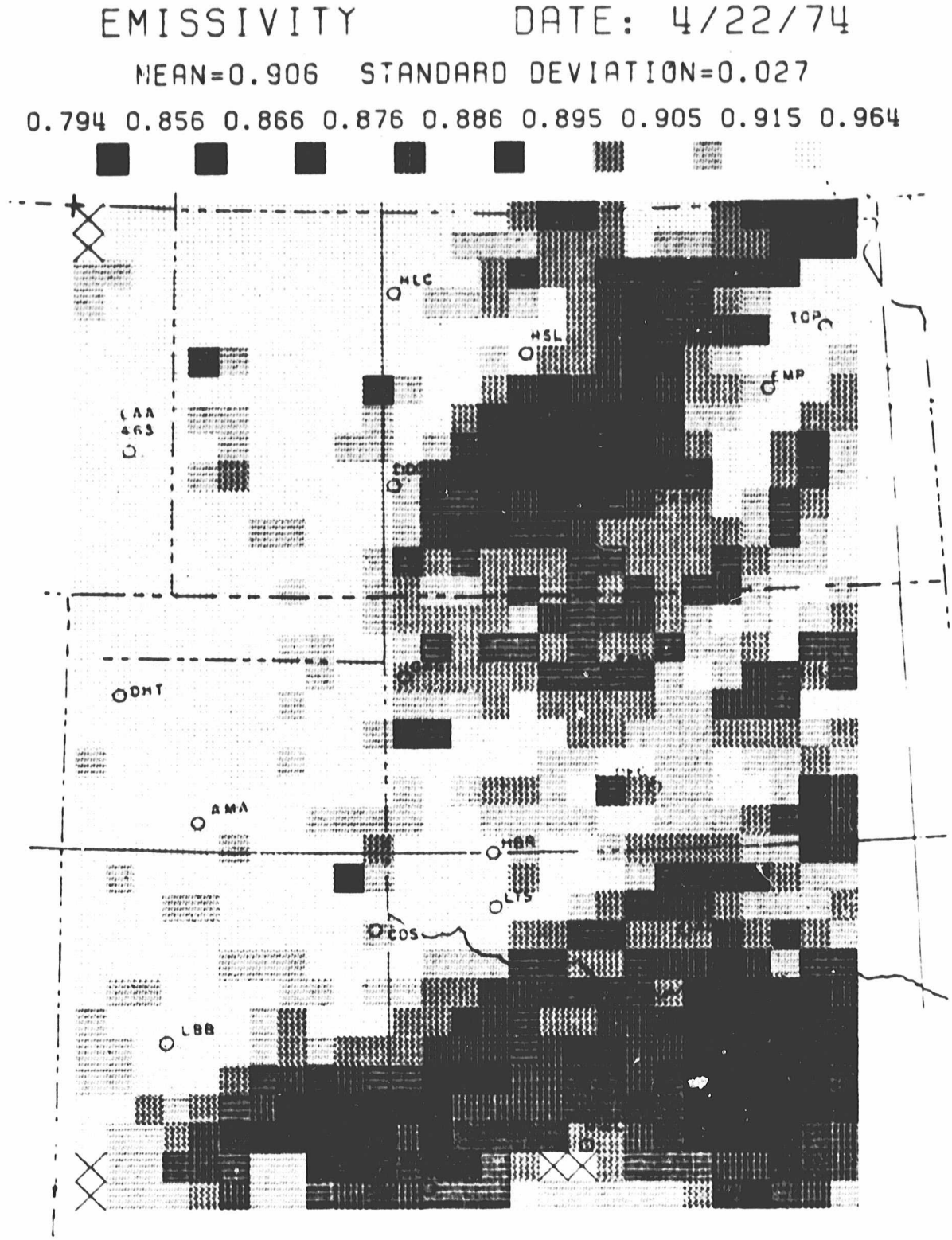
EMISSIVITY DATE: 4/22/74
MEAN=0.906 STANDARD DEVIATION=0.027
0.794 0.856 0.866 0.876 0.886 0.895 0.905 0.915 0.964
MLC
HSL
TOP
EMP
LAA
DHT
AMA
HBR
LTS
CDS
LBB

Figure 21

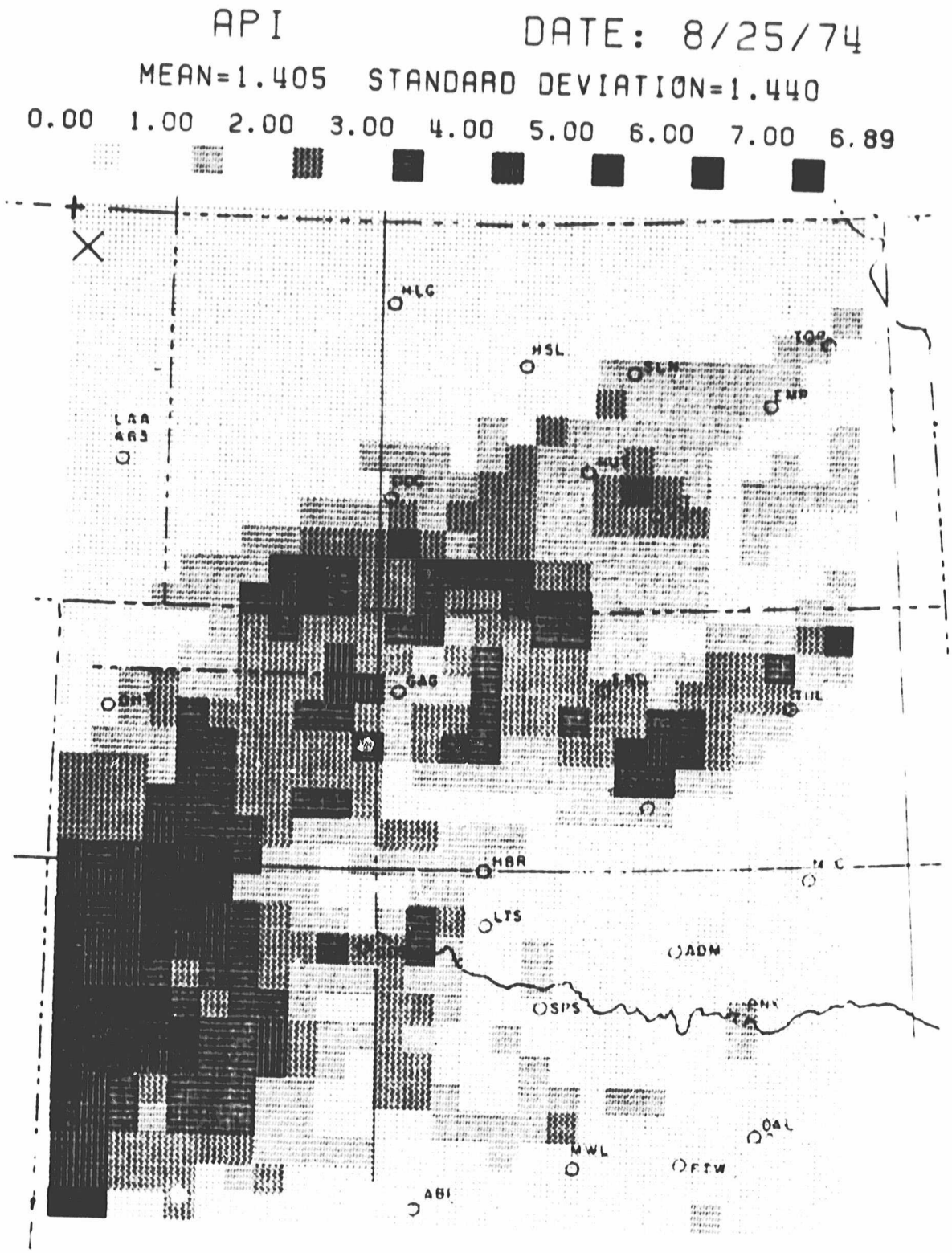
API
DATE: 8/25/74
MEAN=1.405 STANDARD DEVIATION=1.440
0.00 1.00 2.00 3.00 4.00 5.00 6.00 7.00 6.89
HLG
HSL
LAA
ABJ
GAG
HBR
LTS
ADM
SPS
MWL
FTW
ABI
OAL

Figure 22

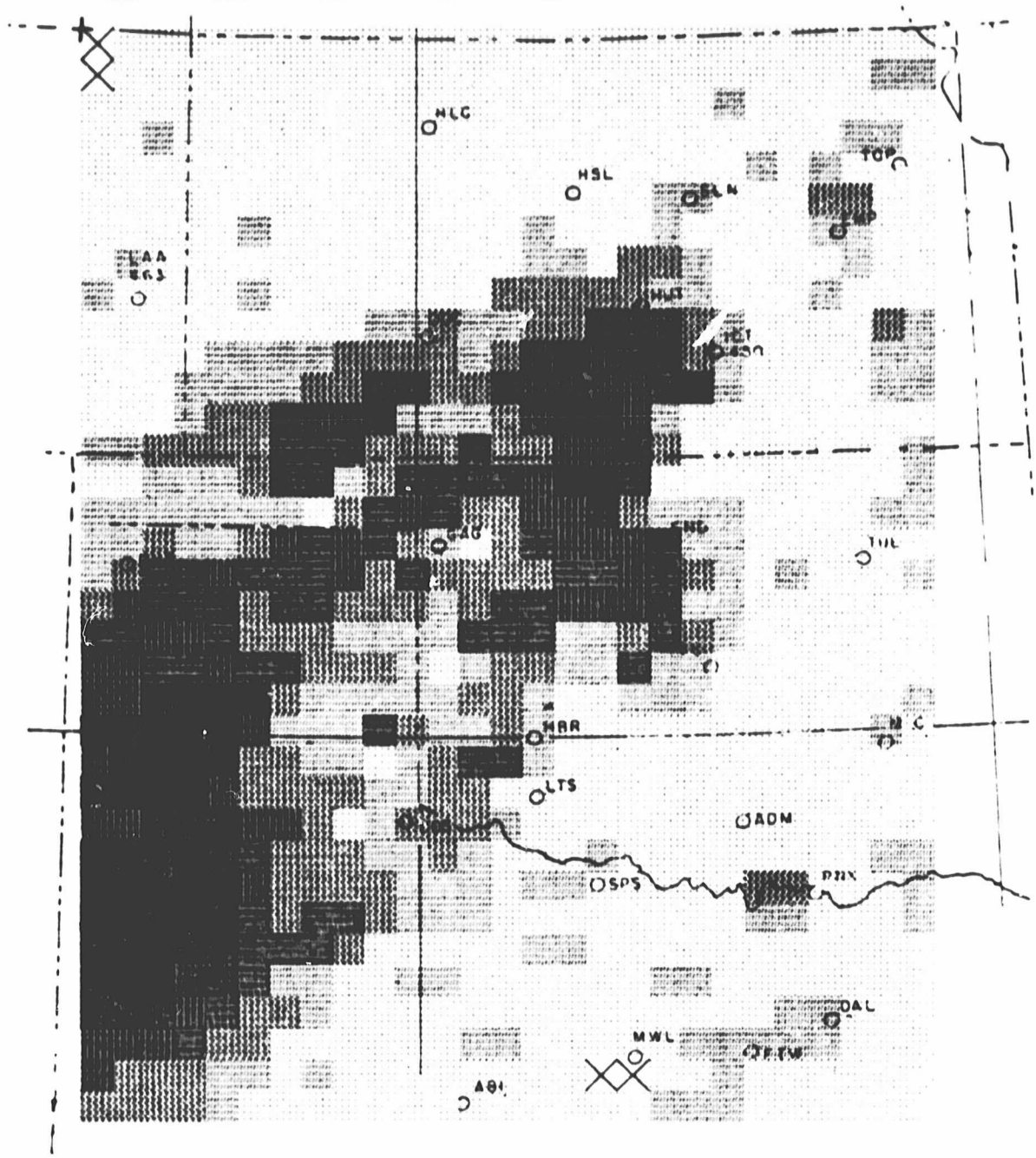
EMISSIVITY DATE: 8/25/74
MEAN=0.904 STANDARD DEVIATION=0.036
0.785 0.799 0.817 0.836 0.855 0.874 0.893 0.911 0.973
HLC
HSL
TOP
TUL
HRR
LTS
ADM
SPS
PHX
DAL
MWL

Figure 23

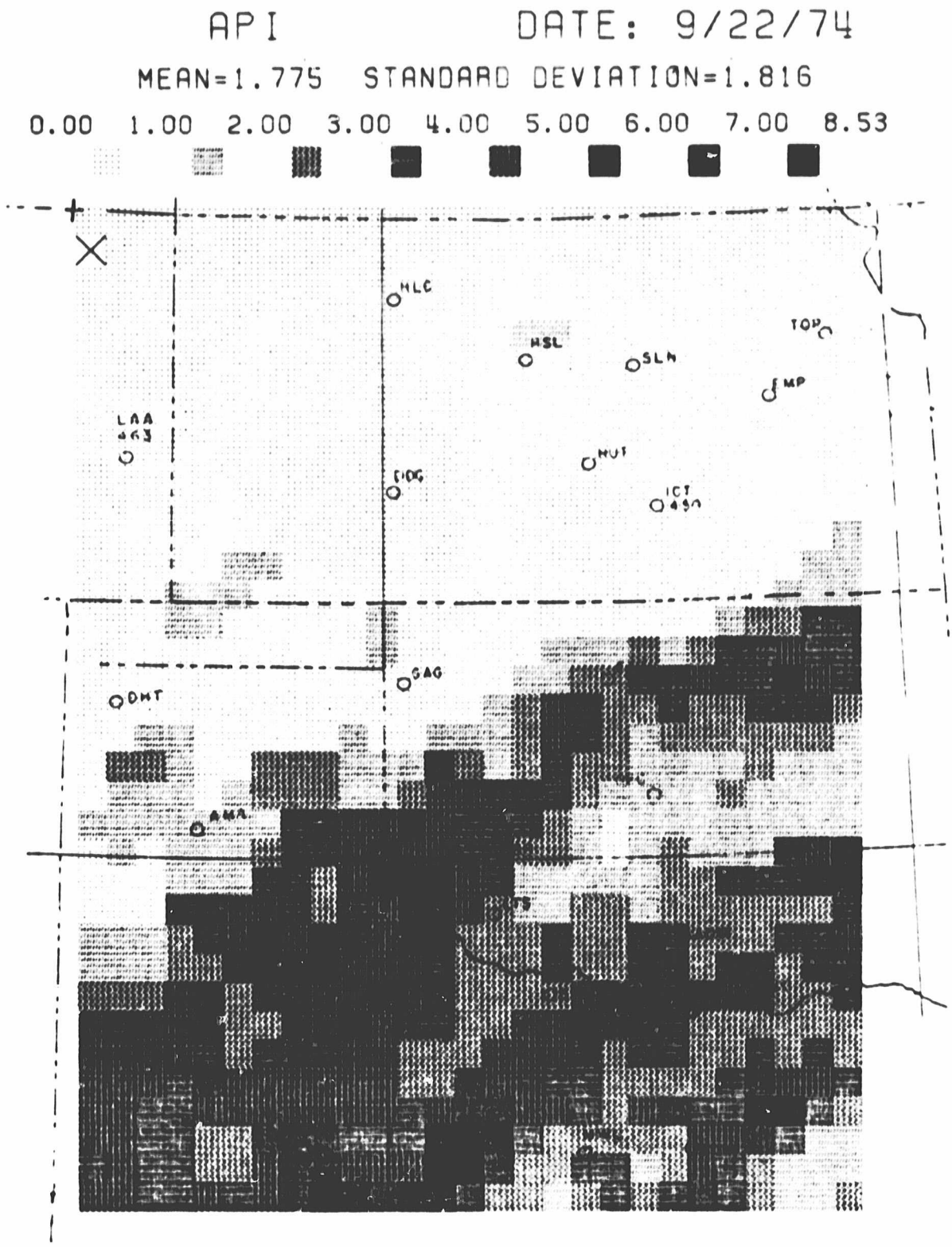
API
DATE: 9/22/74
MEAN=1.775 STANDARD DEVIATION=1.816
0.00 1.00 2.00 3.00 4.00 5.00 6.00 7.00 8.53
HLC
HSL
SLN
TOP
MP
LAA
463
HUT
P.DG
ICT
490
GAG
DHT
AMA

Figure 24

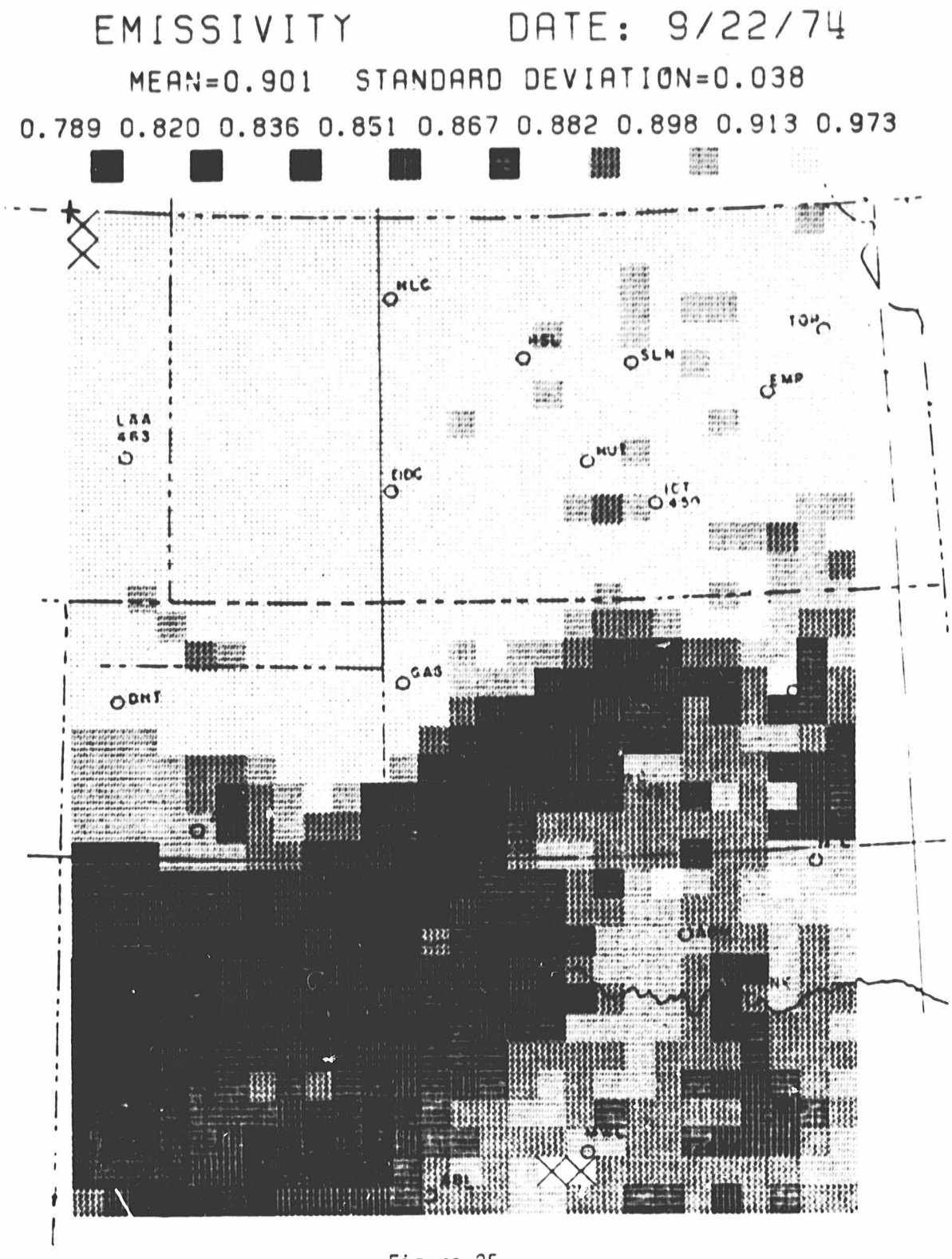
EMISSIVITY DATE: 9/22/74
MEAN=0.901 STANDARD DEVIATION=0.038
0.789 0.820 0.836 0.851 0.867 0.882 0.898 0.913 0.973
HLC
HSL
SLN
EMP
LAA
MUE
DDC
ICT
GAS
DNT

Figure 25

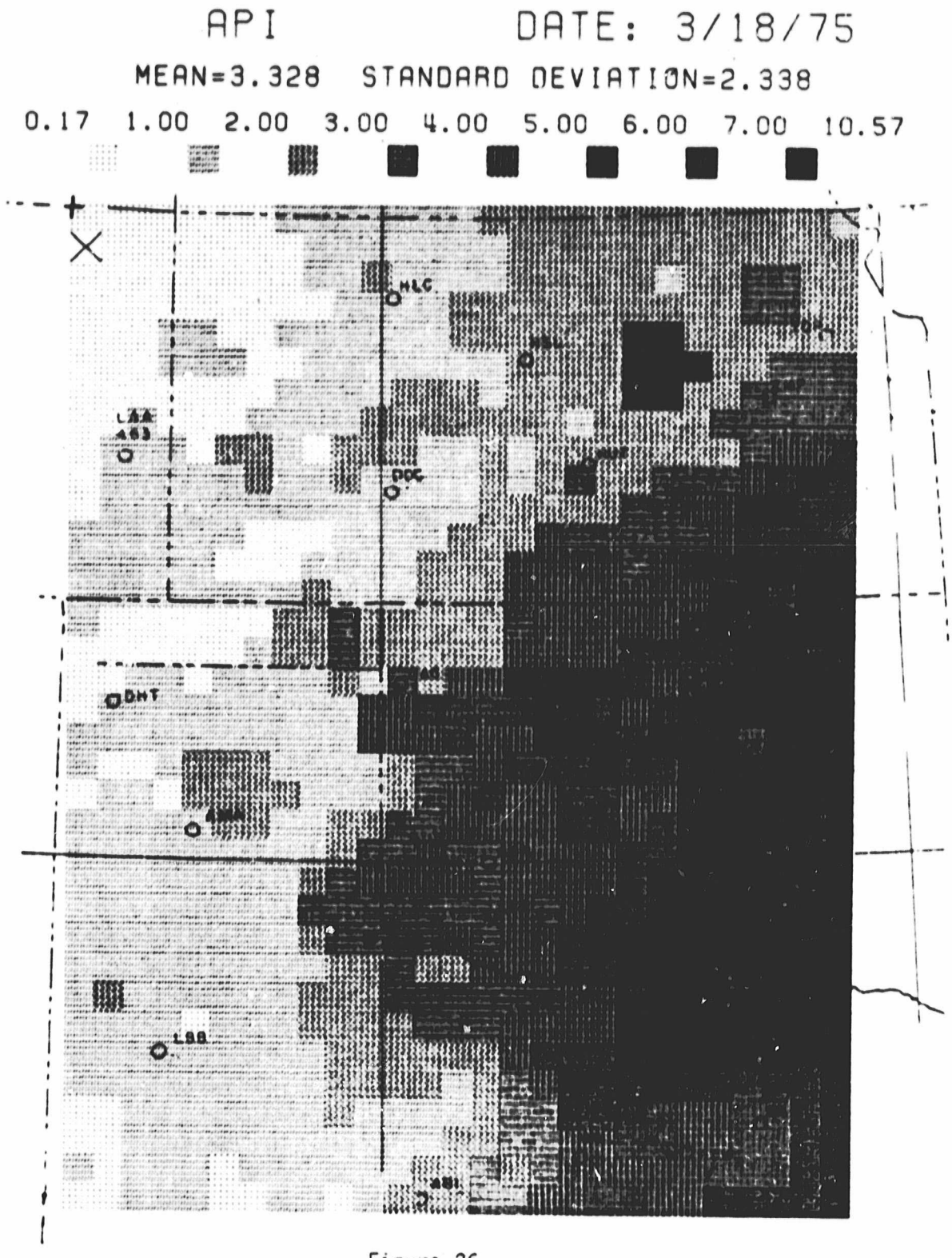
API
DATE: 3/18/75
MEAN=3.328 STANDARD DEVIATION=2.338
0.17 1.00 2.00 3.00 4.00 5.00 6.00 7.00 10.57
HLC
DHT
LSB

Figure 26

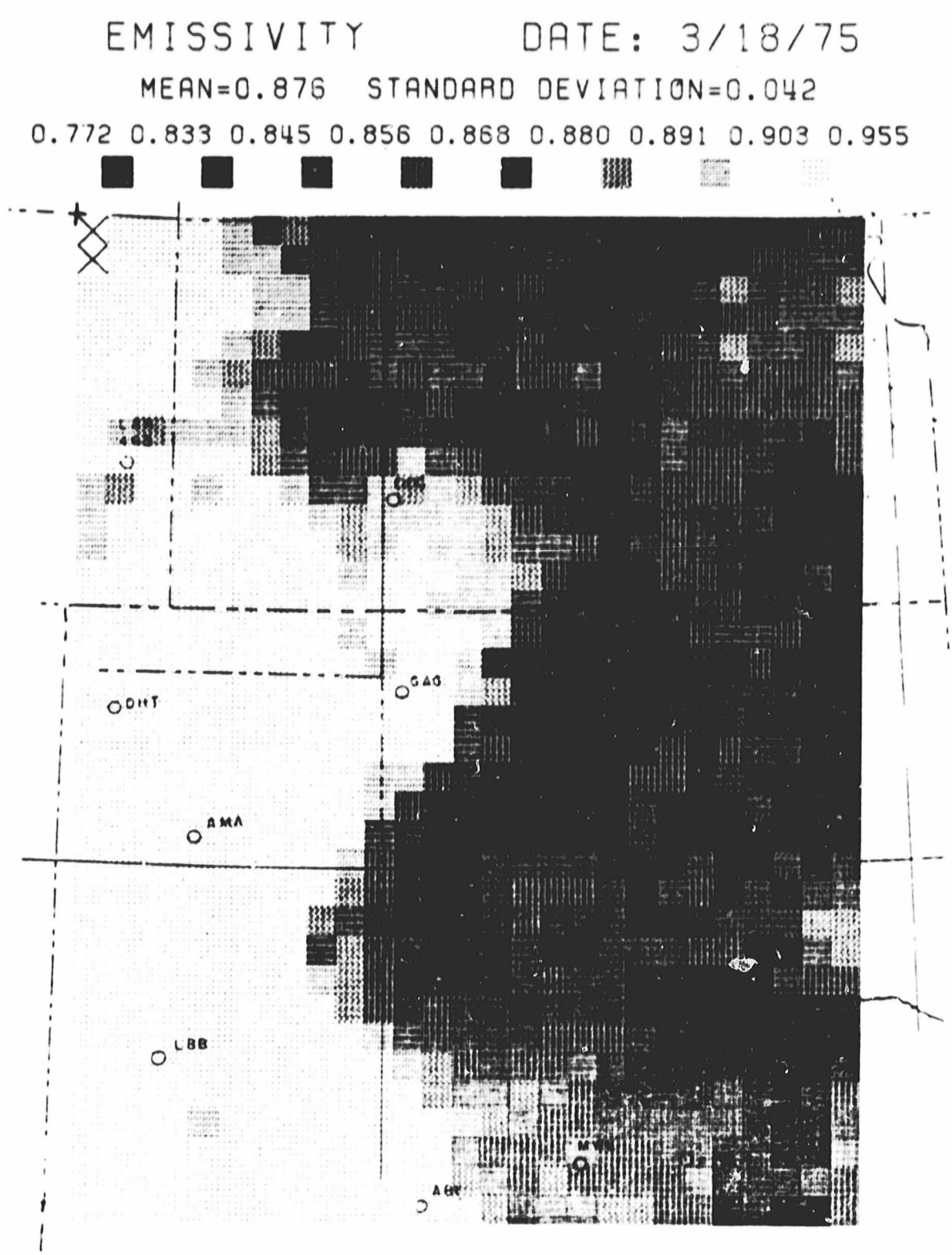
EMISSIVITY DATE: 3/18/75
MEAN=0.876 STANDARD DEVIATION=0.042
0.772 0.833 0.845 0.856 0.868 0.880 0.891 0.903 0.955
DHT
GAG
AMA
LBB
AMA
ABR

Figure 27

months indicate that there is insufficient depletion in the API model after a significant rainfall event. The winter time recession factor (k) was developed fo. soil moisture to a depth of 9 in. and it appears that values of k are too high during the winter period. The values of k may also have a latitudinal dependence when applied to the soil surface.

Correlation coefficients for each cell were calculated after dividing the entire data set into four parts to represent major portions of the growth cycle for winter wheat. The planting, emergence and stooling of the plant take place in the fall. August 12 to November 1 was selected as an appropriate time period for what we define as the fall period. Vegetation during this period seldom exceeds 15 centimeters in height and large percentages of bare soil are normal. Winter, as defined for this study, extends from November 2 through February 27. The winter season is characterized by periods of frozen ground when upward movement of moisture due to temperature gradients can be expected and downward movement or infiltration may be restricted when rain occurs.

The spring period from February 28 to April 15 is characterized by rapid growth to the booting stage of wheat. In areas where heavy winter grazing is practical in Oklahoma and Texas, it is common to remove cattle prior to April 15 to prevent loss in the grain crop. Near the northern edge of Kansas, the boot stage for winter wheat may be two to three weeks later, while this stage may be reached in the south end of the study area as early as April 1. After April 15 to the time of wheat harvest has been defined as early summer. During all of this period, the grain crop is forming and a minimum of bare soil is visible until the plant begins senescence.

A map showing the distribution of wheat crop as a percentage of each cell, Figure 28, provides an overview of the agricultural distribution within the study area. This map points out the portions of the area that are of significant economic importance if we wish to predict moisture availability for wheat yield estimates. Figures 29, 30, 31 and 32 illustrate the fact that the portions of the study devoted to wheat show better correlation between the emissivity and API values during the fall season, Figure 30. An examination of all four figures depicting correlation indicates that there is always low correlation in the eastern central portion of Oklahoma. This area of poor correlation is recognized as the moderately rough timbered area typical of the cross timber region. In general, these illustrations indicate that the relatively flat farming areas of the great plains lend themselves to the use of the ESMR system as a moisture monitoring tool.

Another measure of the usefulness of the ESMR system can be determined from examination of the slope of a regression line relating emissivity to the API value within each cell. Grouping the data in the same four periods used before, regression slopes were calculated for each cell and the slope was tnen scaled to produce the grayscale maps shown in Figures 33, 34, 35 and 36. These figures show that sensitivity of the system to changes in API tends to be greatest in the northwest quadrant of the study area. Again, the slope appears to be even more closely related to the smoothness of the terrain. The lowest sensitivity, as well as the poorest correlations, was found in the winter period. Fortunately, this period seldom has drought severe enough to endanger wheat yield.

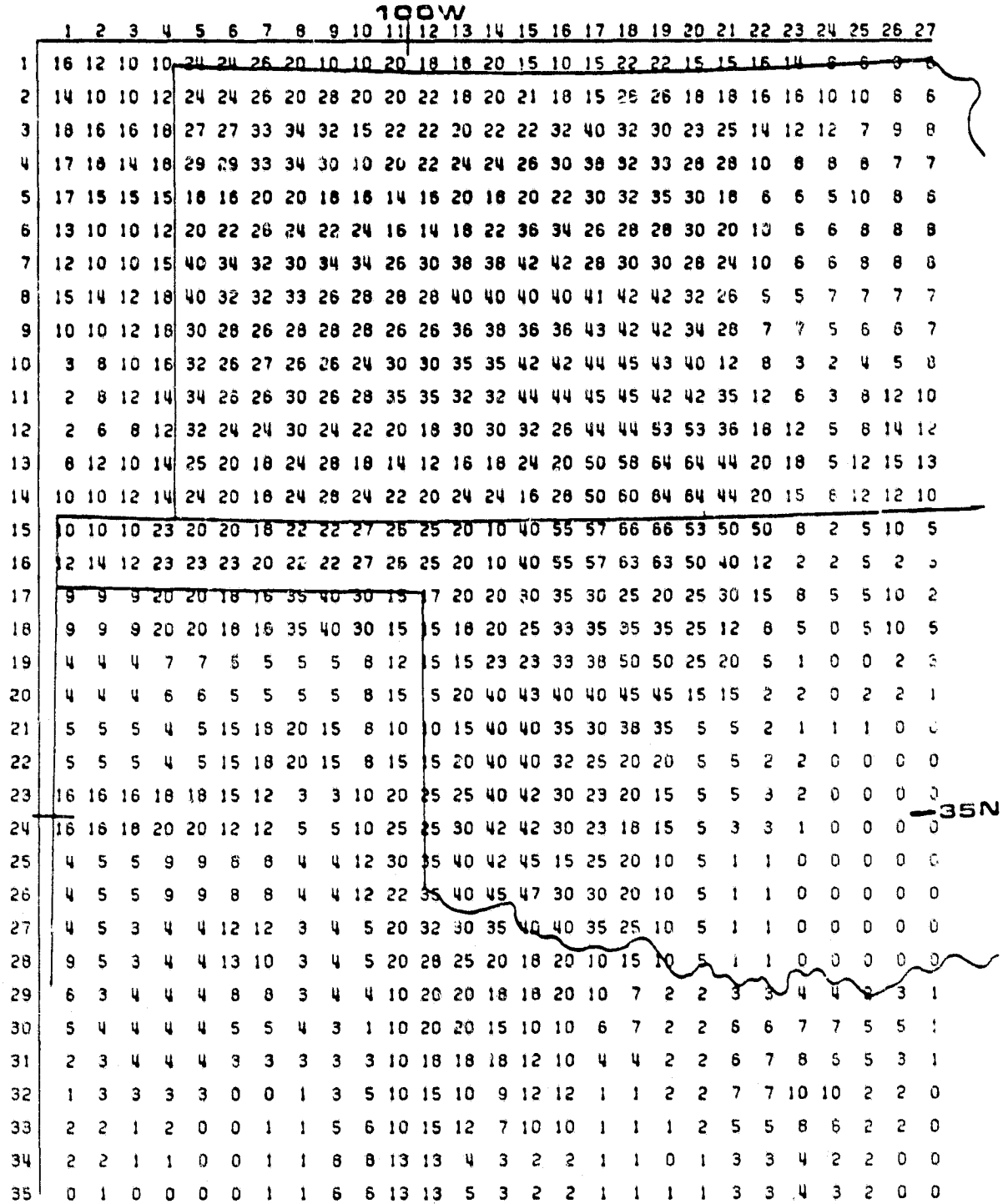

Figure 28. Percent of each grid area covered by winter wheat (derived by state agricultural statistics).

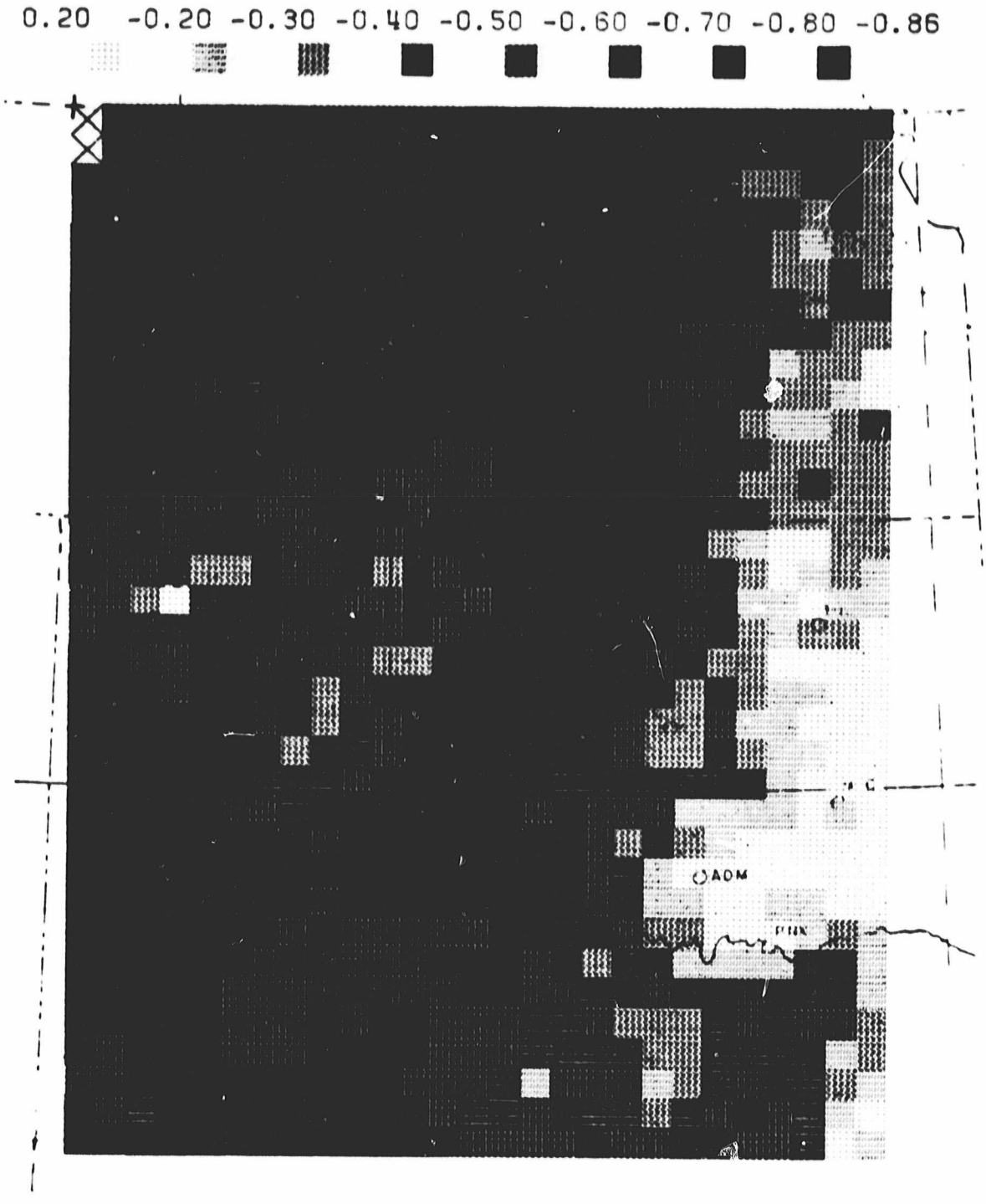

Figure 29. Linear correlation coefficients as an indicator of scatter in the data between emissivity and API for Fall (August 12-November 1).

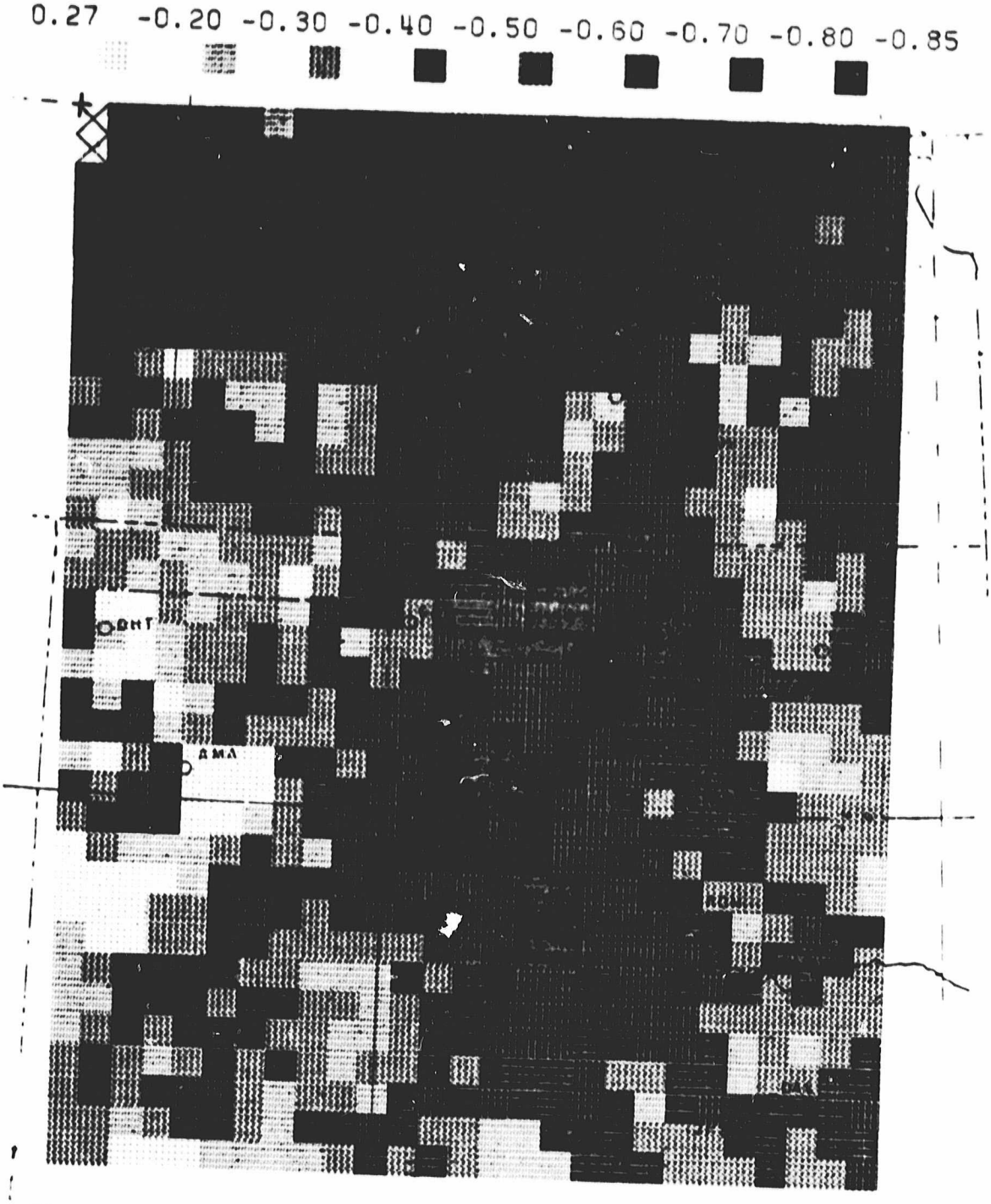

Figure 30. Linear correlation coefficients as an indicator of scatter in the data between emissivity and API for Winter (November 2-February 27).

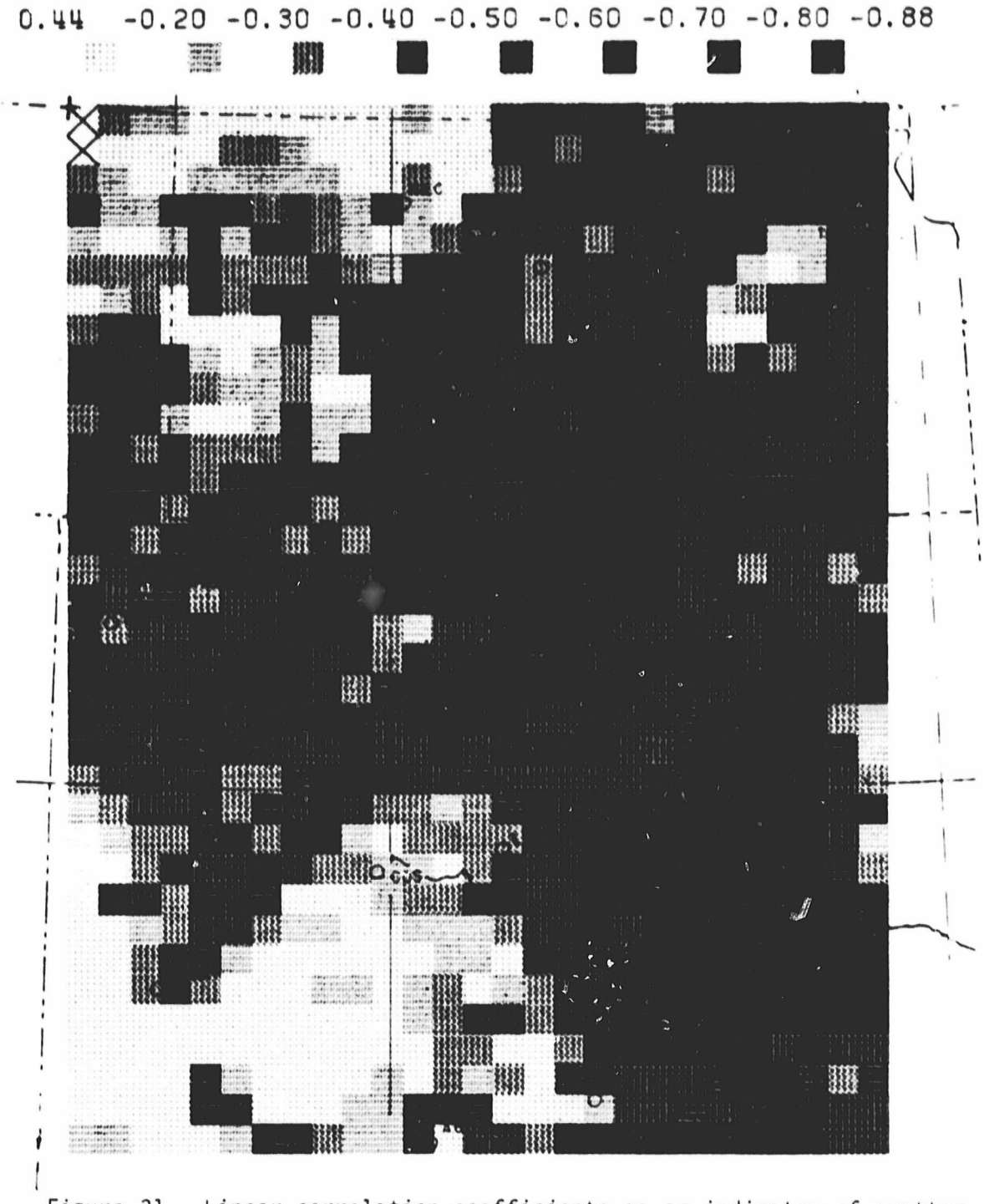

Figure 31. Linear correlation coefficients as an indicator of scatter in the data between emissivity and API for Spring (February 28-April 15).

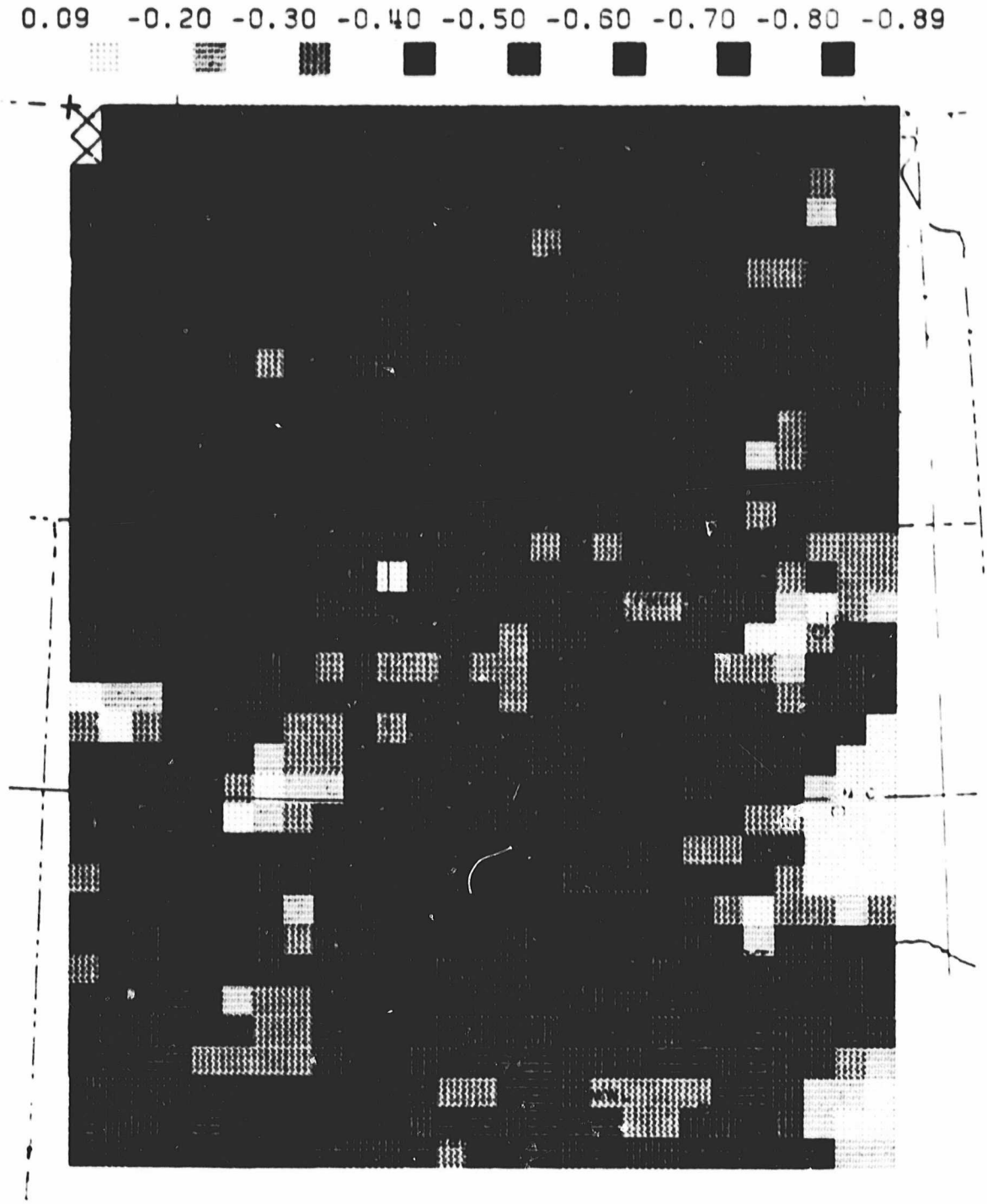

Figure 32. Linear correlation coefficients as an indicator of scatter in the data between emissivity and API for Summer (April 16-June 8).

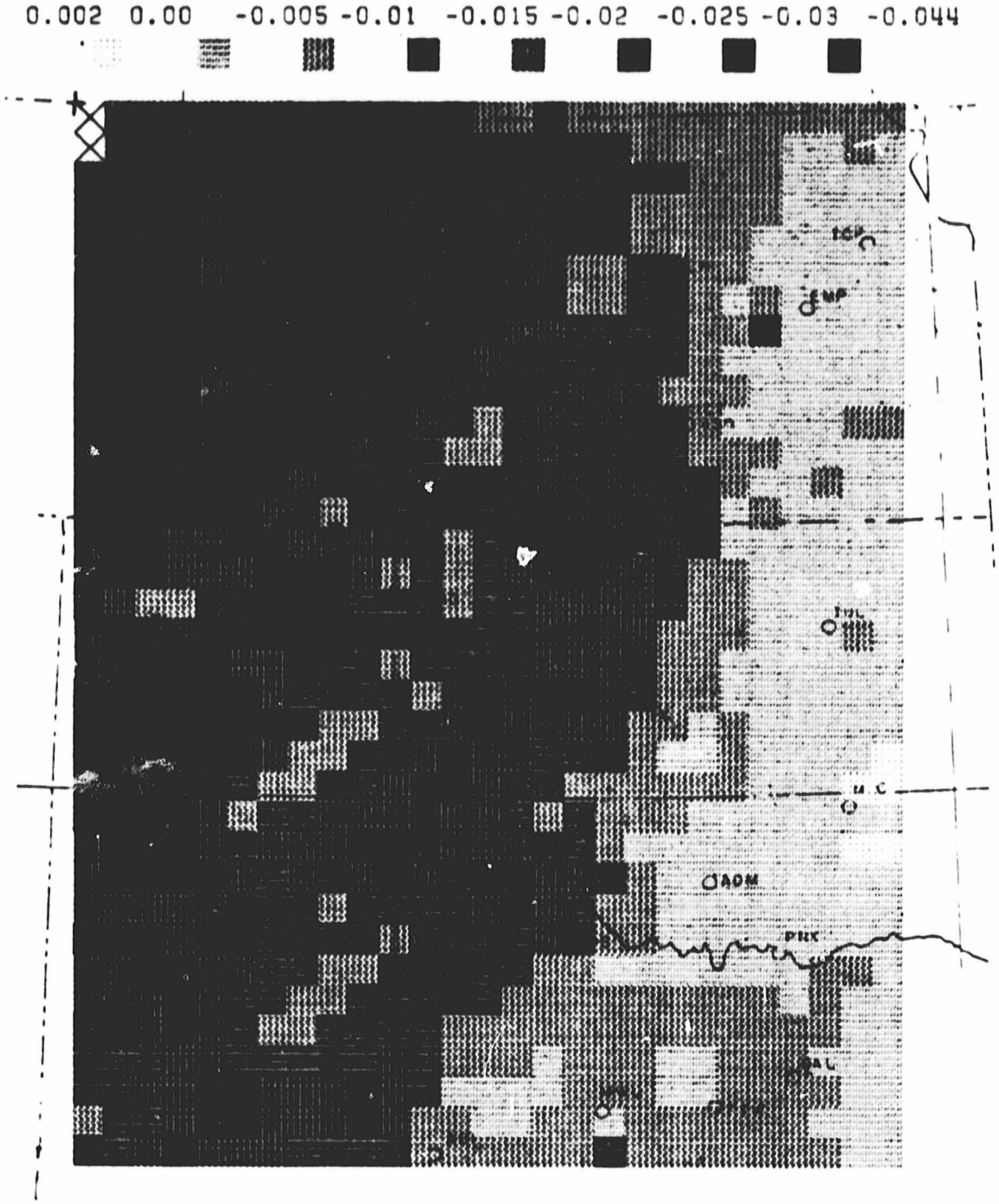

Figure 33. Linear regression slopes as an indicator of the sensitivity of the ESMR sensor to API for Fall (August 12-November 1).

Figure 34. Linear regression slopes as an indicator of the sensitivity of the ESMR sensor to API for Winter (November 2-February 27).

Figure 35. Linear regression slopes as an indicator of the sensitivity of the ESMR sensor to API for Spring (February 28-April 15).

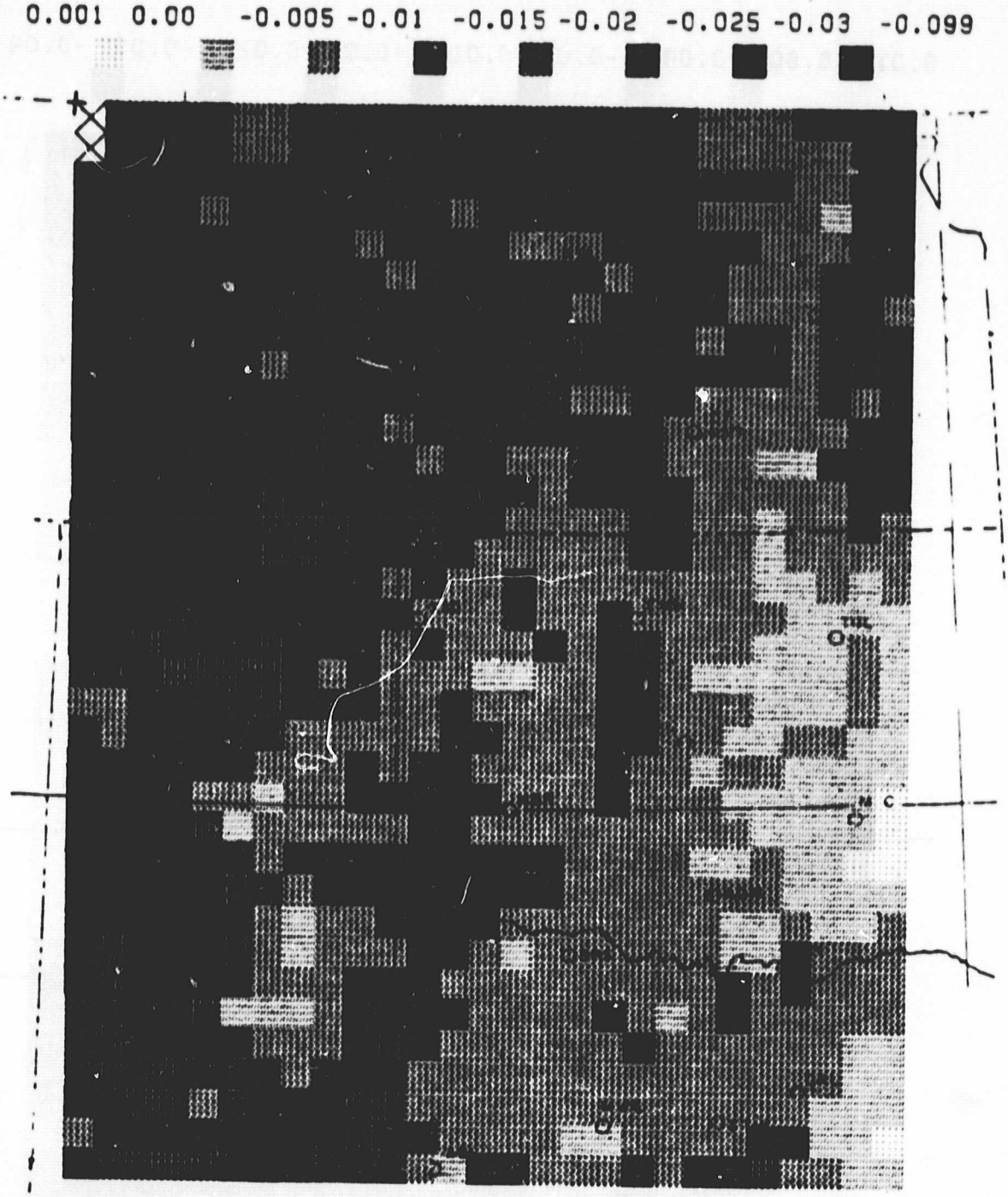

Figure 36. Linear regression slopes as an indicator of the sensitivity of the ESMR sensor to API for Summer (April 16-June 8).

5.3 Drought Conditions and Winter Wheat Yield

The results of this section were presented in a thesis by Richter (1980) (abstract in Appendix A).

As this study of stress indications from the ESMR data progressed, some restrictions were made that limited the area used for final analysis. Grid points that did not represent areas of at least 30 percent winter wheat were not used. This was to insure that wheat emission made a significant contribution to the brightness temperature. A further restriction was imposed that the wheat fields comprising the 30 percent must be continuously cropped. This removed from consideration areas of summer fallowed and irrigated wheat land. Both of these cropping methods increase plant available moisture in comparison to continuous cropping that depends on rainfall in the same year the crop is grown. A total of 95 grid points fit the above criteria.

Contrary to expectations, it was found for both models that the crop susceptibility curve acted to decrease model accuracy. The computed curve in Figure 10 has a factor of 10 difference between maximum and minimum values. The shape of the curve was vertically compressed to study the effect of a smaller range in susceptibility. This was accomplished by taking the CS to an exponent before multiplication with the SDD. The exponents that were tested are listed in Table 1 along with the resulting correlation coefficients. The highest overall correlations between SDI and winter wheat yield resulted when the curve was compressed into a horizontal line. In effect, this study found that all springtime stress had an equal effect on yield reduction. This is in contradiction to the findings that a stress period near heading

TABLE 1

A comparison of CS weighting factors for Model 1

	CS_λ	Correlation Coefficient
where	λ = 1.0 (Fig.6)	- 0.17
	= 1.5	- 0.10
	= 0.4	- 0.35
	= 0.2	- 0.43
	= 0.03	- 0.49
	= 0.0	- 0.51

reduces yield more than if the period came earlier (Chinoy 1962). However, other studies of wheat by Robins and Domingo (1962) have found little difference in CS magnitude between different phenological stages. The importance of early stress is related to the storage of soil moisture. If a crop receives abundant moisture in the early months, it not only reduces stress then but also throughout the season. Since the CS curve acted to reduce the importance of this period, the curve also reduced the accuracy of the yield estimate. Because of this, a value of 1.0 was used for CS at all times. This has the effect of not using a CS curve at all. Figures 37-42 are time series plots of SDI and API grid points that differ in yield. The inverse relationship between SDI and API is quite evident. A close examination shows that if the API is greater than 3.0 cm, then neither model shows stress occurring. After a large rainfall event, with an API above 8 cm, the models do not show stress until the API decays to around 2.0 cm. In this study daily values of T_{VEG} were obtained by linear interpolation of T_{VEG} between the days of ESMR data. This leads to a dependence of SDI on air temperature because the T_{VEG} values could not fluctuate with air temperature when the values were interpolated.

A seasonal summation of weekly SDD totals for the models is shown in Figs. 43 and 44. A representative gridpoint from each of three categories, i.e., low, medium and high yield, was chosen for the plots. The figures show additional justification for not using the CS curve in Fig. 10. Note that much of the yield reducing stress came in the first three months. The importance of this period is greatly decreased when the CS curve is used.

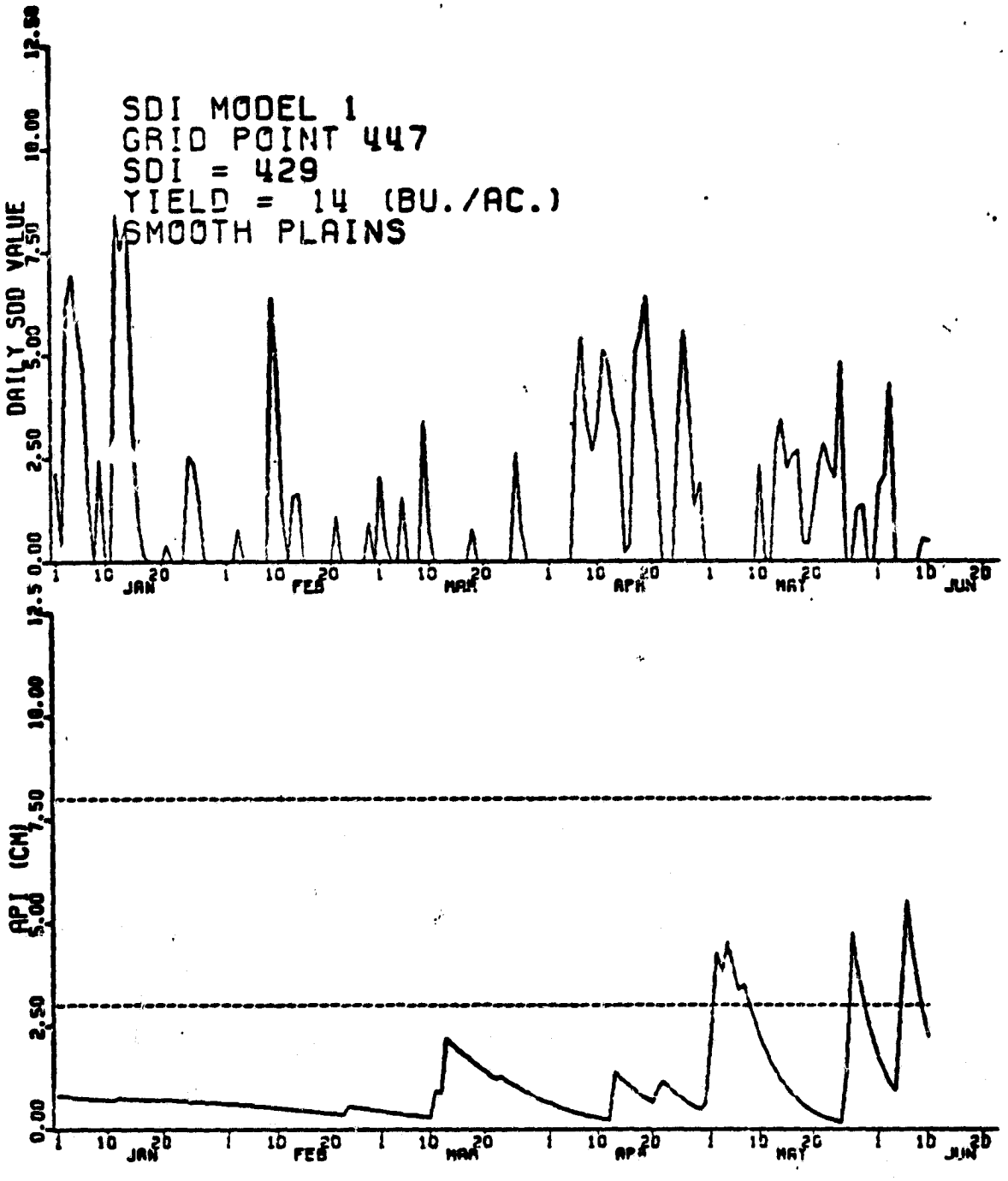

Figure 37. A plot of SSD (Model 1) and API for a low yield area.

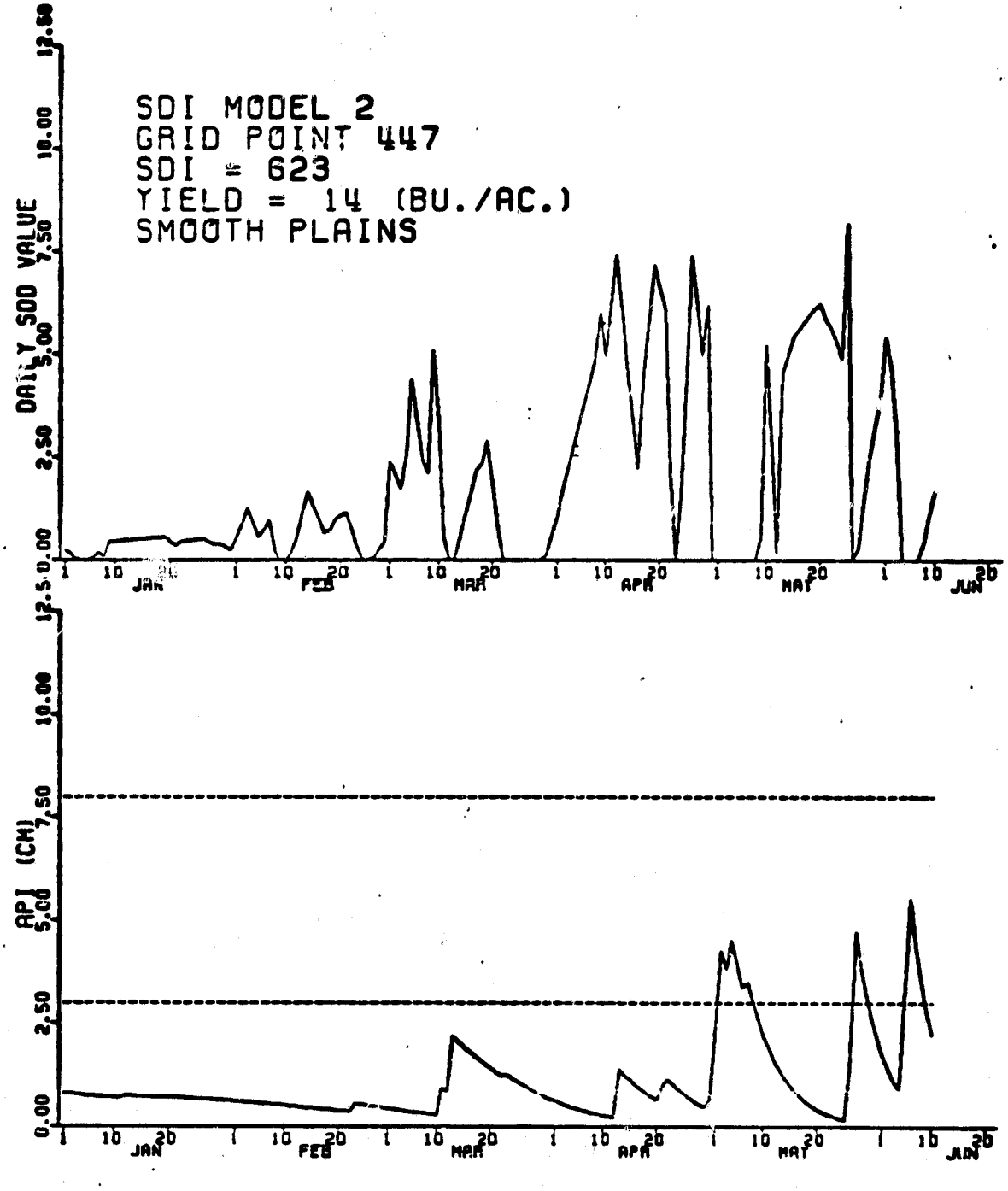

Figure 38. A plot of SDD (Model 2) and API for a low yield area.

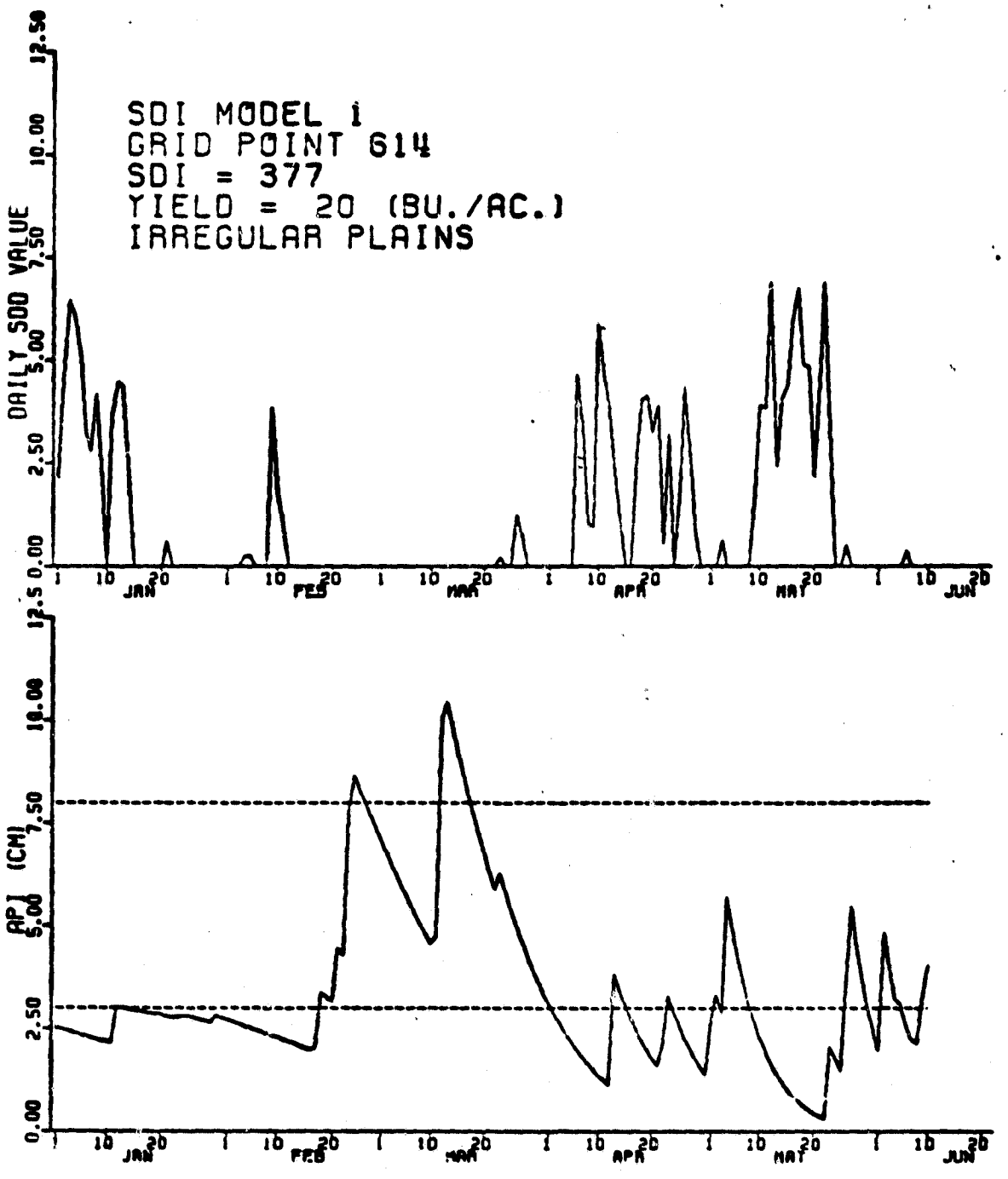

Figure 39. A plot of SSD (Model 1) and API for a medium yield area.

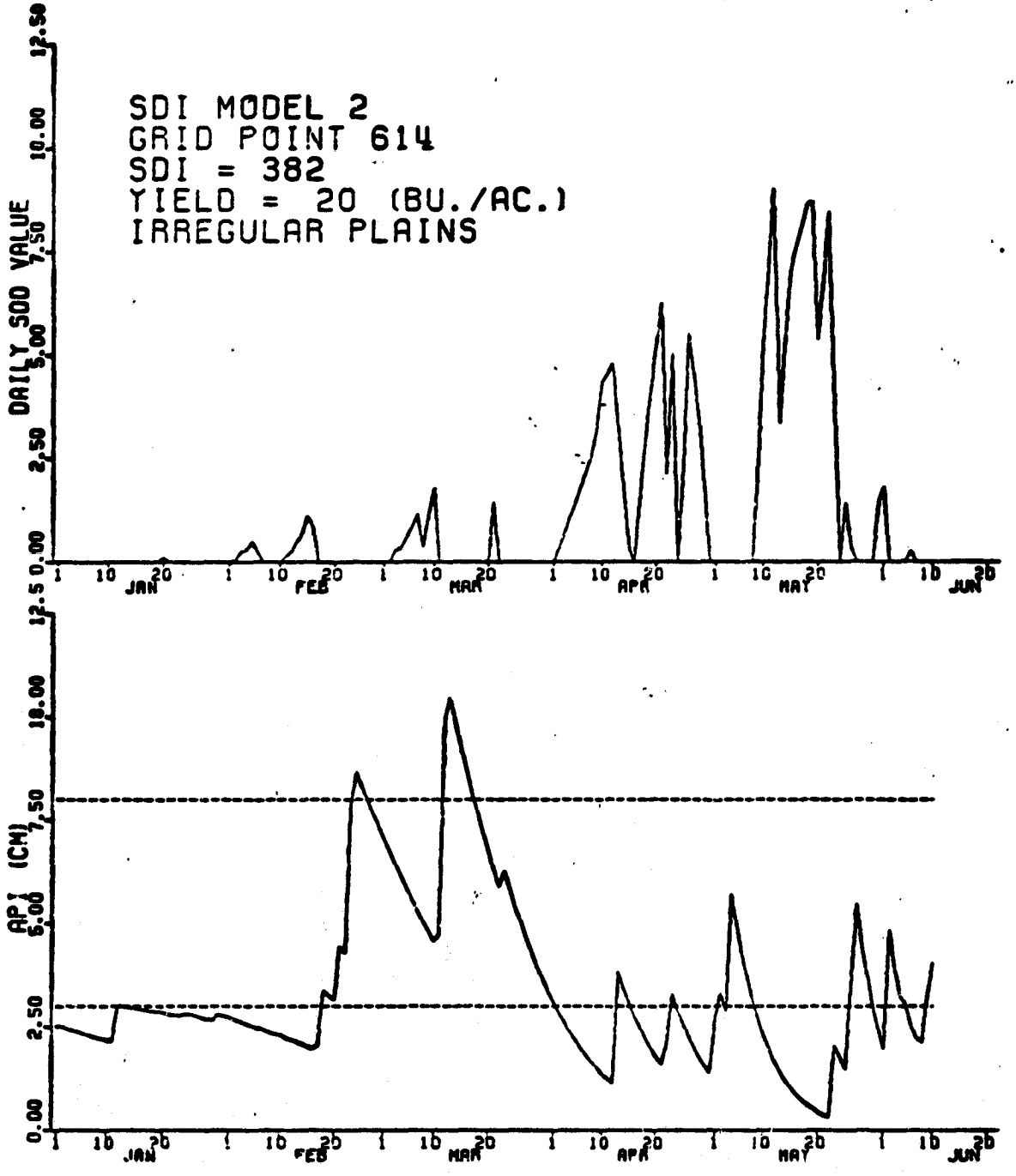

Figure 40. A plot of SSD (Model 2) and API for a medium yield area.

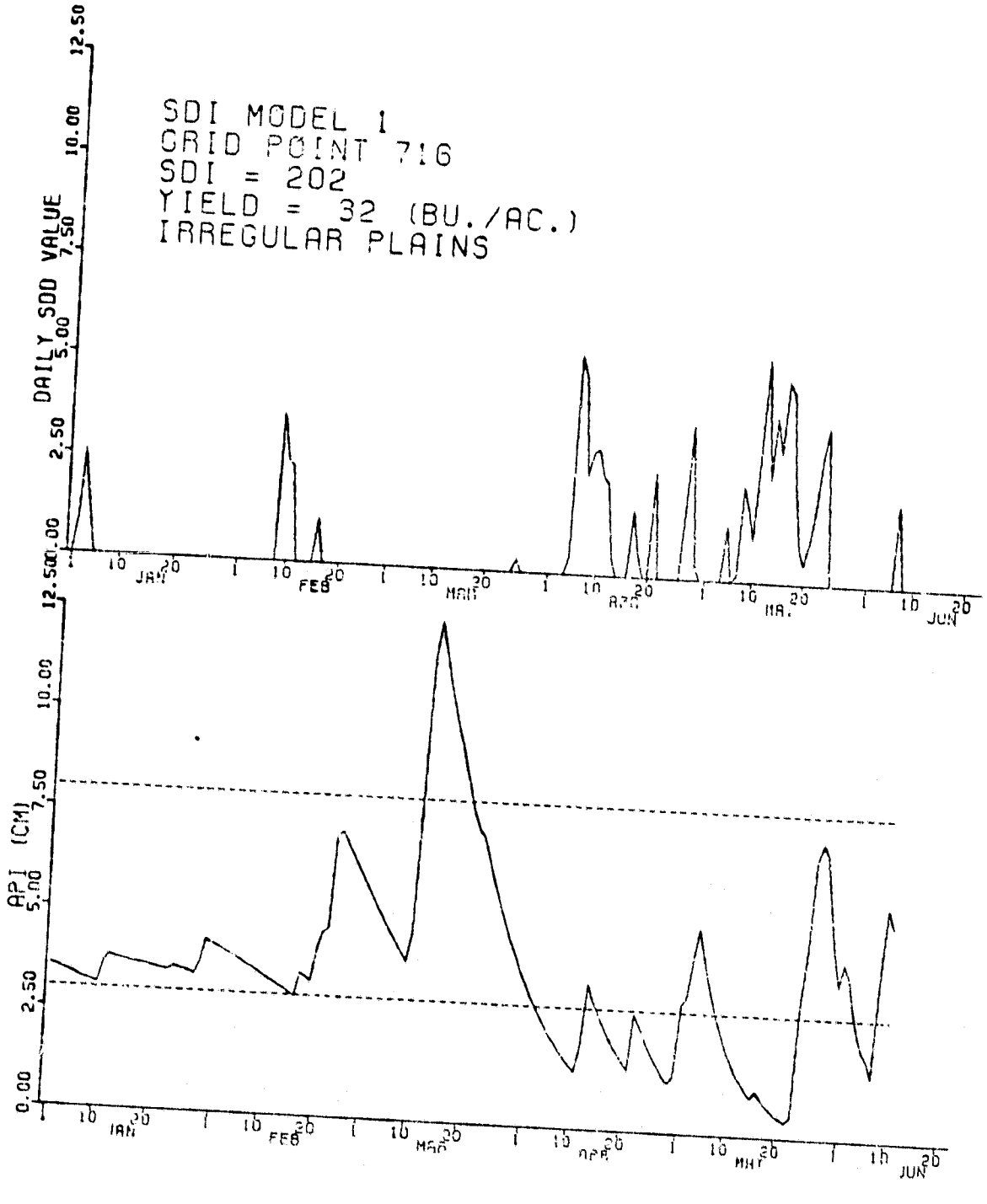

Figure 41. A plot of SDD (Model 1) and API for a high yield area.

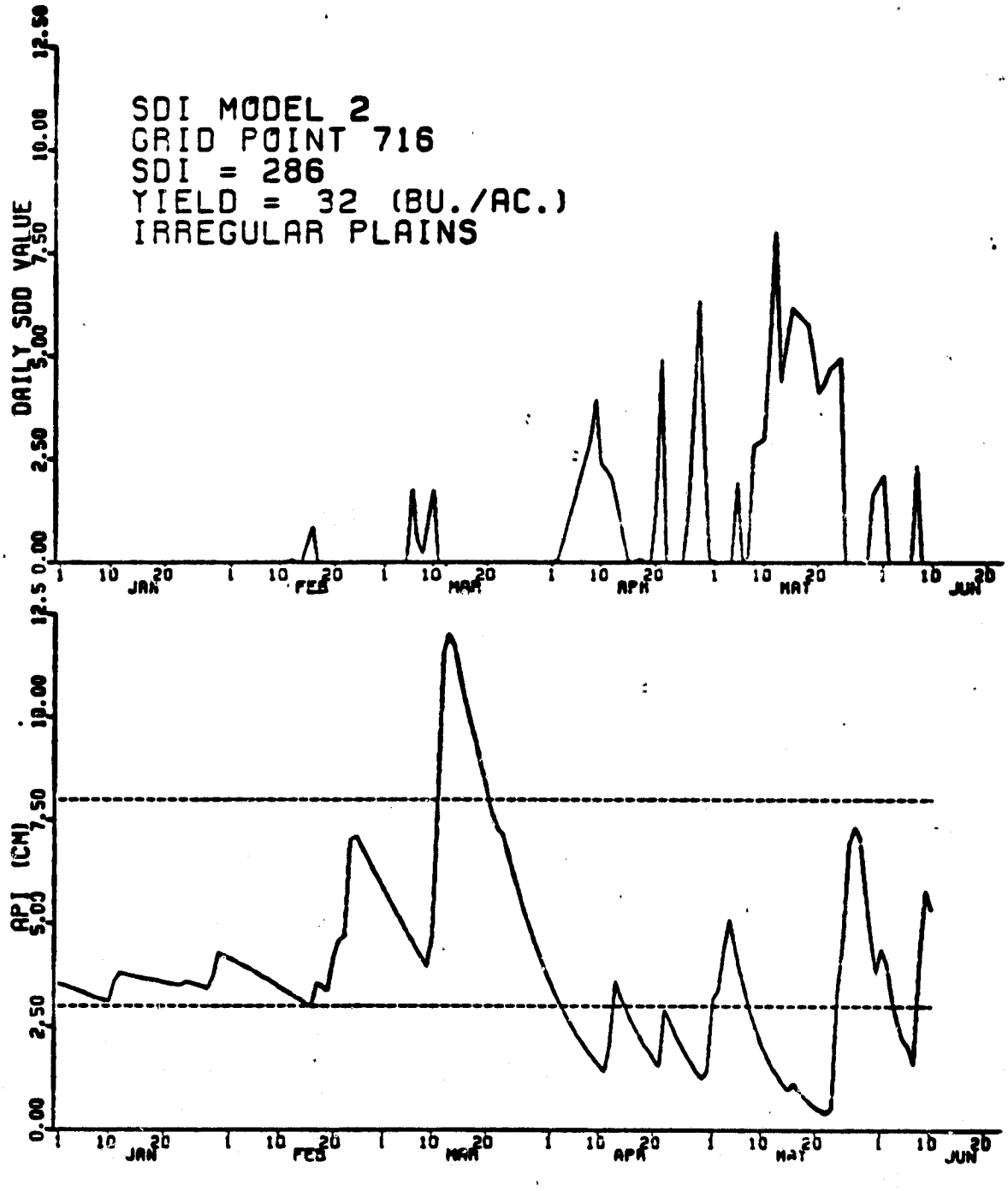

Figure 42. A plot of SDD (Model 2) and API for a high yield area.

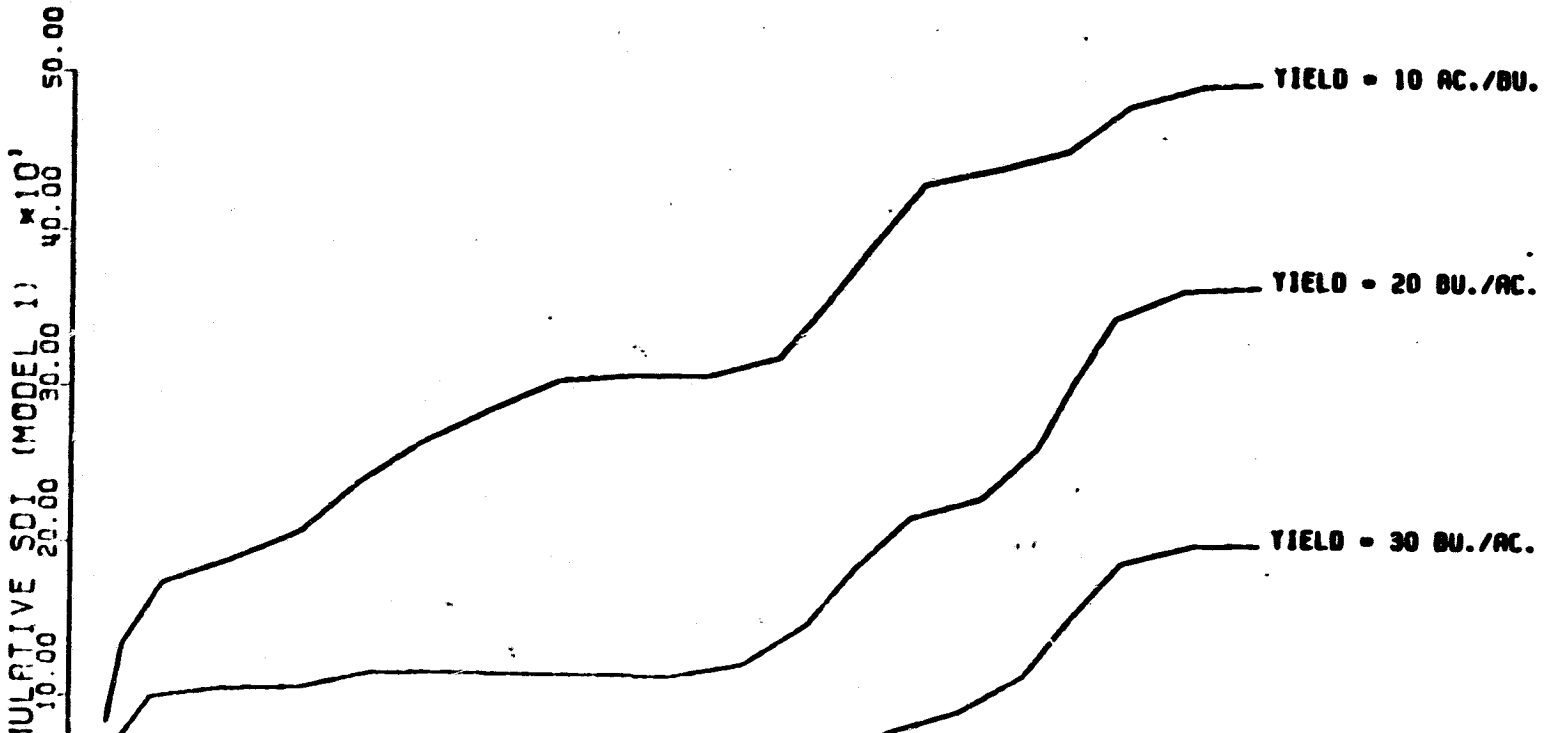

Figure 43. A time series plot of cumulative SDD (Model 1) for three selected grid points.

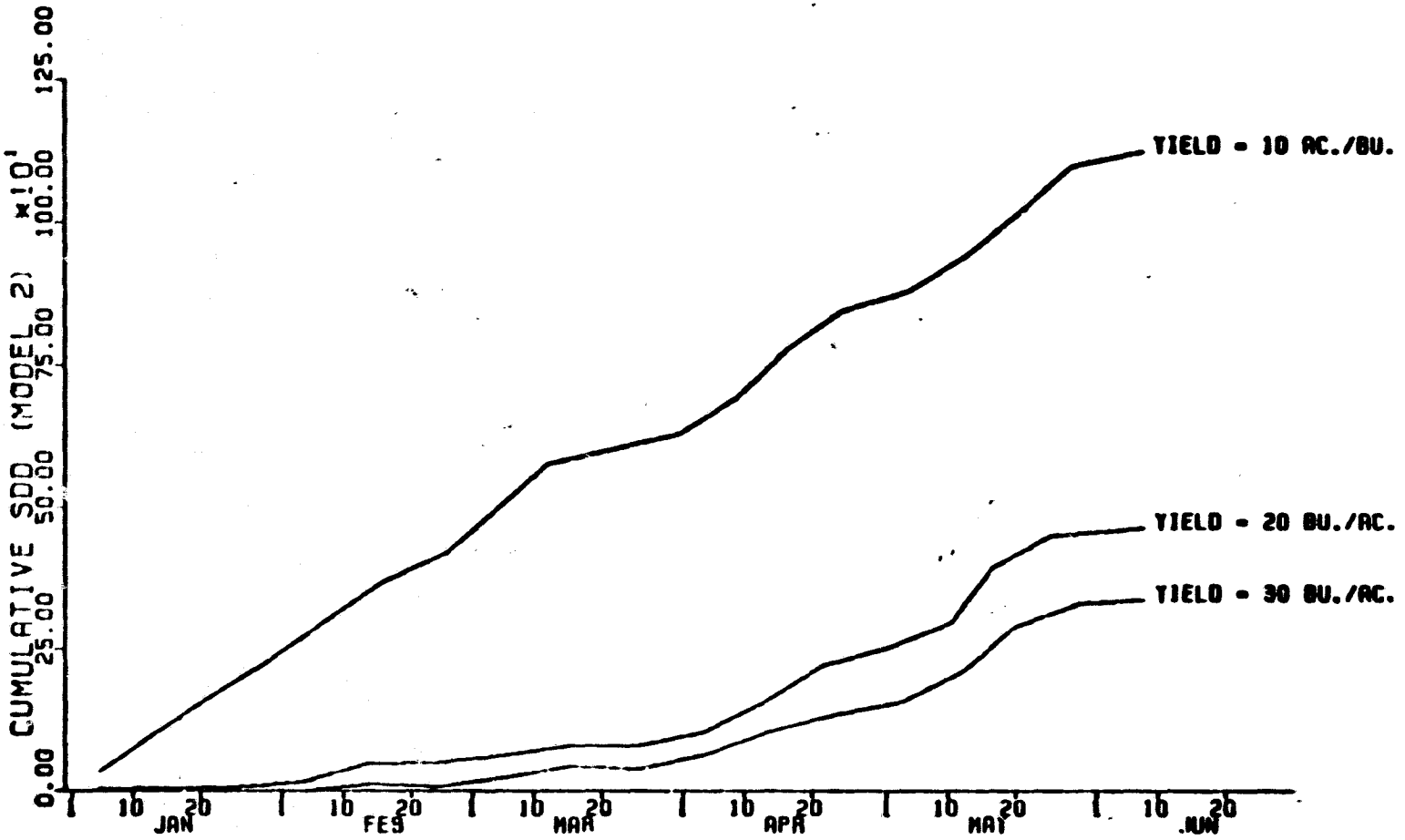

Figure 44. A time series plot of cumulative SDD (Model 2) for three selected grid points.

Figs. 43 and 44 are good illustrations of the yield prediction capability of the models. The yields are forecast in the following manner. First, within areas of homogeneous roughness, all SDI totals for a particular yield are averaged. The yields would then be plotted on the right-hand side of the figure across from the corresponding average SDI. For this study, gridpoints in areas of irregular plains were used to compute the averages. The result is shown in Fig. 45. The figure also shows an example of yield prediction. The current date and SDD total are located on the graph. The curves from Fig. 43 representing maximum and minimum stress, with yields of 10 and 30 bu/ac respectively, are vertically shifted until they pass through the point. The intersection of these curves with the yield axis gives an estimate of maximum and minimum yields. From the example in Fig. 45, the estimate would be between 18 and 22 bu/ac.

The task of predicting most probable yield is much more difficult. While it would certainly be between the maximum and minimum forecast yields, the exact location is difficult to predict. This problem could best be solved by the incorporation of a meteorological forecast. For example, if the long range forecast predicted above average temperatures and below normal precipitation, an above average amount of plant stress would be expected. If this were the case, the probable yield would be closer to the maximum stress estimate of yield rather than the minimum stress estimate. Thus, the forecast of probable yield would then be adjusted with the amount of adjustment dependent upon the forecasted departure from normal weather conditions.

Figs. 46 and 47 are plots showing the variation between SDI and yield for the 95 grid points. Correlation coefficients, as well as the

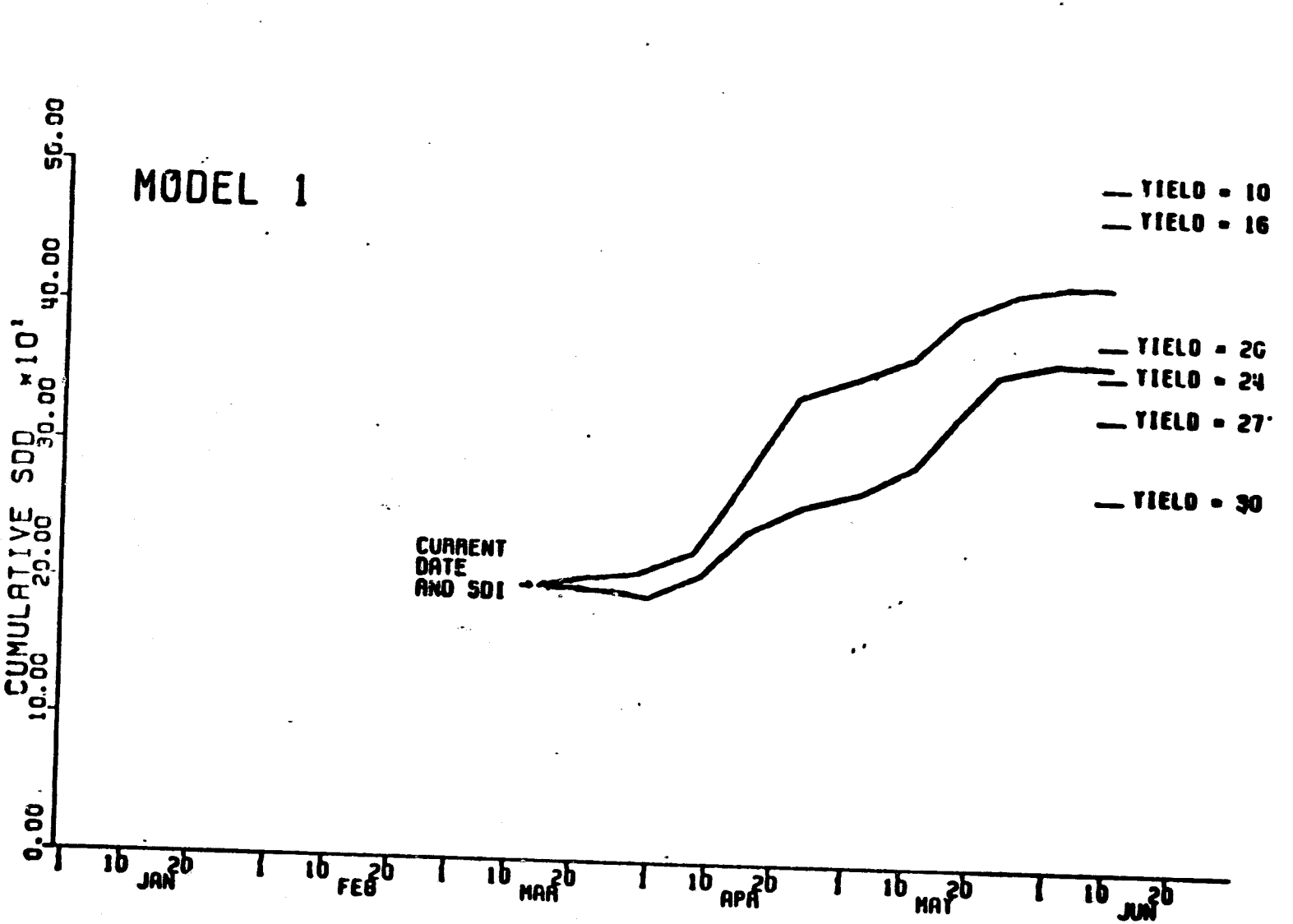

Figure 45. An example of the technique used to forecast yield.

Figure 46. A scatterplot of final SDI (model 1) versus yield.

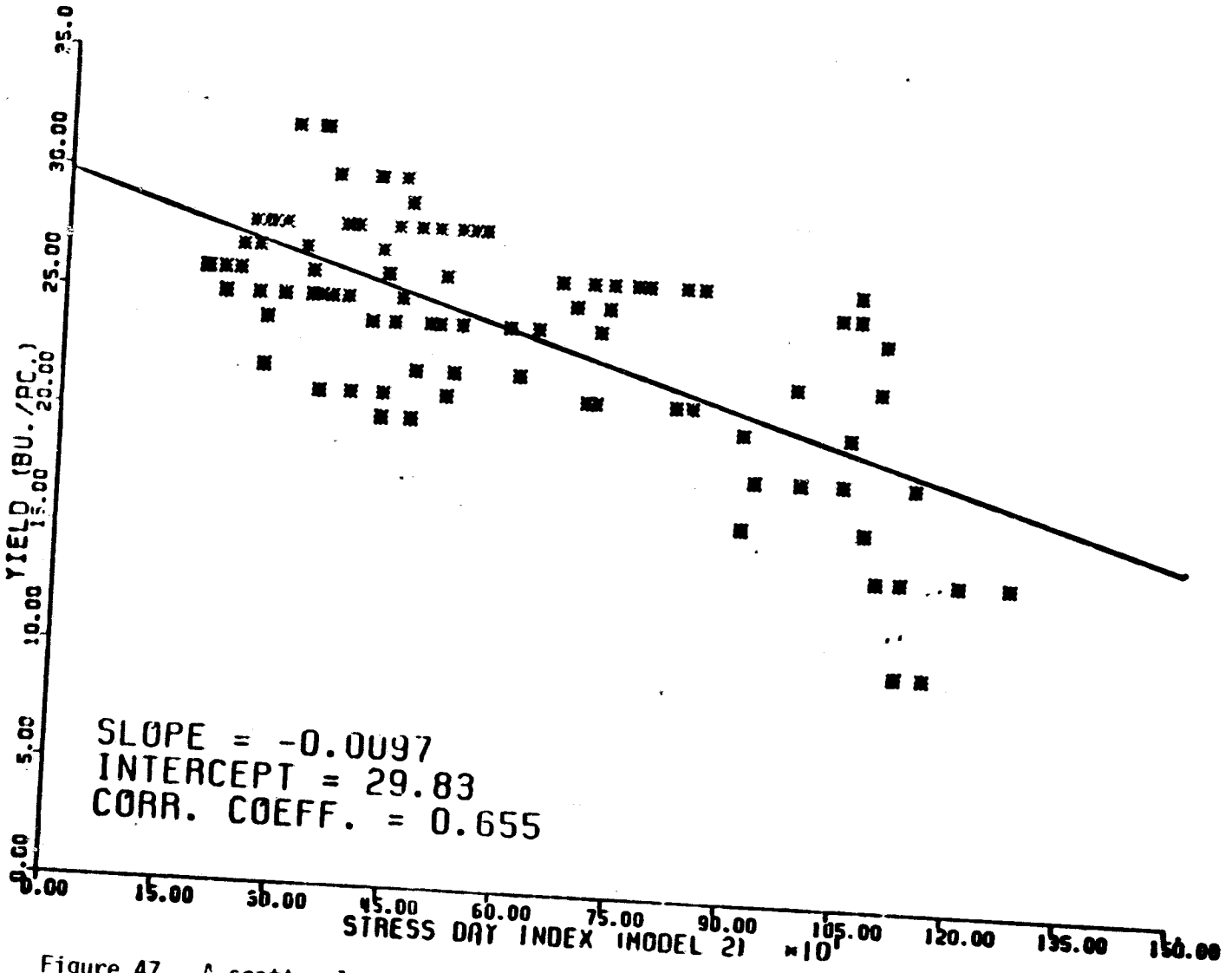

Figure 47. A scatterplot of final SDI (model 2) versus yield.

slope and intercept, are shown in each figure. It is interesting to note that Model 2 has a higher correlation coefficient than Model 1. This was unexpected because Model 2 uses climatological air temperatures instead of the measured temperatures used in Model 1. The encouraging results obtained with Model 2 indicate that a yield forecasting technique using only remotely sensed data is feasible.

Figs. 48 and 49 are graymaps showing the residuals calculated by linear regression. The slopes and intercepts shown in Figs. 46 and 47 were used to calculate the residuals. For each grid, residuals were compared to the percentage of continuously cropped winter wheat. There was no decernable pattern when residuals were plotted against percent winter wheat. The accuracy of the models was therefore unresponsive to differences in the grid point's wheat content.

The effect of surface roughness is shown in Figs. 50 - 52. For each of three yields, three gridpoints were chosen that represented the widest range of final SDI. The gridpoints were then located on a map of USGS classification of land form. This map outlined areas of smooth plains, irregular plains, tableland, low hills, and mountains. As the figures show, the magnitude of the SDI is directly related to the roughness of the land. Thus, much of the scatter in Figs. 46 and 47 is due to variations in roughness.

An investigation was undertaken to examine the method of SDD summation. That is, do ten days of one SDD per day have the same yield reducing effect as one day of ten SDDs? To answer this question, three additional SDD summations were made. Each daily SDD value was taken to exponents of 1.3, 0.7, and 2.0. Table 2 shows the effect of the exponents on the summation and the resulting effect on the correlation

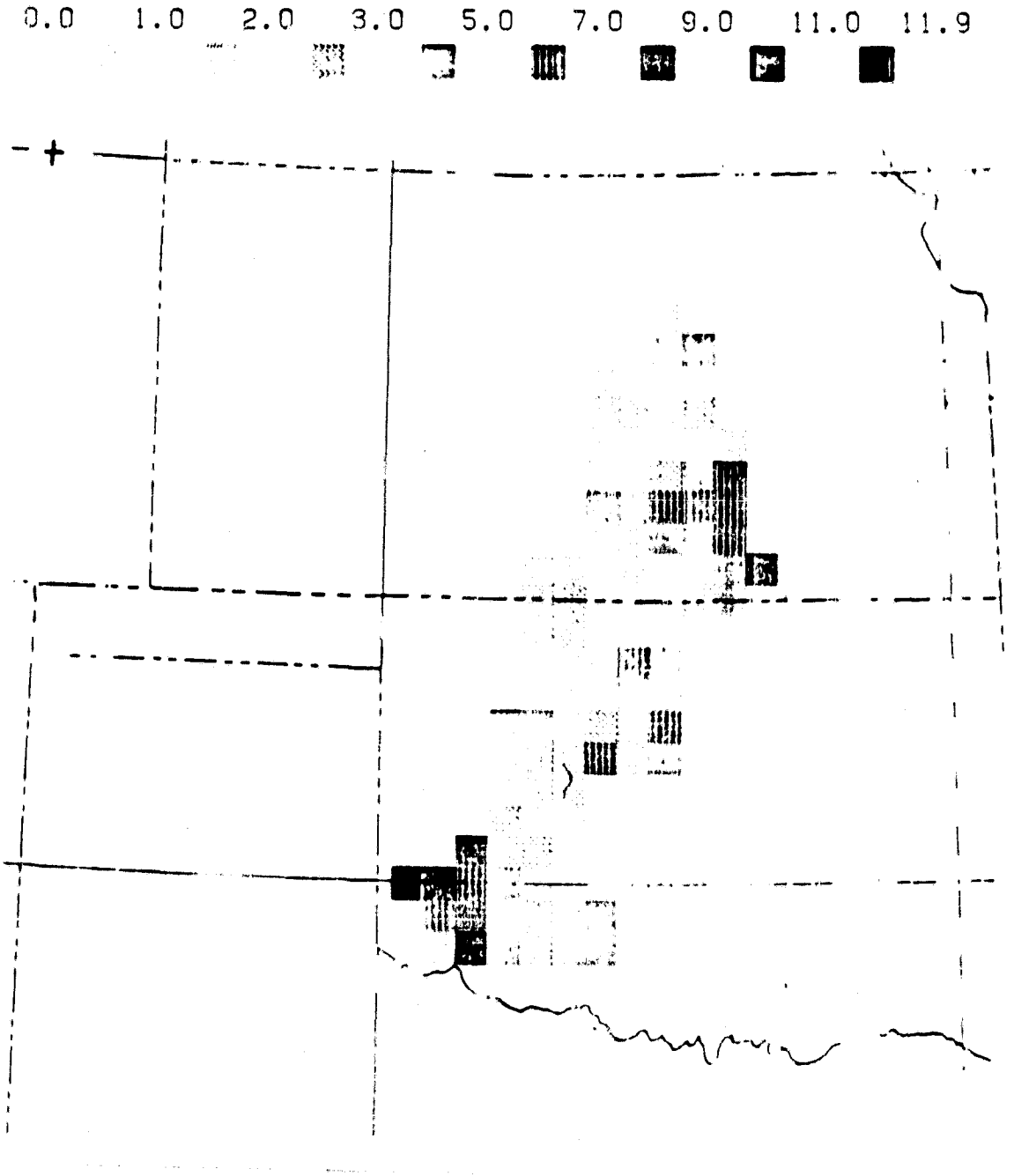

Figure 48. A graymap depicting the residuals from Model 1. The residuals were calculated as the difference between actual and predicted values of yield.

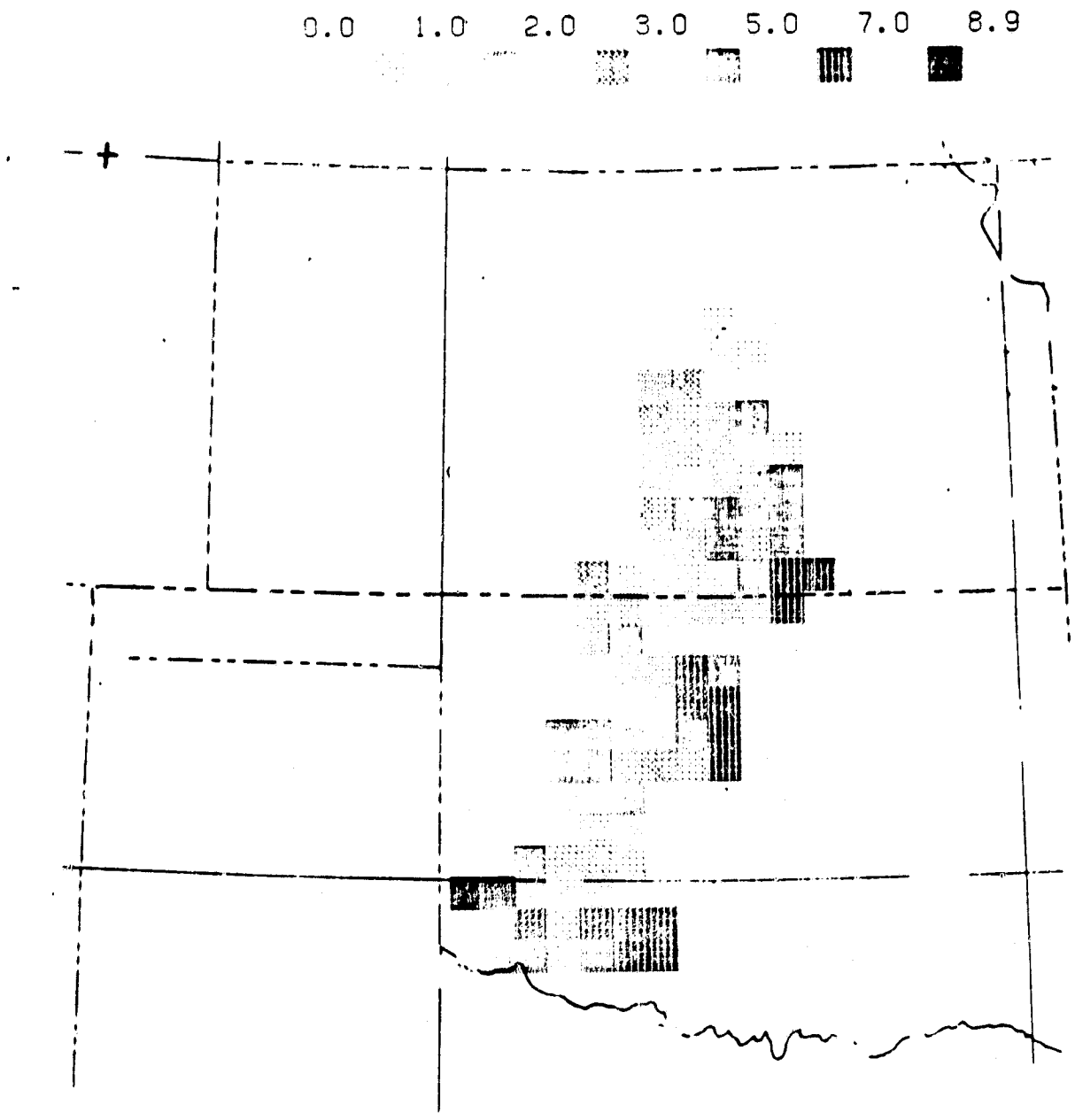

Figure 49. A graymap depicting the residuals from Model 2. The residuals were calculated as the difference between actual and predicted values of yield.

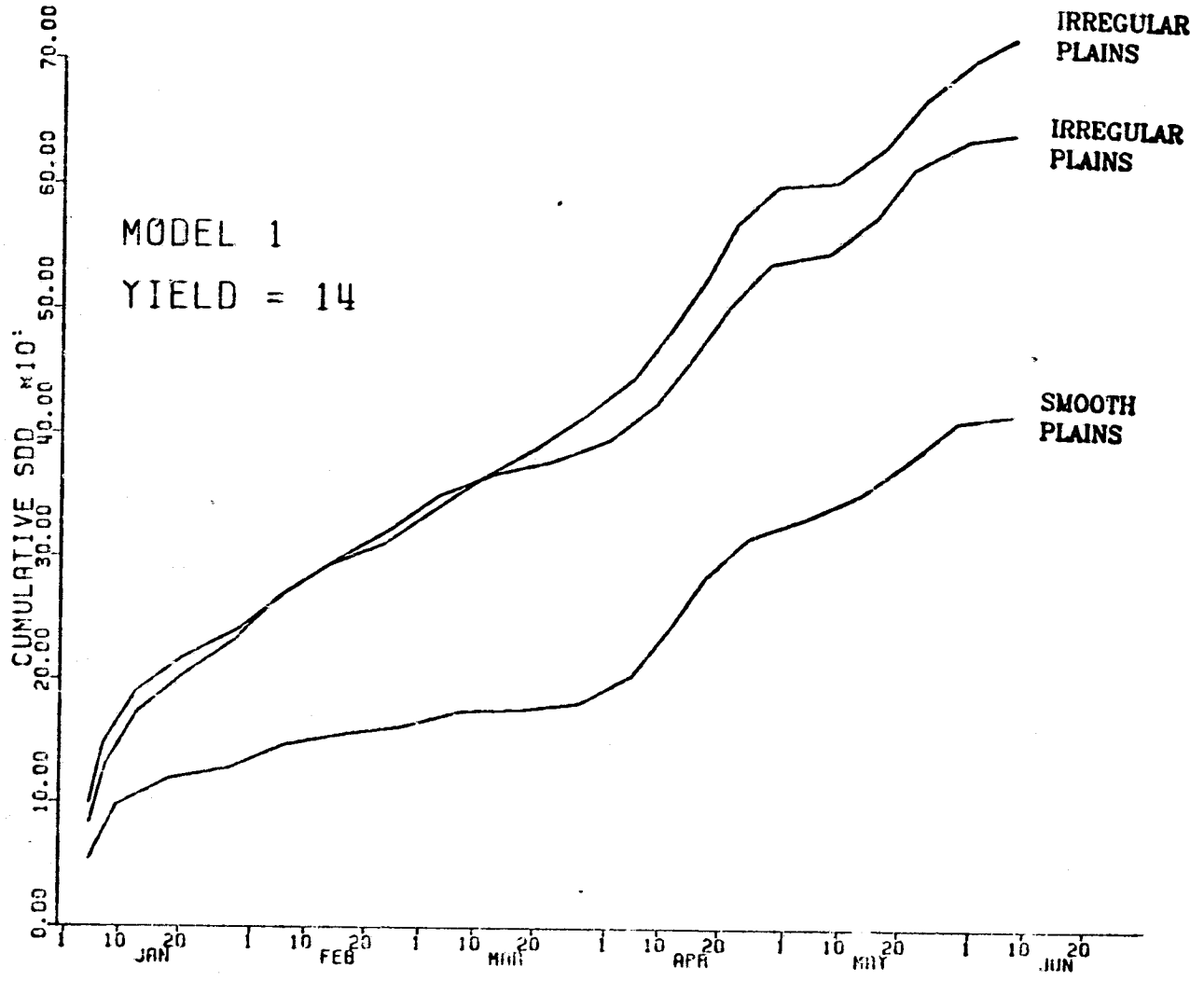

Figure 50. A plot of cumulative SDD (Model 1) for three low yield grid points.

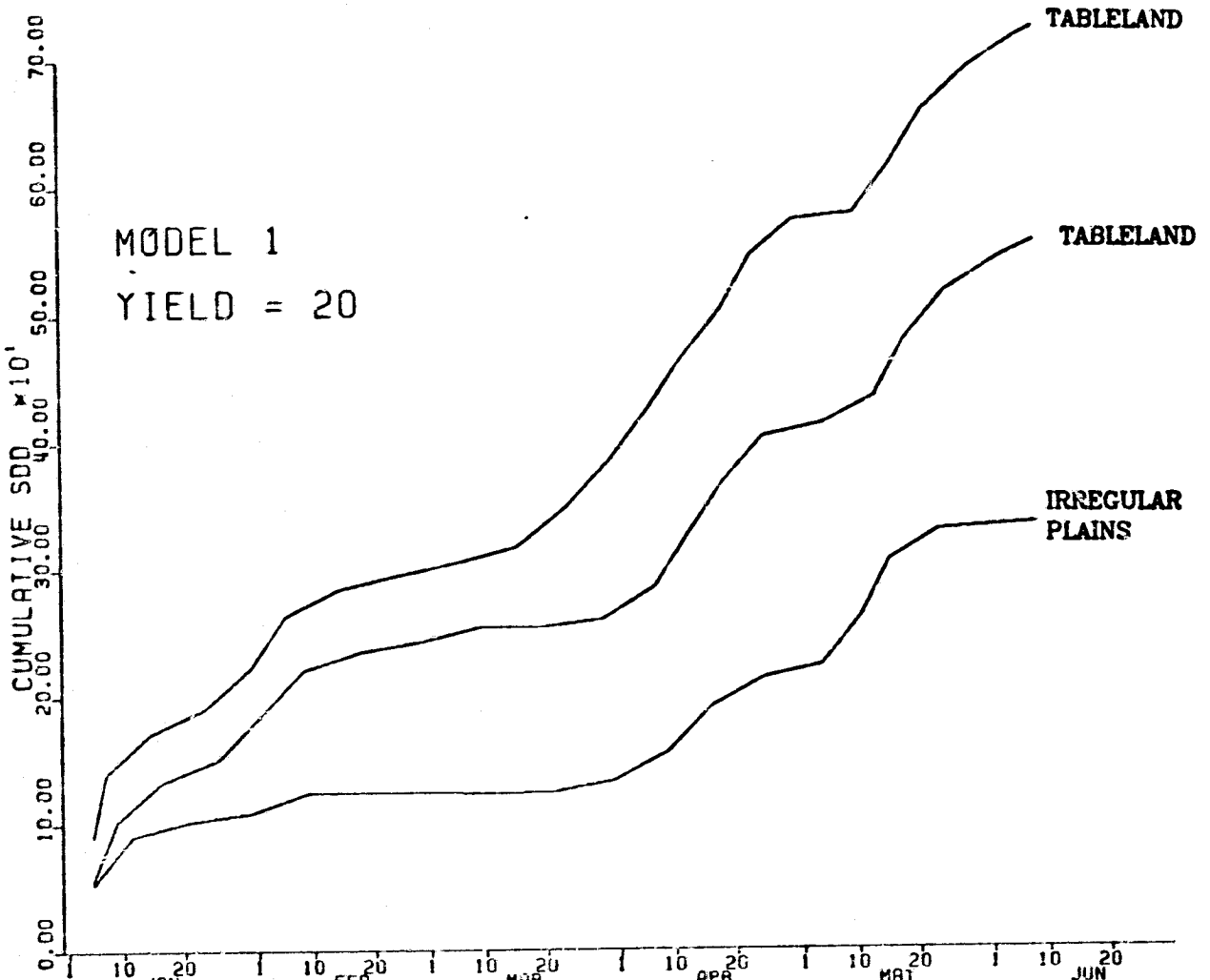

Figure 51. A plot of cumulative SDD (Model 1) for three medium yield grid points.

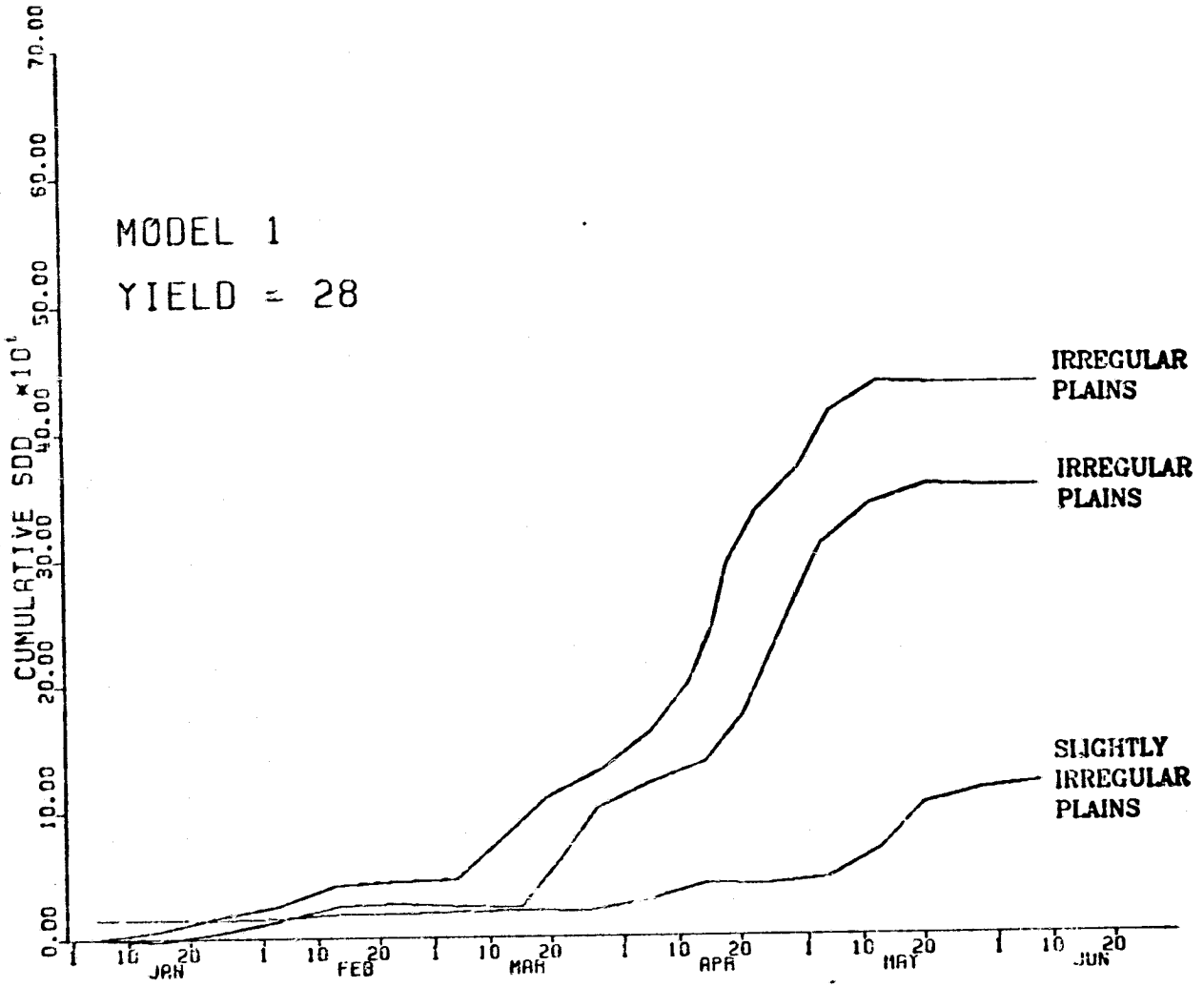

Figure 52. A plot of cumulative SDD (Model 1) for three high yield grid points.

TABLE 2

Comparison of SDD weighting schemes

SDD Exponent	10 days of 1 SDD	1 day of 10 SDD	Correlation Coeff.
1.0	10.0	10.0	.655
2.0	10.0	100.0	.120
1.3	10.0	20.0	.642
0.7	10.0	5.0	.644

6.0 CONCLUSION

Agricultural lands show the greatest potential to use the Electrically Scanning Microwave Radiometer to infer soil moisture. These usually are better soils situated on smoother, less hilly or less eroded land. Tillage practices are such as to afford periods of smooth and bare soils during the year. In contrast, pastures, rangelands and cross timber region usually are situated on poorer soils (some rocky) and the terrain which is unsuitable for agriculture. The surface of untilled lands is almost never completely bare. As a rule, it is covered with growing or dead vegetation or with timber.

Results over the predominant winter wheat areas indicate that the best potential to infer soil moisture occurs during fall and spring. These periods encompass the growth stages when soil moisture is most important to winter wheat's yield.

This study has also shown that it is possible to identify wheat stress periods with the ESMR using the stress degree day approach. However, the amount of scatter indicates that the models need further development. The scatter in the results is attributable to several sources. The effect of variations in the look angle is noticeable in the data. There were instances when the ESMR sensed the same grid point on consecutive days. Usually one of the brightness temperatures was much too low. Upon close examination, it was found that the anomalously low temperature was usually sensed at the extremes of the scan angle. The major sources of inaccuracy are the subjective yield estimates used for comparison with the SDI. These estimates gave one value of yield for an entire county, which often contained several grid points. Thus, one inaccurate county estimate can cause high residuals for several grid

points. A possible example of this is the two grid points with a 10 bu./ac. yield estimate. Both points used the same county for a yield estimate. The models predicted yields of 16 to 20 bu./ac., similar to yields in surrounding counties. These two points had the highest residuals for both models.

Due to the availablity of only one year of data, analysis of stress detection was limited. A multi-year study is needed to validate these results. This would allow the calibration of each grid point separately, minimizing point to point variations. Graphs such as those in Figs. 43 and 44 could be compiled for each grid point. This should allow for more accurate forecasts.

The model which used climatological air temperatures was more accurate than the model that used actual temperatures. This is probably due to a chance variation and cannot be expected to hold true for succeeding years. However, the high correlation coefficient obtained with Model 2 indicated that a good forecast can be made using only remotely sensed data. Perhaps the best combination would be simultaneous measurement by a microwave radiometer and a thermal scanner. In this way, inaccuracies due to the air temperature estimation can be eliminated.

While this study concentrated on winter wheat, the SDI concept could be applied to other crops. However, the crop must meet certain criteria. The vegetation must be dense, so the sensor measures only plant canopy temperature. Sorghum, corn and rangeland grasses are likely candidates for this type of monitoring. For reasons explained earlier, two further restrictions must be remembered. First, the crop cannot have a moisture supply that is unavailable to the surrounding

area. Second, the crop must fill a significant proportion of the grid cell.

The results of this research clearly demonstrate the feasibility of using the short wavelength ESMR (1) to infer soil moisture when surface conditions are acceptable, (2) to map the spatial distribution of moisture from storms resulting from frontal passages, and, (3) with further refinement, to develop an alorithn to identify drought conditions and to forecast crop yield. Atmospheric contributions, vegetation, and roughness produce detrimental effects to soil moisture detection at short microwave wavelengths. Longer wavelength radiometers such as the Scanning Multifrequence Microwave Radiometer (SMMR) should lessen these effects when they become available.

The ESMR or a similar system might be used operationally in the interim period before longer wavelength passive microwave sensors are available.

References

1. Agricultural Statistics 1978, 1979: U. S. Govt. Printing Office, Washington, D. C., 421pp.

2. Barnes, S. L., 1973: Mesoscale objective map analysis using weighted time-series observations. NOAA Tech. Memo., ERL NSSC-62, Norman, OK., 60pp.

3. Bartholic, J. F., L. N. Namken, and C. L. Wiegand, 1972: erial thermal scanner to determine temperatures of soils and crop canopies differing in water stress. Agron. J., 64, 603 08.

4. Blanchard, B. J., M. J. McFarland, T. J. Schmugge, and E. hoades, 1979: Estimation of soil moisture with API algorithms and microwave emmission. (Unpublished manuscript), 32pp.

5. Chilar, J. and F. T. Ulaby, 1975: Microwave remote sensing of soil water content. Remote Sensing Lab. Tech. Rep. 264-6, University of Kansas Space Technology Center, Lawrence, KS., 183 pp.

6. Chinoy, J. J., 1962: Physiology of drought resistance in wheat. IV. Effect of wilting at different growth and developmental stages on plant characters determining yield of grain in eight varieties of wheat. Phyton, 19, 5-10.

7. Day, A. D. and M. A. Barmore, 1971: Effects of soil moisture stress on the yield and quality of flour from wheat (Triticum aestivum L.). Agron. J., 63, 115-116.

8. Day, A. D. and S. Intalap, 1970: Some effects of soil moisture stress on the growth of wheat (Triticum aestivum L. em Thell). Agronomy J., 62, 27-29.

9. DeCoursey, D. G , 1974: Unpublished data.

10. Ehrler, W. L., 1973: Cotton leaf temperatures as related to soil water depletion and meteorological factors. Agron J., 65, 404-409.

11. -----, and C. H. M. van Bavel, 1967: Sorghum foliar responses to changes in soil water content. Agron. J., 59, 242-246.

12. -----, S. D. Idso, R. D. Jackson and R. J. REginato, 1978: Wheat Canopy temperature; relation to plant water potential. Agron. J., 70, 251-256.

13. Hayami, Y. and W. Peterson, 1972: Social returns to public information services: Statistical reporting of U.S. farm commodities. Am. Econ. Rev., 62, 119-130.

14. Heilman, J. L., E. T. Kanemasu, N. J. Rosenberg and B. L. Blad, 1976: Thermal scanner measurements of canopy temperature to estimate evapotranspiration. Remote Sensing of Environ., 5, 137-145.

15. Hess, S. L., 1959: Introduction to theoretical meteorology. Holt, Rinehard and Winston, New York 355pp.

16. Hiler, E. A. and R. N. Clark, 1971: Stress day index to characterize effects of water stress on crop yields. Transactions of the ASAE, 14, 757-761.

17. Idso, S. B., R. D. Jackson, R. J. Reginato, 1975: Detection of soil moisture in the root zone of crops: A technique adaptable to remote sensing. J. Geophy. Res., 81, 23-25.

18. -----, and W. L. Ehrler, 1976: Estimating soil moisture in the root zone of crops: A technique adaptable to remote sensing. J. Geophy. Res., 81, 23-25.

19. -----, R. D. Jackson and R. J. Reginato, 1978: Remote sensing for agricultural water management and crop yield prediction. Agric Water Management, 1, 299-310.

20. Linsley, R. K., M. A. Kohler and J. L. H. Paulhus, 1975: Hydrology for engineers (2nd ed.), McGraw-Hill, New York, 482 pp.

21. Lintz, J. and D. S. Simonett, 1976: Remote sensing of environment. Addison-Wesley Publishing Co., Reading, MA., 694pp.

22. -----, and B. J. Blanchard, 1977: Temporal correlations of antecedent precipitation with Nimbus 5 ESMR brightness temperatures. Preprints 2nd Conf. Hydrometeorology, Toronto, Ont., Canada, American Metecrology Society, Boston, MA., 311-315.

23. Marion, J. B., 1965: Classical electromagnetic radiation. Academic Press, New York, 479pp.

24. Meneely, J. M., 1977: Application of the Electrically Scanning Microwave Radiometer (ESMR) to classification of the moisture content of the ground. Earth Satellite Corporation, Washington, D. C., Final Report, 39pp.

25. Newton, R. W., 1977: Microwave remote sensing and its application to soil moisture detection. Tech. Rep. RSC-81, Remote Sensing Center, Texas A&M University, College Station, TX., 500pp.

26. -----, S. L. Lee, J. W. Rouse, Jr. and J. F. Paris, 1974: On the feasibility of remote monitoring of soil moisture with microwave sensors. Preprints, 9th Int. Symp. Remote Sensing of Environ., April 15-19, 1974. Environmental Research of Michigan, Ann Arbor, MI., 725-738.

27. Paris, J. F., 1969: Microwave radiometry and its application to marine meteorology and oceanography. Ref. No. 69-11, Contract No. 2119(04), Dept. of Oceanography, Texas A&M University, College Station, TX., 210pp.

28. -----, 1971: Transfer of thermal microwaves in the atmosphere. NASA Grant NGR--44-001-098, Dept. of Meteorology Rep., Texas A&M University, College Station, TX. 257pp.

29. Richter, J. C., 1980: Wheat stress measurement with the electrically scanning microwave radiometer (ESMR). M. S. Theis, Texas A&M University, College Station, TX., 55pp.

30. Robins, J. S. and C. E. Domingo, 1962: Moisture and nitrogen effects on irrigated spring wheat. Agron. J., 54, 135-138.

31. Saxton, K. E. and A. T. Lenz, 1967: Antecedent retention indexes predict soil moisture. J. Hydraul. Div., Proc. Am. Soc. Civ. Eng. Vol. 93, No. HY4, 223-241.

32. Schmugge, T., 1976: Preliminary results from the March 1975 soil moisture flight. Goddard Space Flight Center Rep. 913-76-216, Greenbelt, MD., 23pp.

33. -----, 1977: Remote sensing of surface soil moisture. Preprints, 2nd Conf. Hydrometeorology, October 25-27, 1977 Toronto, Ontario. American Meteorology Society, Boston, MA., 304-310.

34. -----, P. Gloersen, T. Wilheit, and F. Geiger, 1974: Remote sensing of soil moisture with microwave radiometer. J. Geophys. Res. Vol. 79, No. 2, 317-323.

35. -----, B. J. Blanchard, W. J. Burke, J. F. Paris and J. R. Wang, 1976a: Results of soil moisture flight during April 1974. NASA Tech. Note TN-D-8321, National Aeronautics and Space Administration, Washington, D. C., 34pp.

36. -----, T. Wilheit, W. Webster, Jr. and P. Gloersen, 1976b: Remote sensing of soil moisture with microwve radiometers-II. NASA Tech. Note TN-D-8321, National Aeronautics and Space Administration, Washington, D. C., 34pp.

37. Theis, S. T., 1979: Surface soil moisture estimation with the electrically scanning microwave radiometer (ESMR). M. S. Theis, Texas A&M Univeristy, College Station, TX., 46pp.

38. Whitehead, V., 1979: Unpublished data.

39. Wilheit, T. T., 1972: The electrically scanning microwave radiometer (ESMR) esperiment. Nimbus 5 Users Guide, NASA Goddard Space Flight Center, Greenbelt, MD., 55-105.

APPENDIX A

ABSTRACT

CORRELATION OF BRIGHTNESS TEMPERATURES FROM THE ELECTRICALLY SCANNING MICROWAVE RADIOMETER (ESMR) WITH ANTECEDENT PRECIPITATION INDICES (API)

M. J. McFarland (Dept. of Agricultural Engineering, Texas A&M University, College Station, Tx.)

B. J. Blanchard, S. W. Theis (Remote Sensing Center, Texas A&M University, College Station, Tx.)

Estimates of soil moisture in a large area context are primarily useful for large area crop monitoring and for estimation flood hazards on large and small drainage areas. Such estimates may also provide indications of soil moisture below the surface as well as provide a means for the determination of drought and areal extent of drought conditions. A preliminary study correlated digital data from the ESMR to API that in turn is correlated to soil moisture over the northwestern third of Oklahoma. Encouraging results were obtained for a three month period in the fall of 1973 when vegetation was sparse. Since the ESMR is a quasi-operational system, data can be acquired over the same area on a three day repeat cycle. This provides the opportunity to investigate changes in soil moisture through a time series. Temporal mapping reduces the effects of the point to point variations in vegetative cover, surface roughness, and soil characteristics.

The moisture content and temperature of the emitting layer integrated over the sensor footprint forms the major variations of the

temporal brightness temperature changes. Since the emitting layer temperature can be approximated, the brightness temperature changes may provide a fairly accurate indication of soil moisture changes for rainfall and subsequent drying.

ABSTRACT

ESTIMATION OF SOIL MOISTURE WITH API ALGORITHMS AND MICROWAVE EMISSION

Bruce J. Blanchard, Marshall J. McFarland

Thomas J. Schmugge, and Edd Rhoades[1]

Large area soil moisture estimations are required for global systems of crop yield estimation and flood prediction. Microwave sensor systems that as yet can only detect moisture at the surface have been suggested as a means of acquiring large area estimates. Measurements of soil moisture were studied to understand the correlation and intercorrelation between moisture in surface soil layers and moisture in deeper layers. Relations previously discovered between microwave emission at the 1.55 cm. wavelength and surface moisture as represented by an antecedent precipitation index were used to provide a pseudo infiltration estimation. Infiltration estimation based on surface wetness estimated on a daily basis were used to estimate soil moisture at a depth of 15 cm. by use of a modified antecedent precipitation index with good results (R^2 = .7010 and R^2 = .7383). The technique was modified and

[1]Respectively, Remote Sensing Center, Texas A&M University, College Station, Texas 77843; Remote Sensing Center, Texas A&M University, College Station, Texas 77843, NASA/Goddard Laboratory for Atmospheric Sciences, Goddard Space Flight Center, Greenbelt, Maryland 20771; SEA-AR, Chickasha, Oklahoma.

used to estimate soil moisture at 15 cm. depth when only an estimate of surface moisture each three days was available. Predictions based on estimation of surface wetness at three day intervals resulted in R^2 value of .6811 and .7076 for the same date sets. The algorithms developed in this study can be used over relatively flat agricultural lands to provide improved estimates of soil moisture to a depth greater than the depth of penetration for the sensor.

ABSTRACT

Wheat Stress Measurement with the
Electrically Scanning Microwave Radiometer (ESMR). (December 1980)
John Charles Richter, B. S., Texas A&M University
Chairman of Advisory Committee: Dr. George Huebner

This study has examined the feasibility of using a stress degree index (SDI) to predict winter wheat yield. Microwave brightness temperatures in the spring of 1974 were used as an input. Two formulations of the SDI model were studied. The difference was in the amount of real time data needed for the computation. The first method used only microwave brightness temperatures as sensed by the Nimbus-5 ESMR. The second method also required data to estimate air temperature at the time of satellite overpass.

Good correlations were found between winter wheat yield and SDI for both models. Forecast inaccuracies were attributed to several sources. The primary source is roughness variations between gridpoints. Other sources included inaccurate county agricultural statistics and differences in wheat content among gridpoints.